Journal of Medicinal Chemistry

pubs.acs.org/jmc

Article

Hinge Binder Scaffold Hopping Identifies Potent Calcium/Calmodulin-Dependent Protein Kinase Kinase 2 (CAMKK2) Inhibitor Chemotypes

Benjamin J. Eduful,[⊥⊥] Sean N. O'Byrne,[⊥⊥] Louisa Temme,[⊥⊥] Christopher R. M. Asquith, Yi Liang, Alfredo Picado, Joseph R. Pilotte, Mohammad Anwar Hossain, Carrow I. Wells, William J. Zuercher, Carolina M. C. Catta-Preta, Priscila Zonzini Ramos, André de S. Santiago, Rafael M. Couñago, Christopher G. Langendorf, Kévin Nay, Jonathan S. Oakhill, Thomas L. Pulliam, Chenchu Lin, Dominik Awad, Timothy M. Willson, Daniel E. Frigo, John W. Scott,* and David H. Drewry*

Cite This: *J. Med. Chem.* 2021, 64, 10849−10877

Read Online

ACCESS | Metrics & More | Article Recommendations | Supporting Information

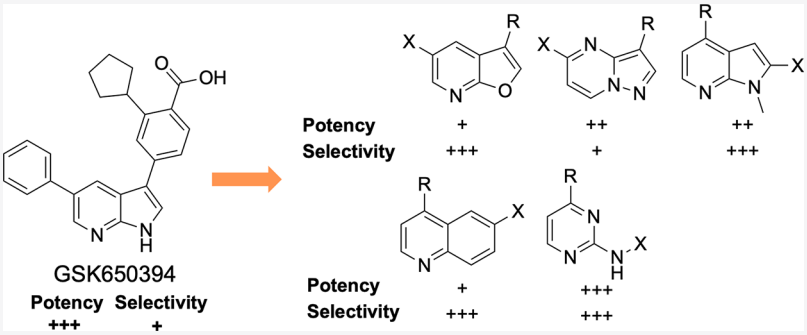

ABSTRACT: CAMKK2 is a serine/threonine kinase and an activator of AMPK whose dysregulation is linked with multiple diseases. Unfortunately, STO-609, the tool inhibitor commonly used to probe CAMKK2 signaling, has limitations. To identify promising scaffolds as starting points for the development of high-quality CAMKK2 chemical probes, we utilized a hinge-binding scaffold hopping strategy to design new CAMKK2 inhibitors. Starting from the potent but promiscuous disubstituted 7-azaindole GSK650934, a total of 32 compounds, composed of single-ring, 5,6-, and 6,6-fused heteroaromatic cores, were synthesized. The compound set was specifically designed to probe interactions with the kinase hinge-binding residues. Compared to GSK650394 and STO-609, 13 compounds displayed similar or better CAMKK2 inhibitory potency *in vitro*, while compounds **13g** and **45** had improved selectivity for CAMKK2 across the kinome. Our systematic survey of hinge-binding chemotypes identified several potent and selective inhibitors of CAMKK2 to serve as starting points for medicinal chemistry programs.

INTRODUCTION

Calcium (Ca^{2+})/calmodulin-dependent protein kinase kinase 2 (CAMKK2) is a serine/threonine kinase that is one of the calmodulin (CaM)-binding proteins of the CaMK family.[1−3] Ca^{2+} is an important second messenger that aids in the regulation of a wide range of signaling events in part through binding to its intracellular receptor CaM.[4] Ca^{2+}-bound CaM modulates various cellular responses *via* activation of an array of downstream proteins including CAMKK2.[5] Upon activation, CAMKK2 phosphorylates and activates its substrates including CAMK1, CAMK4, AMP-activated protein kinase, (AMPK) and in some cases AKT. This signal transduction results in the regulation of many important physiological and pathological processes.[6−16]

Due to CAMKK2's important role in cell signaling, dysregulation of CAMKK2 has been implicated in several diseases. Aberrant activation and overexpression of CAMKK2 have been linked to multiple cancer types including prostate, breast, ovarian, gastric, and hepatic cancers.[8−14,17,18] Knockdown of CAMKK2 *via* siRNA or pharmacological inhibition of CAMKK2 reduced cell proliferation, migration, and invasion as well as induced apoptosis and cell cycle arrest in numerous cancer cell lines and tumor models.[8,12−14,17,19−21] Mechanistically, CAMKK2 is an important regulator of metabolic and

Received: December 31, 2020
Published: July 15, 2021

inflammatory processes, which are contributory factors to its impact on cancer growth.[9,14]

In addition, therapeutic interventions targeting CAMKK2 may be beneficial beyond oncology. For example, hepatocellular carcinoma (HCC) is often preceded by non-alcoholic fatty liver disease (NAFLD), which is driven by several risk factors including obesity and type 2 diabetes.[22−24] Inhibition of CAMKK2 reduced food intake in mice, and *Camkk2*-null mice are leaner than wild-type mice when fed a high-fat diet.[25,26] Consistent with these findings, CaMKK2 was recently shown to be inhibited by liraglutide, a glucagon-like peptide-1 receptor agonist that decreases food intake and promotes weight loss.[27] In relation to skeletal disease, CAMKK2 is expressed in osteoblasts and osteoclasts, which play an essential role in bone tissue maintenance.[28] Inhibition of CAMKK2 stimulated bone formation and reversed age-associated decline in bone health by promoting osteoblast differentiation and inhibiting osteoclast differentiation.[29] Taken together, these findings suggest that inhibition of CAMKK2 may be effective for the treatment of a variety of diseases including various types of cancers, metabolic disorders, and bone diseases like osteoporosis. While CAMKK2 has emerged as an attractive therapeutic target, there remains a shortage of high-quality CAMKK2 inhibitors, which has impaired progress in the field.

At present, almost all CAMKK2-related pharmacological studies rely on the use of the ATP-competitive inhibitor STO-609 to study CAMKK2 signaling events (Figure 1).[8,11,17,28−32]

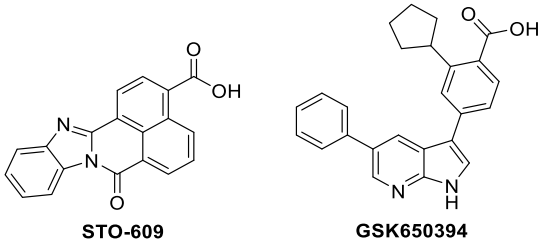

Figure 1. Structures of known CAMKK2 inhibitors: STO-609 and GSK650394.

However, STO-609 is not an ideal chemical tool.[33] It binds to multiple kinases beyond CAMKK2. When screened against a panel of over 400 wild-type human kinases (KINOME*scan*, Eurofins DiscoverX) at 1 μM, STO-609 bound with strong affinity to 14 kinases (<20% activity remaining).[33] Among these kinases were CDKL2, GRK3, and CK2, which are all overexpressed in several cancer types.[34−36] In addition to these collateral kinase targets, STO-609 potently activates the aryl hydrocarbon receptor.[37] STO-609 is a planar molecule with poor aqueous solubility, yet it is routinely used at high doses in cell culture (>10 μM) and *in vivo*.[24] Due to the liabilities of STO-609, the field would benefit from the discovery and development of potent and highly selective small-molecule inhibitors of CAMKK2 as high-quality probes.

We recently conducted an extensive literature search for CAMKK2 inhibitors to identify starting points for medicinal chemistry optimization.[33] A promising series of potent CAMKK2 inhibitors were recently disclosed by GlaxoSmithKline (GSK).[25] The 7-azaindole GSK650394 (also called a pyrrolopyridine) (Figure 1) was a potent CAMKK2 inhibitor (IC_{50} = 0.63 nM). The co-crystal structure of GSK650394 with CAMKK2 (PDB 6BKU) revealed the critical role of the carboxylic acid and cyclopentyl moiety (Figure 2a), which was consistent with the reported structure−activity relationship (SAR) studies.[25] The co-crystal structure reveals that the nitrogen atoms of the pyridine and pyrrole rings act as hydrogen bond acceptor and donor pairs, respectively, and form interactions with the protein backbone of the ATP-binding site. The acid functionality contributes to critical hydrogen bonding interactions with both the protonated amine of Lys194 and the carboxylate group of Glu236 in a water-mediated manner.[38] Additionally, CH−π interactions (aromatic edge−face interactions) between the aromatic ring of gatekeeper Phe267 with both the CH in the 2-position of the 7-azaindole and the methine group in the ortho-position of the 3-aryl moiety of the inhibitor stabilize GSK650394 in this orientation. The pendant phenyl group in the 5-position of the 7-azaindole scaffold occupies a hydrophobic pocket which can potentially be exploited to gain selectivity and potency and modulate physical properties to optimize pharmacokinetic parameters. Although a crystal structure of CAMKK2 co-crystallized with ATP is not available, the cyclopentyl group appears to mimic at least the position of the ribosyl moiety of ATP based on the proximity of the cyclopentyl group to the P-loop of CAMKK2. The 7-azaindole pharmacophore in GSK650394 is commonly found in kinase inhibitors and is considered a powerful but sometimes promiscuous hinge binder.[39−43] When screened against a panel of 334 kinases (Reaction Biology Corporation), GSK650394 inhibited 29

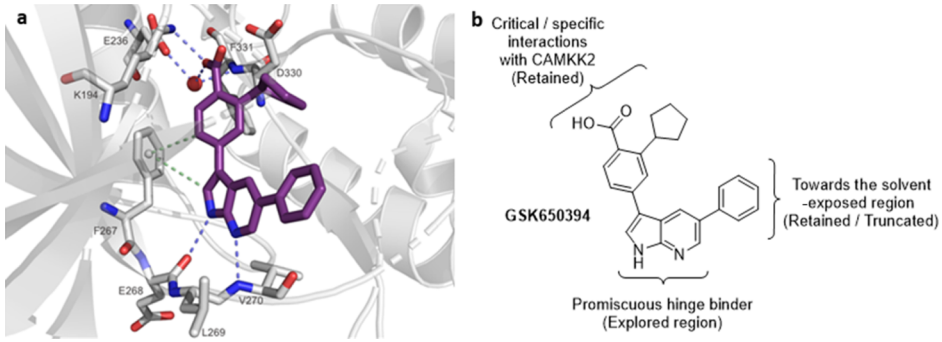

Figure 2. (a) Binding mode of the co-crystallized ligand GSK650394 in the ATP-binding site of CAMKK2 (PDB-ID: 6BKU). The image was generated with PyMOL. The protein is colored in gray. Blue-dashed lines indicate H-bond interactions; green-dashed lines display CH−π interactions. GSK650394 is shown as purple sticks and the water molecule as a red sphere. Oxygen and nitrogen atoms are colored in red and blue, respectively. (b) Structure of GSK650394 highlighting important sites for design of new CAMKK2 inhibitors.

https://doi.org/10.1021/acs.jmedchem.0c02274
J. Med. Chem. 2021, 64, 10849−10877

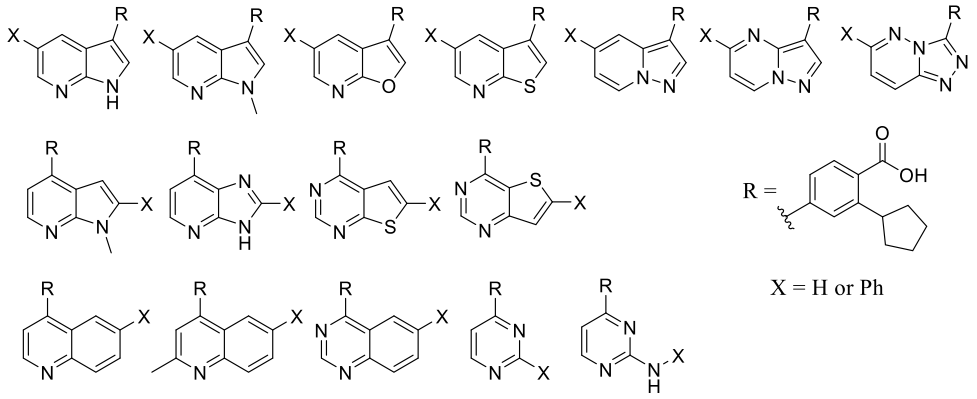

Figure 3. New molecules based on scaffold hopping from GSK650394 designed to interrogate several aspects of hinge binding interactions between CAMKK2 and the proposed inhibitors. Top row: Inhibitors retaining the topology of GSK650394 (5,6-fused ring systems with the cyclopentyl-substituted benzoic acid moiety attached to the 5-membered ring). Middle row: 5,6-fused systems with the cyclopentyl-substituted benzoic acid moiety appended to the 6-membered ring. Bottom row: Inhibitors with ring expansion (6,6-fused ring system) or ring deletion (single 6-membered ring as the hinge-binding core).

Scheme 1. Synthesis of Pinacol Boronate Esters 3 and 4[a]

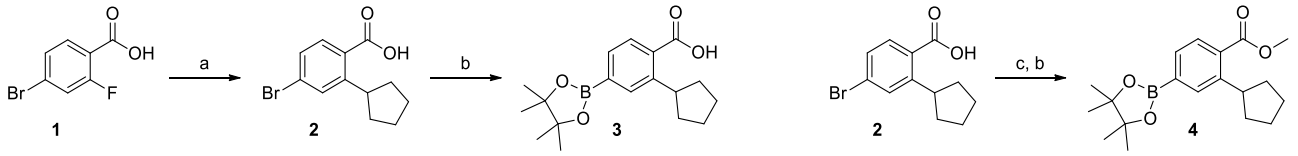

[a]Reagents and conditions: (a) cyclopentylmagnesium bromide, THF, −10 to 25 °C, 5 h, then aq HCl; (b) $PdCl_2(dppf)\cdot CH_2Cl_2$, KOAc, bis(pinacolato)diboron, 100 °C, 2 h; (c) $SOCl_2$, MeOH, 16 h, 75 °C.

kinases by more than 90%, limiting its utility as a tool compound for studying CAMKK2 or any other kinase.[33]

To improve the kinase selectivity of GSK650394, we targeted replacement of the 7-azaindole with other heterocycles that would modulate interactions with the hinge-binding residues and in some cases reduce interactions with the hinge-binding residues. Our compound design strategy is depicted in Figure 2b. Our central hypothesis was based on the belief that the 3-position aryl ring, decorated with the carboxylic acid and cyclopentyl groups, plays a dominant role in CAMKK2 recognition and that inhibitors with enhanced selectivity would arise from compounds with the binding contribution from the hinge binder diminished. This led to the synthesis and evaluation of structurally diverse novel chemotypes as potential inhibitors of CAMKK2 (Figure 3).

Thus, we performed a scaffold-hopping exercise wherein the hinge-binding 7-azaindole core of GSK650394 was substituted with structurally diverse alternate hinge-binding moieties. We retained the *ortho*-cyclopentyl benzoic acid moiety hypothesizing that the interactions observed in the crystal structure would bias the new set toward CAMKK2 affinity.

RESULTS

Chemistry. To develop analogues of GSK650394 that could be potent and selective CAMKK2 inhibitor scaffolds, all our synthesized compounds incorporated the critical pharmacophore, *ortho*-cyclopentyl benzoic acid. In parallel, to investigate the importance of the pendant phenyl ring, we synthesized matched pairs with and without this group. We theorized that removal of the phenyl ring could significantly lower the cLog *P* and increase ligand efficiency (LE) if it was dispensable without being detrimental to potency. To this end, we first synthesized pinacol borate esters **3** and **4** to enable attachment to the various hinge-binding pharmacophores *via* Suzuki coupling reactions (Scheme 1). 4-Bromo-2-fluorobenzoic acid **1** underwent a Grignard reaction with cyclopentylmagnesium bromide to afford the *ortho*-cyclopentyl-substituted benzoic acid **2**, which was then converted into the corresponding pinacol boronate ester using Miyaura borylation conditions yielding **3**.[44] The analogous methyl ester **4** was made in a similar fashion following esterification of **2** in methanol in the presence of thionyl chloride.

3- and 3,5-Substituted Fused 6,5-Ring Systems. Initial analogues were fused 5,6-ring systems with 3- and 3,5-substitution patterns that retained the topology of GSK650394 but modify the nature and/or location of heteroatoms in the ring system and thus can alter the compound's ability to form H-bond interactions with the hinge region. GSK650394 is commercially available, but its matched pair **7**, truncated at the 5-position, required synthesis (Scheme 2). 3-Bromo-7-

Scheme 2. Synthesis of Azaindole 7, the Matched Pair for GSK650394[a]

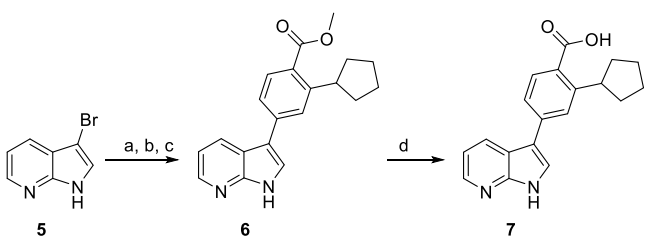

[a]Reagents and conditions: (a) SEM-Cl, NaH, DMF, 0−21 °C, 2 h; (b) **4**, $Pd(OAc)_2$, K_3PO_4, $P(Cy)_3$, $PhMe/H_2O$, 80 °C, 16 h; (c) CF_3COOH, CH_2Cl_2, then NaOAc, EtOH, 21 °C, 24 h; (d) aq NaOH, MeOH, 75 °C, 1 h, then aq HCl.

https://doi.org/10.1021/acs.jmedchem.0c02274
J. Med. Chem. 2021, 64, 10849−10877

Scheme 3. Synthesis of *N*-Methyl Azaindole Hinge Binders 10 and 11[a]

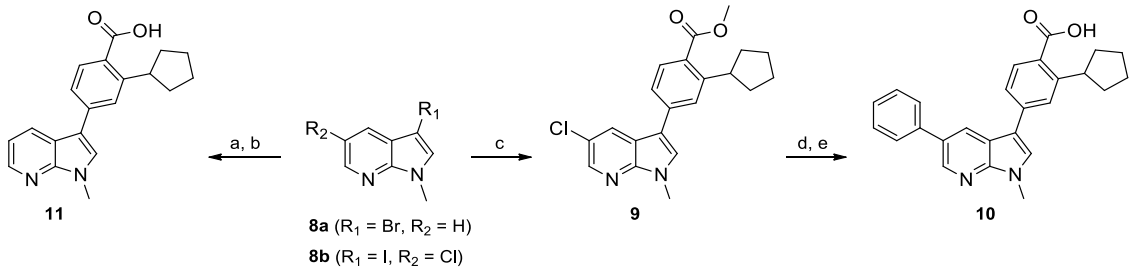

[a]Reagents and conditions: (a) **3**, $Pd_2(dba)_3$, XPhos, Cs_2CO_3, dioxane, H_2O, 120 °C, 16 h; (b) aq LiOH, dioxane, 100 °C, 16 h, then aq HCl; (c) **4**, $PdCl_2(dppf)\cdot CH_2Cl_2$, Cs_2CO_3, dioxane, H_2O, rt, 16 h; (d) $PhB(OH)_2$, $Pd_2(dba)_3$, XPhos, Cs_2CO_3, dioxane, H_2O, 120 °C, 16 h; (e) aq LiOH, dioxane, 100 °C, 16 h, then aq HCl.

Scheme 4. General Route to the Furo- and Thienopyridines[a]

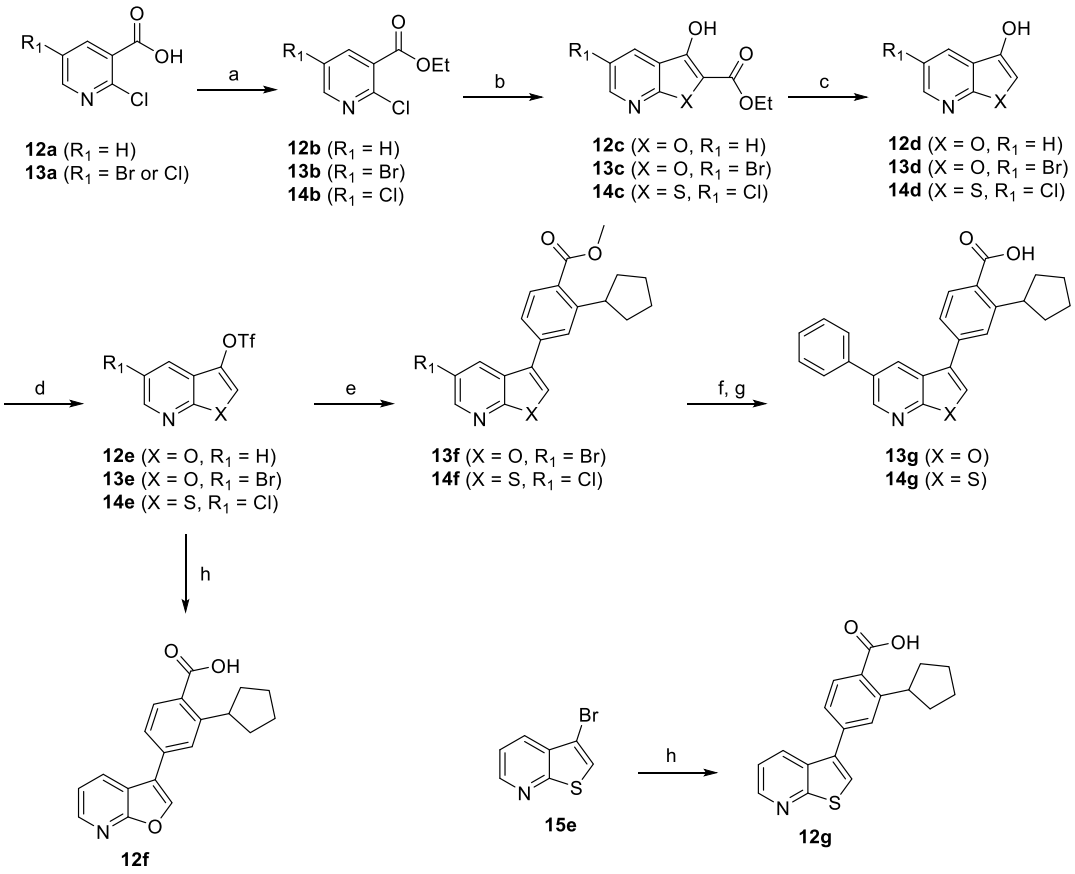

[a]Reagents and conditions: (a) $(EtO)_3CH$, PhMe, 100 °C, 2 h or H_2SO_4, EtOH, reflux, 24 h; (b) ethyl glycolate or ethylthioglycolate, NaH, DME, 0−75 °C, 2.5 h; (c) aq NaOH, EtOH then aq HCl, 100 °C, 2 h; (d) Tf_2O, DIPEA, CH_2Cl_2, −10 to 25 °C, 3 h; (e) **4**, $Pd(PPh_3)_4$, Na_2CO_3, $MeOH/CH_2Cl_2$, 90 °C, 1 h; (f) $PhB(OH)_2$, $Pd(PPh_3)_4$, Na_2CO_3, $MeOH/CH_2Cl_2$, 90 °C, 1 h or $PhB(OH)_2$, $Pd_2(dba)_3$, XPhos, Cs_2CO_3, dioxane/H_2O 90 °C, 16 h; (g) aq NaOH, MeOH then aq HCl, 1 h; (h) **3**, $Pd(PPh_3)_4$, Na_2CO_3, $MeOH/CH_2Cl_2$, 90 °C, 1 h.

azaindole **5** was converted to the silylethoxymethyl (SEM)-protected azaindole and then subjected to Suzuki−Miyaura conditions to afford cyclopentyl analogue **6**. SEM deprotection, followed by base-mediated saponification, afforded the target azaindole **7**.

The *N*-methyl analogues of GSK650394 and **7** were synthesized as depicted in Scheme 3. To access **10**, 5-chloro-3-iodo azaindole **8b** was *N*-alkylated.[45] Consecutive Suzuki reactions with the *ortho*-cyclopentyl methyl benzoate **4** and then phenyl boronic acid placed the key pharmacophore in the 3-position and a phenyl ring in the 5-position. Saponification of the methyl ester proceeded smoothly affording azaindole **10**. Coupling of boronate ester **4** with 3-bromo-*N*-methyl azaindole, followed by saponification of the methyl ester, afforded target molecule **11**.

The synthesis of the structurally similar furopyridine and thienopyridine cores is described in Scheme 4. Nicotinic acid derivatives **12a** and **13a** were converted into ethyl esters **12**−**14b** and then treated with ethyl glycolate or ethyl thioglycolate in the presence of sodium hydride (NaH) to give the respective furopyridines or thienopyridines **12**−**14c**.[46] A one-pot saponification−decarboxylation of the *β*-keto esters

https://doi.org/10.1021/acs.jmedchem.0c02274
J. Med. Chem. 2021, 64, 10849−10877

Scheme 5. Synthesis of Pyrazolopyridine and Pyrazolopyrimidine Analogues[a]

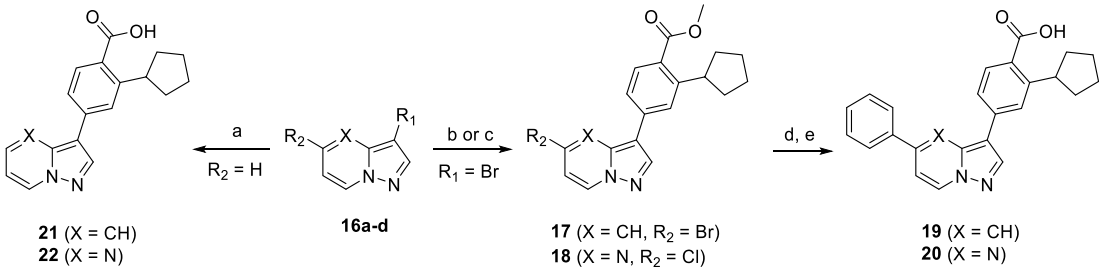

[a]Reagents and conditions: (a) **3**, $Pd_2(dba)_3$, XPhos, Cs_2CO_3, dioxane, H_2O, 120 °C, 16 h; **17** *via* (b) **4**, $Pd_2(dba)_3$, XPhos, Cs_2CO_3, dioxane, H_2O, 120 °C, 16 h; **18** *via* (c) $PdCl_2(dppf)\cdot CH_2Cl_2$, Cs_2CO_3, dioxane, H_2O, 80 °C, 16 h; (d) $PhB(OH)_2$, $Pd(PPh_3)_4$, Cs_2CO_3, dioxane, H_2O, 120 °C, 30 min, μW; (e) aq LiOH, dioxane, 100 °C, 16 h then aq HCl.

Scheme 6. Synthesis of the Triazolopyridazine Analogues 25 and 26[a]

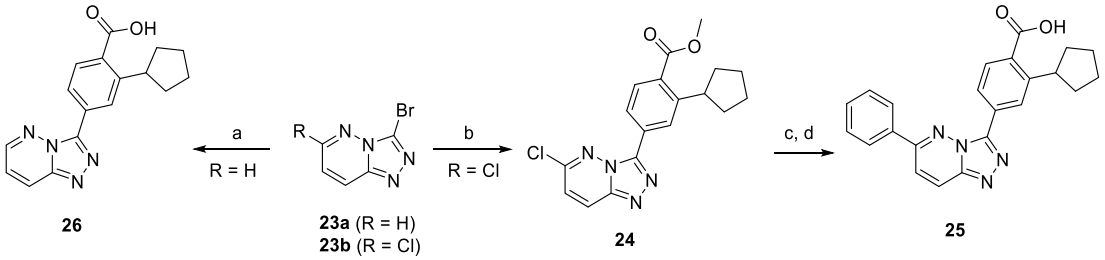

[a]Reagents and conditions: (a) **3**, $Pd_2(dba)_3$, XPhos, Cs_2CO_3, dioxane/H_2O, 90 °C, 16 h; (b) **4**, $Pd(PPh_3)_4$, K_2CO_3, dioxane/H_2O, 90 °C, 16 h; (c) $Pd_2(dba)_3$, XPhos, Cs_2CO_3, dioxane/H_2O, 90 °C, 16 h; (d) aq NaOH, MeOH 75 °C, 1 h, then aq HCl.

Scheme 7. Synthesis of 2,4-Substituted *N*-Methyl Azaindoles[a]

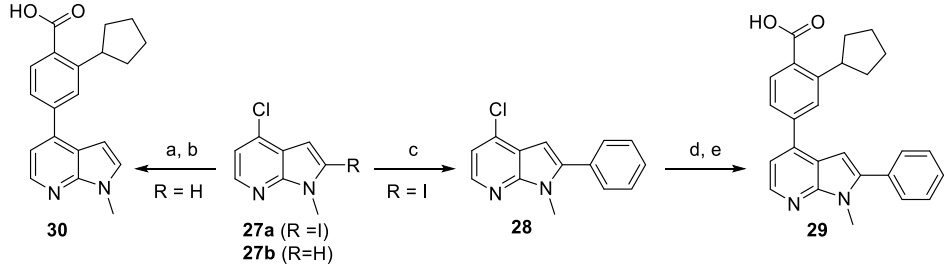

[a]Reagents and conditions: (a) **4**, $Pd(PPh_3)_4$, Cs_2CO_3, dioxane/H_2O, 120 °C, 30 min; (b) aq LiOH, dioxane, 100 °C, 16 h, then aq HCl; (c) $PhB(OH)_2$, $Pd(PPh_3)_4$, Cs_2CO_3, dioxane/H_2O, 120 °C, 30 min; (d) **4**, $Pd(PPh_3)_4$, Cs_2CO_3, dioxane/H_2O, 120 °C, 30 min; (e) aq LiOH, dioxane, 100 °C, 16 h, then aq HCl.

Scheme 8. Synthesis of the Imidazopyridine Hinge Binders[a]

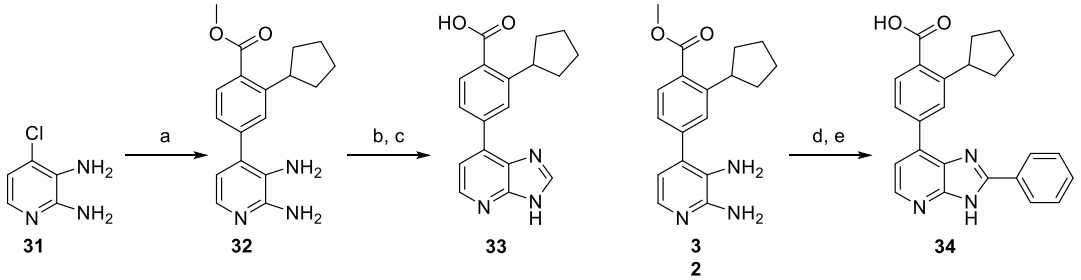

[a]Reagents and conditions: (a) **4**, $Pd_2(dba)_3$, XPhos, Cs_2CO_3, dioxane, H_2O, 100 °C, 16 h; (b) $CH(OMe)_3$, H_3NSO_3, MeOH, rt, 1 h; (c) aq LiOH, dioxane, 100 °C, 16 h, then aq HCl; (d) benzoic acid, CDI, DMF, 0 °C, 30 min, then **32**, 200 °C, 10 min; (e) aq LiOH, dioxane, 100 °C, 16 h, then aq HCl.

afforded the 2-unsubstituted heterocycles **12**−**14d**. These aryl alcohols were converted to the corresponding triflates **12**−**14d**, which were able to undergo Suzuki−Miyaura reactions to yield analogues **12f**, **13g**, and **14g**.[47] **12g** was obtained directly from the commercially available 3-bromothieno[2,3-*b*]pyridine **15e** using Suzuki−Miyaura reaction.

The subsequent set of fused 5,6-ring derivatives synthesized in Scheme 5 (pyrazolopyridines and pyrazolopyrimidines)

https://doi.org/10.1021/acs.jmedchem.0c02274
J. Med. Chem. 2021, 64, 10849−10877

Scheme 9. Synthesis of Thieno[3,2-*d*]pyrimidine and Thieno[2,3-*d*]pyrimidine Hinge Binders[a]

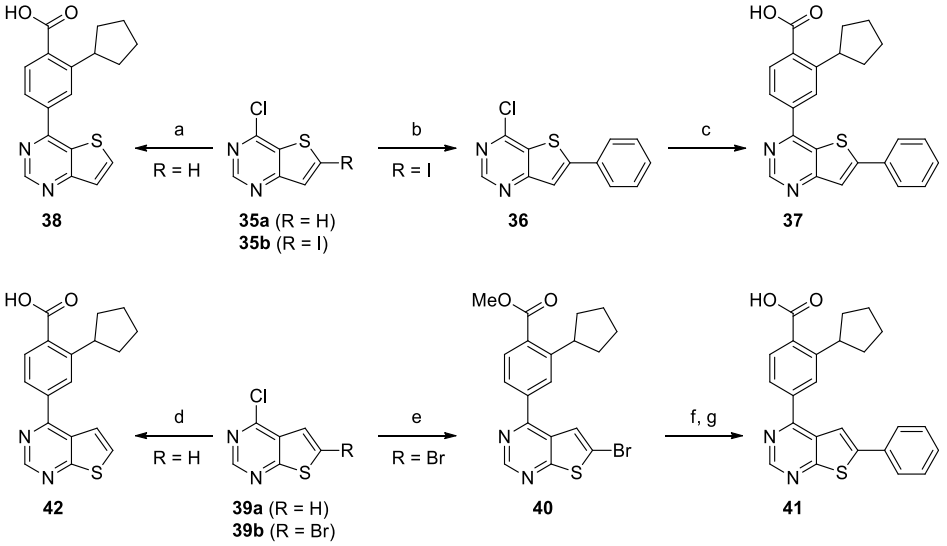

[a]Reagents and conditions: (a) **3**, $Pd(PPh_3)_4$, Cs_2CO_3, dioxane/water, 125 °C, μW, 15 min; (b) $PhB(OH)_2$, $NaHCO_3$, CsF, $Pd(PPh_3)_4$, dioxane/H_2O, 95 °C, 3 h; (c) **3**, $Pd(PPh_3)_4$, Cs_2CO_3, dioxane/water, 125 °C, 15 min; (d) **3**, $Pd(PPh_3)_4$, Cs_2CO_3, dioxane/water, 125 °C, μW, 15 min; (e) **4**, $Pd(PPh_3)_4$, Cs_2CO_3, dioxane/water, 145 °C, μW, 15 min; (f) $PhB(OH)_2$, $NaHCO_3$, CsF, $Pd(PPh_3)_4$, dioxane/H_2O, 80 °C, 4 h; (g) aq LiOH, dioxane, 100 °C, 16 h, then aq HCl.

Scheme 10. Synthesis of Quinoline and Quinazoline Hinge Binders[a]

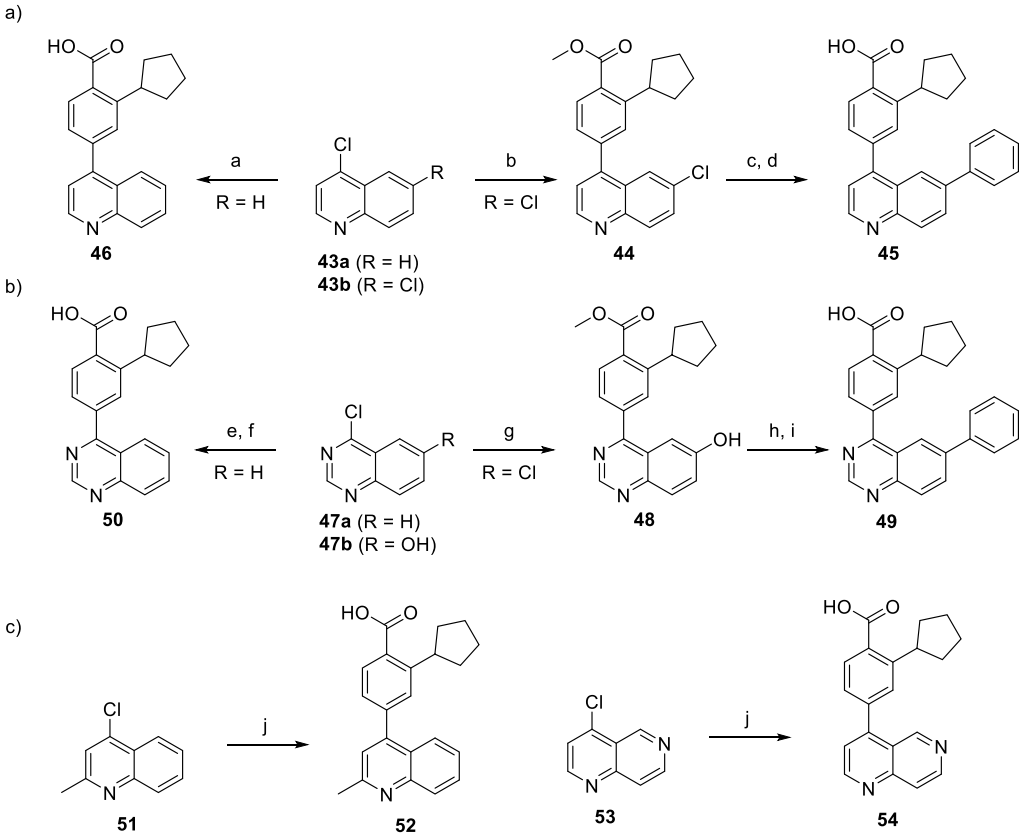

[a]Reagents and conditions: (a) **3**, $Pd_2(dba)_3$, XPhos, Cs_2CO_3, dioxane/H_2O, 90 °C, 16 h; (b) **4**, $Pd_2(dba)_3$, XPhos, Cs_2CO_3, rt, 16 h; (c) $PhB(OH)_2$, $Pd_2(dba)_3$, XPhos, Cs_2CO_3, 120 °C, 16 h; (d) aq LiOH, dioxane, 100 °C, 16 h, then aq HCl; (e) **4**, $Pd(PPh_3)_4$, K_2CO_3, dioxane/H_2O, 120 °C, 16 h; (f) aq LiOH, dioxane, 100 °C, 16 h, then aq HCl; (g) **4**, $Pd(PPh_3)_4$, K_2CO_3, dioxane/H_2O, 90 °C, 16 h; (h) (i) DIPEA, Tf_2O, CH_2Cl_2, 0–21 °C, 2 h, (ii) $PhB(OH)_2$, $Pd(PPh_3)_4$, K_2CO_3, CH_2Cl_2/MeOH, 90 °C, 1 h; (i) aq NaOH, MeOH, 75 °C, 1 h, then aq HCl; (j) **4**, $Pd_2(dba)_3$, XPhos, Cs_2CO_3, dioxane/H2O, 90 °C, 16 h.

https://doi.org/10.1021/acs.jmedchem.0c02274
J. Med. Chem. 2021, 64, 10849−10877

Scheme 11. Synthesis of Pyrimidine and Aminopyrimidine Hinge Binders[a]

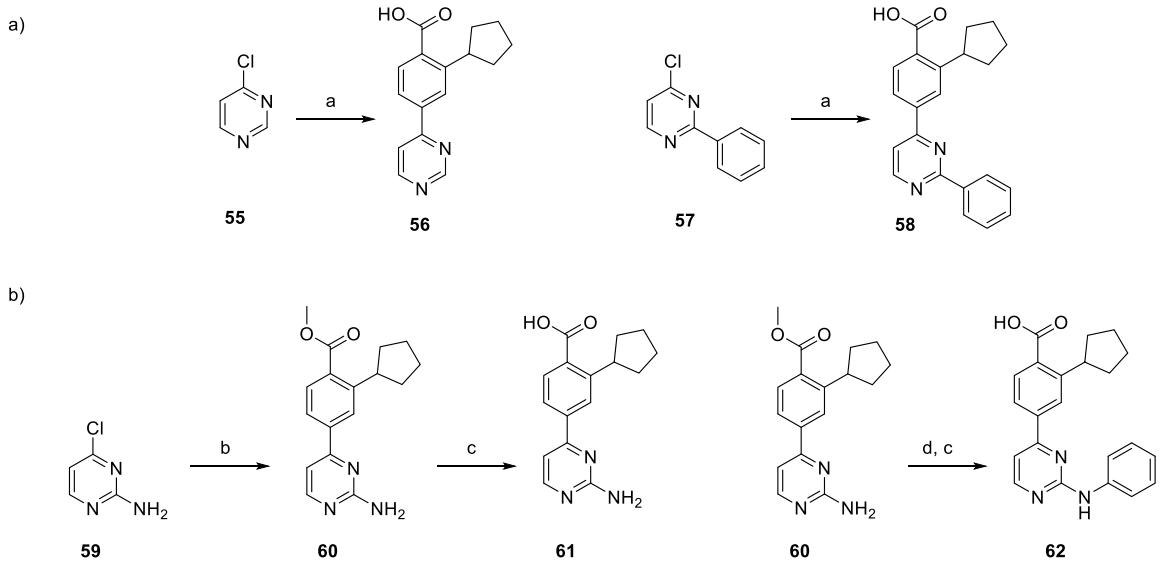

[a]Reagents and conditions: (a) **3**, $Pd(PPh_3)_4$, Cs_2CO_3, 1,2-DME, H_2O, 120 °C, 0.5 h. (b) **4**, $Pd(PPh_3)_4$, Cs_2CO_3, 1,2-DME, H_2O, 120 °C, 0.5 h; (c) aq LiOH, dioxane, 100 °C, 16 h, then aq HCl; (d) PhBr, $Pd_2(dba)_3$, XantPhos, NaO^{t}Bu, PhMe, 80 °C, 19 h.

dramatically altered the placement of the heteroatoms based on the parent compound. Analogues **19** and **20** were obtained by stepwise Suzuki couplings, first with **4** and then with phenylboronic acid, followed by methyl ester hydrolysis. The monosubstituted complementary matched pairs were synthesized from commercially available 3-bromopyrazolo[1,5-*a*]-pyridine or -pyrimidine *via* Suzuki couplings with **4** to afford **21** and **22**. The same set of reaction conditions was used to afford the triazolopyridazine analogues **25** and **26** (Scheme 6).

2- and 2,4-Substituted Fused 5,6-Ring Systems. The first scaffolds in this category were *N*-methyl azaindoles and are described in Scheme 7. The disubstituted azaindole **29** was obtained from coupling phenylboronic acid at the more reactive 2-position of 2-iodo-4-chloro-*N*-methyl azaindole, followed by coupling with intermediate **4** at the 4-position. Saponification of the methyl ester afforded acid **29**. The monosubstituted compound **30** was synthesized from commercially available 4-chloro-*N*-methyl-7-azaindole with a Suzuki coupling reaction, followed by saponification of the methyl ester.

Imidazopyridine analogues were obtained from initial coupling of 2,3-diamino-4-chloropyridine with **4** to afford the aryl-substituted pyridine **32** (Scheme 8). Imidazopyridine **33** was synthesized by condensation of diamine **32** with trimethyl orthoformate in methanol, followed by saponification of the ester to afford the desired carboxylic acid. The 2-aryl analogue **34** was obtained by converting benzoic acid into an activated ester with 1,1′-carbonyldiimidazole (CDI) and addition of diamine **32** to form a putative amide intermediate that underwent a ring closure under thermal conditions resulting in the imidazopyridine intermediate. Ester hydrolysis yielded the desired imidazopyridine **34**.

Mono- and disubstituted thienopyrimidine analogues of the [3,2-*d*] and [2,3-*d*] core scaffolds were synthesized from commercially available starting materials (Scheme 9). The monosubstituted analogues **38** and **42** were easily accessed in one step *via* Suzuki coupling using commercially available **35a** and **39a**, respectively. **37** was synthesized by first coupling **35b** with phenylboronic acid to afford 2-aryl-substituted intermediate **36**, which was then coupled with **3** to yield the disubstituted thieno[3,2-*d*]pyrimidine. The reaction sequence was reversed in the synthesis of the disubstituted thieno[2,3-*d*]pyrimidine **41** since the chlorine substituent in **39b** was found to be more reactive than the thiophene bromine. Intermediate **4** was coupled to the 4-position of **39b** affording **40**. Subsequent Suzuki coupling with phenylboronic acid, followed by saponification of the ester, yielded disubstituted analogue **41**.

Synthesis of Substituted Fused 6,6-Ring Hinge Binders. This set of hinge binders moves from 5,6-fused ring systems to 6,6-fused systems. The disubstituted quinoline analogue **45** was synthesized in a straightforward manner from commercially available 4,6-dichloroquinoline **43b** *via* sequential Suzuki couplings with **4** and phenylboronic acid, followed by saponification of the methyl ester. The monosubstituted quinoline **46** was synthesized in one step *via* Suzuki coupling between the commercially available **43a** and **3**.

The quinazoline hinge binder derivatives were obtained via similar routes utilized in the synthesis of the quinolines (Scheme 10) with the exception of compound **49**. The disubstituted quinazoline **49** was prepared from 4-chloroquinazolin-6-ol **47b** with initial installation of boronate **4** and subsequent conversion of the hydroxy group of **48** into a triflate which readily underwent Suzuki coupling with phenylboronic acid. Saponification then afforded the target compound. 4-Aryl-2-methylquinoline **52** and 1,6-naphthyridine **54** analogues were synthesized in one step *via* Suzuki coupling with **3** (Scheme 10c).

Synthesis of Pyrimidine Hinge Binders. The final set of hinge binders we explored consisted of substituted pyrimidines. The monosubstituted pyrimidine **56** was obtained *via* Suzuki coupling of **55** with **3** (Scheme 11a). 2-Phenyl-4-aryl pyrimidine **58** was synthesized from 2-phenyl-4-chloropyrimidine **57** by Suzuki coupling with **3**. The synthesis of aminopyrimidines **61** and **62** is described in Scheme 11b. Starting from commercially available 4-chloropyrimidin-2-amine **59**, Suzuki coupling with **4** afforded **60**. Saponification of the resulting methyl ester afforded **61**. **60** was utilized in a

https://doi.org/10.1021/acs.jmedchem.0c02274
J. Med. Chem. 2021, 64, 10849−10877

Table 1. CAMKK2 Enzyme Inhibition Data for Compounds with 3- and 3,5-Substituted Fused 5,6-Ring Systems[a]

ID	Hinge Binder	Hinge Binder	X	CAMKK2 PoC			IC_{50} [nM]
				1 μM	0.1 μM	0.01 μM	
GSK 650394	Azaindole	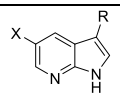	Ph	3	4	14	3
7			H	0	6	83	26
10	*N*-methyl azaindole	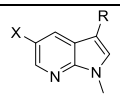	Ph	101	102	103	NG
11			H	95	100	103	NG
13g	Furopyridine	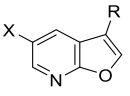	Ph	7	46	71	65
12f			H	28	71	97	NG
14g	Thienopyridine	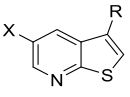	Ph	3	14	30	5
12g			H	19	75	101	NG
19	Pyrazolopyridine	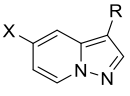	Ph	9	60	85	145
21			H	5	37	81	44
20	Pyrazolopyrimidine	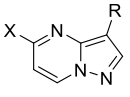	Ph	4	18	71	21
22			H	16	65	100	NG
25	Triazolopyridazine	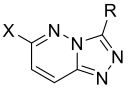	Ph	58	72	91	NG
26			H	83	94	95	NG

[a]R = *ortho*-cyclopentyl benzoic acid moiety; PoC (percent of control = percent of enzyme activity remaining, when compared with the control); IC_{50} (half-maximal inhibitory concentration); NG (not generated); IC_{50} values were generated in an 8-point full dose response assay.

Buchwald−Hartwig coupling with bromobenzene, and subsequent ester hydrolysis yielded 2-phenylaminopyrimidine **62**.

Assays Used for *In Vitro* Compound Affinity Evaluation. *DSF Assay.* We used a thermal-shift assay (differential scanning fluorimetry, DSF) to detect protein−ligand interactions.[48] For many proteins, including kinases, this is a useful high-throughput method to identify compounds that bind to a protein of interest, and in many cases, the melting temperature correlates with binding affinity. CAMKK1 and CAMKK2 are ∼60% identical at the amino acid sequence level.[49] We measured DSF ΔT_m for all analogues against both CAMKK2 and CAMKK1 using the purified kinase domains of these two proteins. As in the end we did not utilize the DSF data to drive the project, all DSF data are reported in the Supporting Information.

In Vitro CAMKK1 and CAMKK2 Enzyme Inhibition Assays. We used purified recombinant CAMKK1 and CAMKK2 in an assay that measured the transfer of radiolabeled phosphate from [γ-^{32}P]-ATP to a synthetic CAMKK2 substrate (CAMKKtide). Initially, we evaluated CAMKK2 inhibitory activity of all synthesized compounds at three different concentrations (10, 100, and 1000 nM) to rank compounds and provide preliminary dose response information. In the percent of control (PoC) experiments, the assay with no inhibitor present serves as the control. Half-maximal inhibitory concentrations (IC_{50}) were then determined for analogues with PoC values <10 at the 1 μM screening concentration. For a subset of CAMKK2 inhibitors, we also determined half-maximal inhibitory concentration (IC_{50}) values. STO-609 and GSK650394 were routinely used as reference compounds in the assay to ensure that the assay performed correctly and CAMKK2 inhibition was observed.

***In Vitro* Compound Screening Results.** The initial set of compounds evaluated was focused on those with similar topology to GSK650394. Data in Table 1 depict compounds, the enzyme CAMKK2 inhibition data (PoC) at three concentrations, and CAMKK2 enzyme inhibition IC_{50} data for selected compounds. Although we collected thermal shift (DSF) data for our inhibitors with both CAMKK1 and CAMKK2, we found that they did not provide enough information to drive chemistry decisions and did not always correlate with the enzymatic activity. The DSF data are provided in the Supporting Information for reference. We thus relied on the CAMKK2 enzyme inhibition data as our primary assay.

Removal of the phenyl group from the 5-position of GSK650394 led to a roughly 3-fold decrease in enzyme inhibitory activity (IC_{50} = 26 vs 3 nM), implying that the phenyl group or an appropriately adorned phenyl group may be useful to enhance CAMKK2 enzyme affinity and/or activity. Similar pairs of analogues for the different hinge binders allowed for direct comparison (Table 1).

The goal of this project was to discover alternate scaffolds for CAMKK2 with sufficient potency and suitable kinome selectivity that can be used as starting points for medicinal chemistry optimization programs. We hypothesized that carefully modulating the hydrogen bonding interactions at the hinge-binding region *via* a variety of heterocyclic scaffolds could identify a new series that maintained CAMKK2 affinity and improved selectivity profiles. Kinase inhibitors with

https://doi.org/10.1021/acs.jmedchem.0c02274
J. Med. Chem. 2021, 64, 10849−10877

Table 2. CAMKK2 Enzyme Inhibition Data for Compounds with 2- and 2,4-Substituted Fused 6,5-Ring Systems[a]

ID	Hinge Binder	Hinge Binder	X	CAMKK2 PoC			IC_{50} [nM]
				1 μM	0.1 μM	0.01 μM	
29	*N*-methyl azaindole	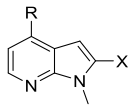	Ph	6	64	84	120
30			H	5	30	97	56
34	Imidazopyridine	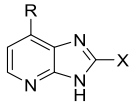	Ph	0	8	78	23
33			H	11	66	97	193
37	Thienopyrimidine	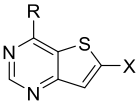	Ph	0	68	101	169
38			H	0	17	73	24
41	Thienopyrimidine	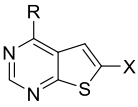	Ph	12	75	91	232
42			H	2	24	77	31

[a]R = *ortho*-cyclopentyl benzoic acid moiety; PoC (percent of control = percent of enzyme activity remaining, when compared with control); IC_{50} (half-maximal inhibitory concentration); IC_{50} values were generated in an 8-point full dose response assay.

multiple hinge-binding interactions can suffer from off-target effects owing to their potential for poor selectivity across the kinome.[39,41,50] However, careful modification of even promiscuous starting points can in some cases lead to desired levels of selectivity. There are examples demonstrating that modifications to the hydrogen bonding interactions between a kinase inhibitor and the hinge region of the kinase can improve selectivity without severely impacting potency.[41] *N*-Methyl azaindoles **10** and **11** (Table 1) offer a particularly drastic change in hinge binding by blocking the H-bonding donor property of the pyrrole ring. This resulted in a complete loss in enzyme inhibition potency *in vitro*. This suggested that the steric bulk of the *N*-methyl group is not accommodated within the binding pocket of CAMKK2 when the cyclopentyl benzoic acid moiety is attached at the 3-position of the azaindole scaffold.

Further structural modifications to the hinge-binding moiety that maintained the fused 5,6-ring system are outlined here. Compounds **13g** and **12f** replaced the pyrrole ring with a furan ring. Compounds **14g** and **12g** replaced the pyrrole ring of GSK650394 with a thiophene ring. The pyridine nitrogen that makes a key hydrogen bond with the hinge is maintained, but the NH hydrogen bonding opportunity has been removed. Compounds **19**, **20**, **21**, **22**, **25**, and **26** all maintain the 5,6-fused core but have key differences from GSK650394. They do not have a nitrogen in a position analogous to the nitrogen in the 7-position of GSK650394, thus necessitating different hinge-binding interactions. They also incorporate nitrogen atoms in other locations within the 5,6-ring system.

Nearly all the phenyl-substituted analogues of active CAMKK2 inhibitor scaffolds showed greater enzyme potency than their corresponding truncated analogues. An exception was compound **19** (phenyl version), which had an IC_{50} = 145 nM compared to an IC_{50} = 44 nM for compound **21** (truncated version). Replacement of the pyrrole ring in the azaindole with either a furan or thiophene ring retained potency in the phenyl-substituted analogues (**13g** IC_{50} = 65 nM, **14g** IC_{50} = 5 nM), but their corresponding truncated analogues (**12f**, **12g**) were relatively inactive. We would like to point out that an analogue of compound **13g** is listed as a CAMKK2 chemical probe (https://www.thesgc.org/chemical-probes/SGC-CAMKK2-1) with the name SGC-CAMKK2-1. The kinome-wide selectivity profiles and cellular potencies of these two close analogues are comparable (*vide infra* and the SGC probe link above). In addition, SGC-CAMKK2-1 is currently commercially available from Sigma-Aldrich. The results depicted in Table 1 demonstrate that the choice of a hinge binder plays a role in the type of substitutions that are tolerated. Both versions of the triazolopyridazine hinge binder (**25**, **26**) showed no activity. We hypothesize that this is due to repulsion between the lone pair on the nitrogen in the 2-position and a backbone protein carbonyl (carbonyl from E268 in CAMKK2). In many kinase/inhibitor co-crystal structures, this carbonyl is engaged in hydrogen bonding with a NH from the inhibitor or at least pointing toward a polarized CH on the inhibitor. In summary, four scaffolds (furopyridine **13g**, thienopyridine **14g**, pyrazolopyridine **19** and **21**, and pyrazolopyrimidine **20**) in this set exhibited robust CAMKK2 enzyme inhibition (IC_{50} values < 150 nM), with **14g** (IC_{50} = 5 nM) exhibiting comparable enzymatic inhibitory activity to GSK650394 (IC_{50} = 3 nM).

To further evaluate fused 5,6-ring structures as CAMKK2 inhibitors, we switched from 3,5- to 2,4-ring substitutions as depicted in Table 2. *N*-methyl azaindoles **29** and **30** were the first pair of analogues synthesized. Interestingly, these two *N*-methyl-substituted azaindole analogues were well tolerated, displaying good CAMKK2 enzyme inhibitory activity (**29** IC_{50} = 120 nM, **30** IC_{50} = 56 nM). This result is in stark contrast to 3,5-*N*-methyl azaindoles **10** and **11** in Table 1. The truncated analogue **30** was significantly more potent than its corresponding phenyl analogue **29**.

The 2,4-substituted analogues of Table 2 are all inhibitors of CAMKK2. Incorporation of an extra nitrogen into the pyrrole ring to create imidazopyridine analogues **33** and **34** was well tolerated, with the phenyl-substituted analogue demonstrating higher potency (**34** IC_{50} = 23 nM) than the corresponding non-phenyl version (**33** IC_{50} = 193 nM). Similar to *N*-methyl azaindole **30**, non-phenyl-substituted thienopyrimidines (**38**

https://doi.org/10.1021/acs.jmedchem.0c02274
J. Med. Chem. 2021, 64, 10849−10877

Table 3. CAMKK2 Enzyme Inhibition Data for Compounds with Fused 6,6-Ring Systems[a]

Entry	Hinge Binder	Hinge Binder	X	CAMKK2 PoC			IC_{50} [nM]
				1 μM	0.1 μM	0.01 μM	
45	Quinoline	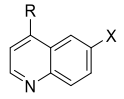	Ph	8	62	92	137
46			H	3	5	51	13
49	Quinazoline	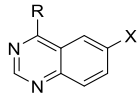	Ph	5	28	48	12
50			H	10	51	96	96
52	2-Methylquinoline	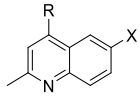	H	97	93	98	NG
54	1,6-Naphthyridine	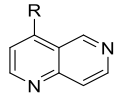	-	86	91	102	NG

[a]R = *ortho*-cyclopentyl benzoic acid moiety; PoC (percent of control = percent of enzyme activity remaining, when compared with the control); IC_{50} (half-maximal inhibitory concentration); NG (not generated); IC_{50} values were generated in an 8-point full dose response assay.

Table 4. CAMKK2 Enzyme Inhibition Data for Substituted Pyrimidines and 4-Aminopyrimidines[a]

ID	Hinge Binder	Hinge Binder	X	CAMKK2 PoC			IC_{50} [nM]
				1 μM	0.1 μM	0.01 μM	
56	Pyrimidine		Ph	0	10	73	21
58			H	26	84	98	NG
62	Aminopyrimidine	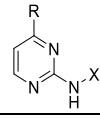	Ph	0	21	97	51
61			H	8	53	95	108

[a]R = *ortho*-cyclopentyl benzoic acid moiety; PoC (percent of control = percent of enzyme activity remaining, when compared with the control); IC_{50} (half-maximal inhibitory concentration); NG (not generated); IC_{50} values were generated in an 8-point full dose response assay.

IC_{50} = 24 nM, **42** IC_{50} = 31 nM) were more potent than their corresponding phenyl-substituted analogues (**37** IC_{50} = 169 nM, **41** IC_{50} = 232 nM). Both [3,2-*d*] analogues **37** and **38** (with the sulfur oriented away from the hinge-binding region) and [2,3-*d*] analogues **41** and **42** (with the sulfur oriented toward the hinge) inhibit CAMKK2. For both these isomeric thienopyrimidines, removal of the pendant phenyl actually increases CAMKK2 potency (**37** with phenyl IC_{50} = 169 nM **38** without phenyl IC_{50} = 24 nM; **41** with phenyl IC_{50} = 232 nM **42** without phenyl IC_{50} = 31 nM).

Next, we explored replacement of the 5,6-bicyclic cores with 6,6-bicyclic structures. Quinazolines and quinolines are frequently used as kinase hinge-binding heterocycles and were identified as active scaffolds for CAMKK2 inhibition (Table 3). Both quinoline **45**, with a phenyl in the 6-position, and **46**, unsubstituted in the 6-position, inhibited CAMKK2 (**45** IC_{50} = 137 nM, IC_{50} **46** = 13 nM). The potency of the low-molecular-weight compound **46** suggests that further exploration may be fruitful. Similarly, the two quinazolines **49** (IC_{50} = 12 nM) and **50** (IC_{50} = 96 nM) were also potent CAMKK2 inhibitors.

As expected, introduction of a methyl group at the 2-position of **52** resulted in a complete loss of CAMKK2 enzyme activity. The steric bulk of the 2′ methyl group is not tolerated and likely hinders the ability of the quinoline nitrogen to effectively participate in hydrogen bonding with the hinge region. Naphthyridine **54** showed poor CAMKK2 enzymatic activity.

Finally, we evaluated a small set of pyrimidines, well-known kinase ATP-competitive inhibitor scaffolds, for their CAMKK2 inhibitory activity (Table 4). Pyrimidine **56**, with a phenyl in the 2-position, had a CAMKK2 IC_{50} = 21 nM. 2-Anilino-pyrimidine **62** was also potent with CAMKK2 IC_{50} = 51 nM. Pyrimidine **58**, unsubstituted in the 2-position, lost considerable activity relative to **56**. 2-Amino-pyrimidine **61** retained CAMKK2 potency (IC_{50} = 108 nM).

X-ray Crystallography and *In Silico* Docking Studies. In order to more fully understand the binding modes and to plan optimization studies on these scaffolds, we turned to X-ray crystallography and in silico docking analysis of key molecules. We previously reported the crystal structure of 7-azaindole GSK650394 bound to CAMKK2 (PDB ID 6BKU).[51] A crystal structure of the closely related 7-azaindole GSK650393 is also available (PDB ID 6CMJ).[25] These two structures clearly demonstrate a hydrogen bond interaction between the NH of the pyrrole in the 7-azaindole to the

https://doi.org/10.1021/acs.jmedchem.0c02274
J. Med. Chem. 2021, 64, 10849−10877

Table 5. Crystallization Conditions and Data Collection Statistics

ligand	13g	UNC10244803
data collection		
X-ray source	APS 24-ID-C	DLS I03
wavelength (Å)	0.9791	0.9763
space group	$P4_32_12$	$P4_32_12$
cell dimensions		
a, *b*, *c* (Å)	73.3, 73.3, 122.0	73.2, 73.2, 120.3
α, *β*, *γ* (deg)	90.0, 90.0, 90.0	90.0, 90.0, 90.0
resolution (Å)	19.74−1.70 (1.73−1.70)	19.61−1.60 (1.63−1.60)
no. of unique reflections	37,374 (1,767)	43,864 (3,161)
R_{merge} (%)	14.7 (183.7)	12.2 (31.5)
mean $I/\sigma I$	14.2 (2.0)	21.3 (10.9)
mean CC(1/2)	1.0 (0.75)	1.0 (0.99)
completeness (%)	99.9 (100)	99.9 (100)
redundancy	21.7 (22.1)	25.8 (25.0)
refinement		
resolution (Å)	19.75−1.70 (1.75−1.70)	19.61−1.60 (1.64−1.60)
R_{cryst}/R_{free} (%)	16.0/18.2	15.3/17.1
no. of non-hydrogen atoms/mean B-factor (Å)		
protein atoms	2230/28.1	2229/21.3
solvent atoms	370/44.3	338/33.6
ligand atoms	29/19.8	26/12.5
rmsd bond lengths (Å)	0.010	0.01
rmsd bond angles (deg)	1.05	1.04
Ramachandran statistics (%)		
favored	98.2	98.2
allowed	1.8	1.8
PDB ID	5UY6	5UYJ
crystallization conditions	25% PEG 3350, 0.2 M ammonium sulfate, 0.1 M bis−tris buffer, pH 6.5	20% PEG 3350, 0.02 M ammonium sulfate, 0.1 M CHC buffer system, pH 8.5

carbonyl group of Glu268 at the CAMKK2 hinge region. The nitrogen atom at the 7-position forms an interaction with the hinge *via* the hydrogen bond with the NH of Val270. We were able to obtain a crystal structure of furopyridine **13g** (PDB ID 5UY6). Data collection statistics and crystallization conditions are shown in Table 5.

Furopyridine **13g** displays a similar binding mode to GSK650394. The 5,6-fused ring systems are oriented in the same way in the CAMKK2 active site, and the pyridine moieties of the two heterocycles form comparable hydrogen bond interactions with the NH group of Val270, and the furan oxygen atom and pyrrole NH group are in the same region of space. Although we have no crystal structure of thienopyridine **14g**, we hypothesize that it would likely bind in a similar fashion.

To assess the binding modes of **14g** and other compounds, we performed in silico docking studies with the docking software Glide version 2014 (Schrödinger).[52] For our docking studies, we utilized three of the X-ray crystal structures of CAMKK2 (PDB-ID: 6BKU, 5UY6, and 5UYJ). We based our choice of the CAMKK2 PDB protein structure to use for our modeling on the structural similarity between the co-crystallized ligand and the compound we planned to use in the in silico docking. In order to ensure reliability of the docking protocol and the ensuing results for hypothesis generation, the co-crystallized ligands GSK650394, **13g**, and UNC10244803 [2-cyclopentyl-4-(7-methoxyquinolin-4-yl)-benzoic acid, CAMKK2 enzyme IC_{50} = 33 nM] were removed from the binding site and the ligands were re-docked into the binding pocket. The docking poses were then compared with the original pose from the crystal structures. The root-mean-square deviation (rmsd) value was lower than 1 Å, indicating a reliable docking procedure. The predicted binding modes of active compounds (Figure 3) show conserved H-bonds or close proximity between the compound's carboxylate group and both the protonated amine of Lys194 and the carboxylate group of Glu236 in a water-mediated manner, analogous to what was observed in the crystal structures. The overall orientation of the tested compounds and their interactions with the hinge region is also of interest.

As expected, the predicted binding mode of thienopyridine **14g** overlaid almost perfectly with the pose of furopyridine **13g** in the X-ray structure (Figure 4a). The backbone NH group of Val270 and the thienopyridine N-atom are well positioned for a hydrogen bond interaction. Interestingly, there appears to be an additional favorable interaction between the sulfur atom of **14g** and the carbonyl group of Glu268. Inter- and intramolecular interactions between sulfur and oxygen atoms are relatively common and can be used to the medicinal chemists' advantage.[53,54]

We were also able to obtain a crystal structure of quinoline UNC10244803 (PDB ID: 5UYJ). The quinoline nitrogen atom is positioned to form a hydrogen bond with the NH group of Val270. The predicted binding pose of **46** (Figure 4b) is highly comparable to the binding mode of the co-crystallized ligand UNC10244803. Similar to quinoline **46**, 2-phenylpyrimidine **56** has only one heteroatom that is capable of forming hydrogen bonds with the hinge (Figure 4c). The N-atom of pyridine in the 1-position of **56** shows a H-bond with the NH group of Val270. Together with the presumed H-bond

https://doi.org/10.1021/acs.jmedchem.0c02274
J. Med. Chem. 2021, 64, 10849−10877

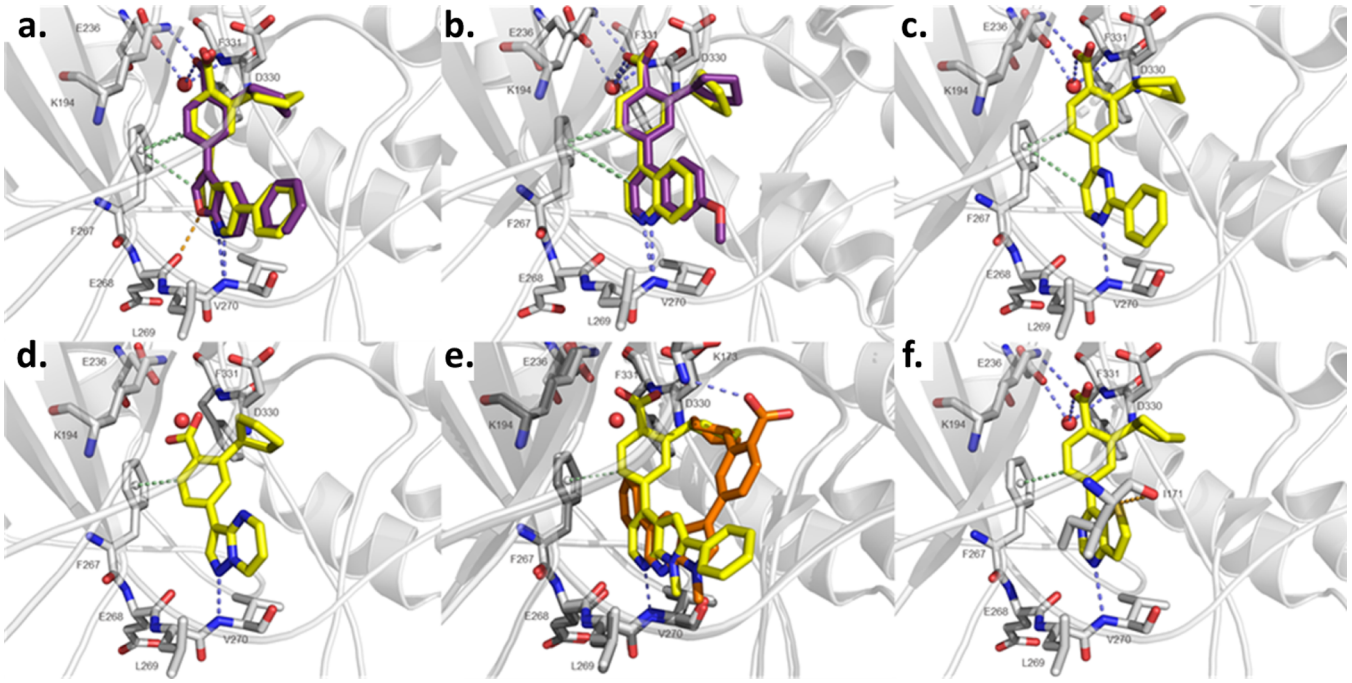

Figure 4. X-ray structures and in silico docking. In silico docking was performed with Glide, and images were generated with PyMOL. The protein is colored in gray. Blue-dashed lines indicate H-bond interactions, while green-dashed lines display CH−π interactions and orange-dashed lines refer to sulfur−σ hole bonding. Docked ligands are shown as yellow sticks or orange sticks, co-crystallized ligands as purple sticks, and the water molecule as a red sphere. Oxygen and nitrogen atoms are colored in red and blue, respectively. (a) Predicted binding mode of **14g** (yellow) using the protein structure from PDB-ID 5UY6 compared to the co-crystallized ligand **13g** (purple). (b) Predicted binding modes of **46** (yellow) using the protein structure from PDB-ID 5UYJ and the co-crystallized ligand UNC10244803 (purple). (c) Predicted binding mode of **56** using the protein structure from PDB-ID 5UYJ. (d) Predicted binding mode of **22** using the protein structure from PDB-ID 6BKU. (e) Predicted binding modes of **10** (orange) and **29** (yellow) using the protein structure from PDB-ID 6BKU (light gray) and 5UYJ (dark gray), respectively. (f) Predicted binding mode of **38** using the protein structure from PDB-ID 5UYJ.

formed between the protonated N-atom of Lys194 and the carboxylate group of **56**, these two interactions anchor **56** in the active site. In this orientation, the phenyl ring in the 2-position is tolerated by the binding pocket. 2-Aryl-pyrimidines are much less common as kinase inhibitors than 2-anilinopyrimidines and so warrant further exploration. The 2-position phenyl ring of **56** is adjacent to Leu269 of CAMKK2. We speculate that kinases incorporating amino acids with larger side chains such as Phe or Tyr in this location at the hinge region will be less tolerant of this scaffold, perhaps offering a path to enhance selectivity.

Pyrazolopyrimidine **22** (Figure 4d) forms one hinge-binding interaction between the N-atom in position 1 and the backbone NH group of Val270. The distance between the NH_3^+ group of Lys194 and the carboxylate group of **22** is greater compared to the predicted binding modes of the other compounds (Figure 4b,e). The *N*-methyl group of compound **10** (Figure 4e) appears to preclude binding of this compound in the same orientation as GSK650394. This compound is inactive in the enzyme assay, and the docking predicts a flipped orientation of the compound. *N*-methyl compound **29**, however, retains activity, and the in silico docking result suggests a conformation that allows the pyridyl nitrogen atom to interact with the NH group of Val270. The methyl group in this orientation is tolerated, perhaps analogously to the 2-phenyl of compound **56**. This flipped binding mode is possibly due to the shift of the attachment position of the cyclopentyl benzoic acid moiety from the 5-position of **10** to the 4-position in **29**. The hinge-binding interactions shown in the predicted binding mode of thienopyrimidine **38** are comparable (Figure 4f) to those of **56**. Additionally, the orientation of **38** is further stabilized by an interaction that is formed between the O-atom of the carbonyl moiety of Ile171 and the S-atom of the thienopyrimidine scaffold.

Compound Selectivity. In order to begin to understand kinome-wide selectivity for these new compounds, we profiled 9 exemplars in a panel of over 400 wild-type human kinases using the Eurofins DiscoverX's KINOME*scan* technology[50] (Freemont, CA USA). A summary of the kinome selectivity results is depicted in Table 6, and the complete KINOME*scan* data sets are available in the Supporting Information. Table 6 contains the structures of the compounds profiled, the PoC values for CAMKK1 and CAMKK2 at the 1 μM screening concentration, and a list of all the kinases in the panel that bound with a PoC < 10. The S-score is a quantitative measure of a compound's selectivity at a particular screening concentration, calculated by dividing the number of kinases that a particular compound binds to at a chosen threshold by the total number of distinct kinases tested. All the compounds we tested from this scaffold-hopping effort have an S_{10} (1 μM) < 0.05, which implies that they bind to fewer than 5% of the wild-type kinases tested in this panel with a PoC of 10 or less, thus offering promising selectivity for a starting point for further optimization.

Figure 5 is a visual representation of the KINOME*scan* data for two of the compounds, azaindole compound **7** and 2-anilino-pyrimidine compound **62**. All kinases bound with a PoC < 10 are depicted as red dots. These kinases are listed in Table 5, and the full data sets are available in the Supporting Information. For compound **7**, 12 kinases have a PoC less than

https://doi.org/10.1021/acs.jmedchem.0c02274
J. Med. Chem. 2021, 64, 10849−10877

Table 6. Selectivity Screening Summary Results for Nine Different Exemplars

Compound	Structure	S_{10} (1 μM)	CAMKK2 PoC (%)	CAMKK1 PoC (%)	Kinases with PoC ≤ 10
7	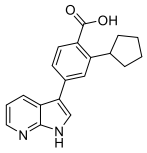	0.03	2.8	2.3	CDK8, SGK, JAK3, YSK4, CDK11, CAMKK1, CAMKK2, CASK, ERK8, CAMK2A, EPHB6, SGK3
13g	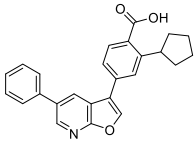	0	12	19	none
20	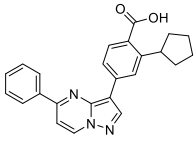	0.05	7	7.7	CSNK2A2, JAK3, CDK11, CSNK2A1, EPHB6, PIK3CG, NEK10, CLK2, ICK, GAK, TYK2, CAMKK2, CAMKK1, DRAK2, MLK3, PIK4CB, ULK3 CDK8, MEK4
21	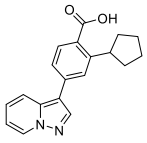	0.01	12	26	MARK1, BRSK2, MARK4, BMPR1B
29	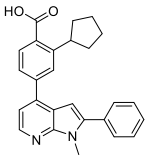	0.01	17	10	p38-delta, MST1R, MAK
34	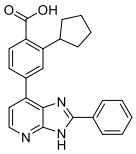	0.04	4.4	2.4	CDK9, JNK1, ICK, JNK3, CAMKK1, EPHB6, CDC2L5, SGK, CDK2, CAMKK2, CDK3, JNK2, JAK3, AURKA, CDKL5, PIP5K2C
38	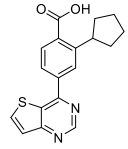	0.01	8.5	9.4	CDK11, CDK8, CAMKK1, CAMKK2
45	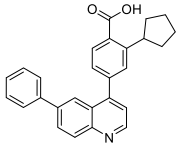	0	18	12	none
62	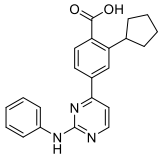	0.01	9.4	5.9	CAMKK1, CAMKK2

or equal to 10, including CAMKK2 and CAMKK1. For compound **7**, S_{10} (1 μM) = 0.03 implies that 3% of the kinases tested had a PoC < 10 at an inhibitor screening concentration of 1 μM. For compound **62**, only two kinases (CAMKK1 and CAMKK2) have a PoC < 10. S_{10} (1 μM) = 0.005 implies that 0.5% of the kinases tested had a PoC < 10 at an inhibitor screening concentration of 1 μM. Next steps will need to include testing of the compounds in enzyme inhibition assays and cell-based assays for the identified kinases for each scaffold.

CAMKK1 activity. CAMKK1 is a closely related and also understudied kinase. In order to learn if selectivity between CAMKK1 and CAMKK2 may be attainable in these series, we determined IC50 values for CAMKK1 inhibition for the 18 compounds with CAMKK2 IC50 < 150 nM, with the results depicted in Table 7. STO-609 is reported to have some selectivity for CAMKK2 over CAMKK1, and this is recapitulated in our assays.[55] In general, the compounds are more potent inhibitors of CAMKK2 than CAMKK1.

https://doi.org/10.1021/acs.jmedchem.0c02274
J. Med. Chem. 2021, 64, 10849−10877

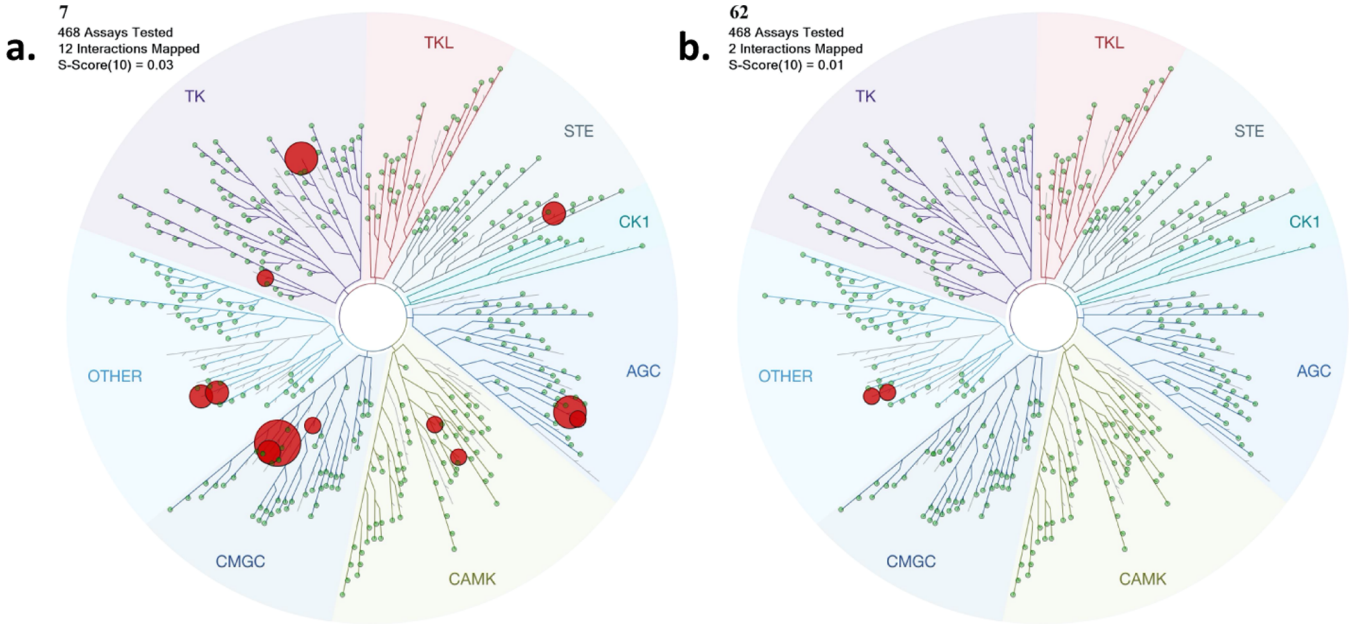

Figure 5. *In vitro* kinase selectivity profile of compound **7** (**5a**) and compound **62** (**5b**) at 1 μM (Eurofins DiscoverX KINOME*scan*). TREEspot interaction maps for **7** and **62** profiled against >400 human kinase targets. In this assay, primary screen binding interactions are reported as PoC, where lower values are an indication of stronger hits. Red dots depict the kinases for which PoC at 1 μM < 10. The size of the dot is based on the PoC values, with larger dots having smaller PoC values (more potent binders). PoC values for all kinases can be found in the Supporting Information.

Table 7. CAMKK1 and CAMKK2 Enzyme Inhibition Data, CAMKK2 NanoBRET in Cell Target Engagement, LE Metrics, and cLog *P* and Solubility Data for Potent CAMKK2 Inhibitors[a]

ID	CAMKK1 enzyme IC_{50} [nM]	CAMKK2 enzyme IC_{50} [nM]	CAMKK2 NB IC_{50} [nM]	cLog *P*	LE	LLE	solubility [μg/mL]
STO-609	408 ± 22	58 ± 5.7	NG	3.59	0.41	3.61	60
GSK650394	33 ± 6.9	3 ± 0.4	<3	5.67	0.40	2.83	2
7	195 ± 25	26 ± 6.1	NG	3.78	0.45	3.82	
13g	961 ± 132	65 ± 15	700 ± 9.3	5.68	0.34	1.52	77
14g	384 ± 53	5 ± 1.1	210 ± 24	6.32	0.39	1.98	1.5
19	1480 ± 120	145 ± 30	530 ± 95	6.01	0.32	0.79	42
20	238 ± 32	21 ± 1.3	190 ± 19	5.17	0.36	2.53	50.5
21	2013 ± 174	44 ± 9.1	200 ± 11	4.13	0.44	3.27	48.3
29	>10,000	120 ± 21	240 ± 7	6.06	0.32	0.84	
30	1345 ± 222	56 ± 14	470 ± 44	3.97	0.42	3.33	40
34	27 ± 4.5	23 ± 4.2	8.1 ± 0.8	5.42	0.36	2.18	55.1
38	407 ± 25	24 ± 1.1	170 ± 18	3.99	0.45	3.61	55.4
42	7280 ± 216	31 ± 4.3	1400 ± 250	3.78	0.45	3.72	62.6
45	1838 ± 348	137 ± 12	540 ± 62	6.59	0.32	0.31	38
46	239 ± 20	13 ± 1.0	140 ± 12	4.7	0.45	3.2	64.4
49	2614 ± 349	12 ± 3.9	890 ± 71	5.86	0.36	2.04	70.4
50	5481 ± 130	96 ± 14	1900 ± 200	3.97	0.40	3.03	
56	>10,000	21 ± 2.6	290 ± 23	4.68	0.41	3.02	19.4
61	>10,000	108 ± 6.9	950 ± 110	2.57	0.46	4.43	
62	31 ± 6.5	51 ± 13	<3	5.38	0.37	1.92	10.6

[a]NB = data from the NanoBRET in the cell target engagement assay; NG = data not generated.

Compound **34** ($CAMKK1\ IC_{50}$ = 27 nM, $CAMKK2\ IC_{50}$ = 23 nM) and compound 62 ($CAMKK1\ IC_{50}$ = 31 nM, $CAMKK2\ IC_{50}$ = 51 nM) are exceptions, being equipotent or slightly more potent on CAMKK1. For STO-609, a switch in a residue near the inhibitor hinge-binding group from a valine in CAMKK2 (Val269) to a leucine in CAMKK1 (Leu233) has been hypothesized as the source of selectivity.[56] Further experiments will need to be done to understand and exploit the differences in CAMKK1 and CAMKK2 activity observed for the inhibitors described here.

Compound Properties. A number of key physicochemical screens and calculations are considered in early-stage drug discovery, including lipophilicity, pK_a, solubility, permeability, and stability. Solubility is one of the most critical physicochemical properties as poor solubility can lead to an underestimation of activity, inaccurate SAR, inaccurate *in vitro* ADMET test results, and downstream compound development

https://doi.org/10.1021/acs.jmedchem.0c02274
J. Med. Chem. 2021, 64, 10849−10877

issues.[57,58] Highlighting the critical importance of solubility, it has been shown that 87% of commercial drugs have solubility ≥65 μg/mL, but only 7% had solubility ≤20 μg/mL.[59] Therefore, solubility data can identify a series liability that needs to be fixed and highlight promising series with enhanced solubility. This information can help guide optimization strategies. LE metrics are also a commonly used tool that can guide hit-to-lead optimization for drug candidates.[60,61] To this end, we calculated LE and lipophilic ligand efficiency (LLE) and collected kinetic solubility data for compounds with IC_{50} values <150 nM in the CAMKK2 enzyme assay (Table 7).[62]

LE values are influenced by molecular size; hence, it was unsurprising to see two clear ranges depending on the presence or absence of the phenyl ring. The hinge binders without the phenyl ring had LE values ranging from 0.41 to 0.46. These are smaller compounds with molecular weights between 300 and 325, and generally, LE values above 0.3 are acceptable for this MW range.[60] The LLE values for these compounds were between 3.02 and 4.43. Aminopyridine **61** had the highest LE and LLE values of 0.46 and 4.43, respectively. Both **7** and **38** had comparable LE values of 0.45 but significantly lower LLE values of 3.82 and 3.61, respectively.

Both the LE and LLE metrics of the phenyl-substituted analogues have lower values. This is reflective of the increased atom count and higher cLog *P* values due to the additional lipophilicity of the phenyl ring. The LE values are between 0.32 and 0.40 for these compounds. GSK650394 has the highest LE and LLE values of 0.40 and 2.83, respectively. The analogous thienopyridine **14g** has the next highest LE value of 0.39 but a lower LLE value of 1.98. Quinoline **45** had the lowest LE and LLE values of 0.32 and 0.31, respectively. Solely relying on LE metrics to select compounds is unadvisable as many other factors, such as solubility, underpin successful drug development. A future direction could be to focus on polar substituents on the pendant phenyl to lower log *P*, enhance solubility, and mitigate the metabolic liability that may be seen in high-logP compounds. Similarly, non-aromatic substituents could be explored to access this same region of the active site.

Of the phenyl-substituted analogues, GSK650394 and **14g** were the most potent, with IC_{50} values of 3 and 5 nM, respectively, and had the best LE and LLE values. Although promising in this regard, these compounds have extremely poor solubility values of 2 and 1.5 μg/mL, respectively. Optimization of these compounds will thus require extensive structure−property-relationship studies in parallel to SAR studies to develop them into useful tools with adequate solubility for further study. Interestingly, furopyridine **13g** had the highest measured solubility value of 77 μg/mL. Substitution of the azaindole's NH with an oxygen greatly improved solubility. The effect was reversed when a more lipophilic sulfur atom is incorporated into the same position, **14g**. Pyrimidine analogues **56** and **62** are also only modestly soluble (10.6 and 19.4 μg/mL). Optimization to tool compounds will likely require the introduction of solubilizing functional groups. A number of the compounds tested had reasonable solubility ranging from 38 to 55 μg/mL. Four compounds had a promising solubility above that recorded for **STO-609**, 60 μg/mL. These were the thienopyrimidine **42** (62.6 μg/mL) and quinoline **46** (64.4 μg/mL), both without the pendant phenyl ring. The phenyl-substituted quinazoline **49** has a solubility of 70.4 μg/mL, second only to furopyridine **13g**. Overall, the solubility of several potent compounds was encouraging but will need to be monitored as optimization proceeds.

CAMKK2 NanoBRET Cellular Target Engagement. Having demonstrated potent CAMKK2 inhibition and promising selectivity profiles for these compounds we tested in kinome-wide profiling, we turned our attention to the cellular activity of the compounds (Table 7). To this end, we developed a CAMKK2 NanoBRET target engagement assay.[63] This assay uses bioluminescence resonance energy transfer (BRET) between nanoluciferase (NL) fused to the kinase domain of CAMKK2 (BRET donor) and a tracer molecule that binds to the ATP-binding site of the kinase (BRET acceptor). The addition of cell penetrant CAMKK2 inhibitors leads to displacement of the tracer molecule and a quantifiable reduction in BRET signal. This assay is conducted in living cells, and the observation of binding not only depends on affinity between the compound and CAMKK2 but also on compound cell penetrance. The parent molecule, GSK650394, was very potent in this assay (NB IC_{50} < 3 nM). Several additional key compounds were evaluated in this assay (Table 7 and the Supporting Information). A key takeaway here is that all the compounds that advanced to this assay (those with CAMKK2 enzyme IC_{50} < 150 nM) demonstrated measurable CAMKK2 target engagement in cells. The potency was below 500 nM for thienopyridine **14g** (210 nM), pyrazolopyrimidines **20** and **21** (190 and 200 nM), *N*-methyl azaindoles **29** and **30** (240 and 470 nM), imidazopyridine **34** (8 nM), thienopyrimidine **38** (170 nM), quinoline **46** (140 nM), 2-phenylpyrimidine **56** (290 nM), and 2-amino-pyrimidine **62** (<3 nM). The results for exemplar compounds from five different scaffolds (**13g**, **45**, **46**, **56**, and **62**) are depicted in Figure 6.

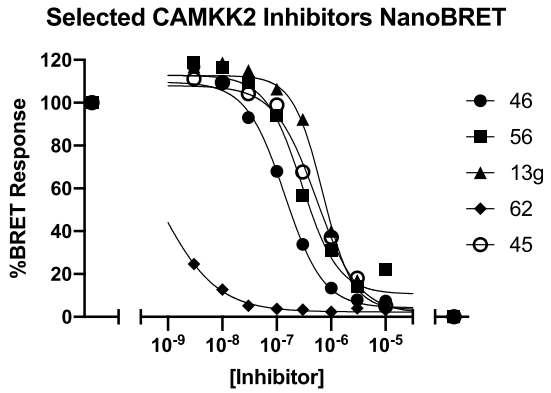

Figure 6. CAMKK2 NanoBRET dose−response curves for compounds **13g**, **45**, **46**, **56**, and **62**.

On-Target Cellular Effect (Phosphorylation Inhibition Assay). We also assessed the impact of our inhibitors on phosphorylation downstream from CAMKK2 using Western blot analysis with C4-2 prostate cancer cells to provide evidence of a phenotypic and on-target effect of our CAMKK2 inhibitors in intact cells. AMPK (Thr172) was chosen because in intact cells, CAMKK2, but not the related CAMKK1, can readily phosphorylate this substrate.[64] We performed preliminary Western blot analysis at a single inhibitor concentration of 1 μM for the 18 compounds with CAMKK2 enzyme IC_{50} < 150 nM along with STO-609. These results are shown in Figure 7.

https://doi.org/10.1021/acs.jmedchem.0c02274
J. Med. Chem. 2021, 64, 10849−10877

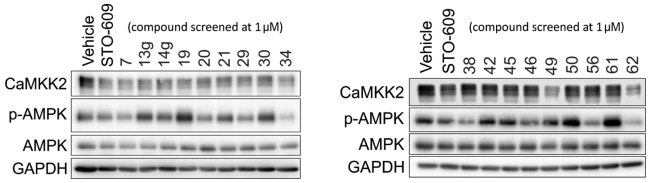

Figure 7. Western blots of the 18 compounds with IC_{50} < 150 nM in the CAMKK2 enzyme assay, together with STO-609, screened at a single inhibitor concentration = 1 μM.

Based on these results from screening at a single concentration, compounds **7**, **20**, **29**, **34**, **38**, **46**, **56**, and **62** showed the most robust reduction of the p-AMPK band and were advanced into full dose response experiments in this same assay format to provide IC_{50} estimates for inhibition of phosphorylation of AMPK at Thr172. The IC_{50} values were determined from dose response experiments using 0−10 μM of the compound. The Western blot dose response experiments for the most potent compound, **62**, are depicted in Figure 8a. The Western blot dose response data for

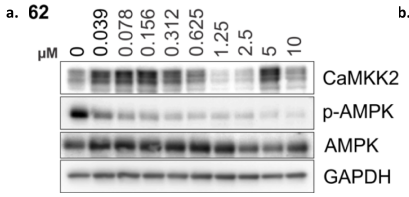

b.

compound	IC50 for inhibition of p-AMPK
62	<39 nM
46	390 nM
56	790 nM
20	900 nM
29	980 nM
34	1800 nM
7	5500 nM
38	8100 nM

Figure 8. (a) Dose response for inhibition of phosphorylation of AMPK at Thr172 in C4-2 prostate cancer cells by compound **62**. (b). Calculated IC_{50} values for inhibition of phosphorylation of AMPK at Thr172 in C4-2 prostate cancer cells for the top compounds from the single concentration experiment depicted in Figure 7.

compounds 7, 20, 29, 34, 38, 46, and 56 can be found in the Supporting Information. In addition, dose response experiments for compound 62 utilizing lower inhibitor concentrations can be found in the Supporting Information. The calculated IC_{50} values for the dose response experiments for all eight compounds are shown in Figure 8b. Compounds **62** (IC_{50} = 10 nM), **46** (IC_{50} = 390 nM), **56** (IC_{50} = 790 nM), **20** (IC_{50} = 900 nM), and **29** (IC_{50} 980 nM) all have IC_{50} values for inhibition of phosphorylation of AMPK at Thr172 below 1 μM, suggesting that optimization into compounds with potent cellular activity will be achievable for these series.

DISCUSSION AND CONCLUSIONS

Through a hinge-binder scaffold hopping strategy, we have designed, synthesized, and biologically evaluated as CAMKK2 inhibitors a series of 32 compounds that utilize 5,6-bicyclic, 6,6-bicyclic, and single-ring hinge-binding moieties that are based on the 7-azaindole GSK650394. These inhibitors were designed with the aim of retaining CAMKK2 potency and improving the kinase selectivity of the promiscuous azaindole by changing the strong H-bond interactions that the parent azaindole makes with the kinase hinge-binding residues. Additionally, we sought to identify inhibitors with improved physicochemical properties, drug likeness, and selectivity all while retaining CAMKK2 inhibitory potency. Several compounds with similar or better potency than GSK650394 and STO-609 have been identified, some of which also showed improved physicochemical properties. We found that a number of these compounds, but not all, have some selectivity over the closely related enzyme CAMKK1 in enzyme assays. Further work will be needed to understand selectivity determinants, to optimize this selectivity, and to determine if the observed selectivity holds in a cellular context. Kinome-wide profiling revealed that the nine exemplars we screened in the Eurofins DiscoverX KINOME*scan* platform are not broadly promiscuous, with S_{10} (1 μM) < 0.05. In addition, we have demonstrated that exemplars have cellular activity in two orthogonal assays, a CAMKK2 NanoBRET in cell target engagement assay, and Western blot experiments looking at inhibition of the production of p-AMPK. Our work has shown that kinase inhibitors with weakened (non-ideal) hinge-binding interactions can show highly selective kinase inhibition and still have useful on-target enzyme potency and cellular potency. This work has led to the identification of several CAMKK2 scaffolds with alternate hinge-binding moieties that hold promise as starting points for the discovery of potent, selective, and cell-active CAMKK2 inhibitors.

EXPERIMENTAL SECTION

Biology. *Protein Expression and Purification/DSF Assay.* Small-molecule screening by DSF was performed as described previously.[48,65] Briefly, the DSF assay was performed in the 96-well format. Purified CAMKK1 or CAMKK2 was diluted to 2 μM kinase in 100 mM potassium phosphate pH 7.5, 150 mM NaCl, and 10% glycerol supplemented with 5 × SYPRO Orange (Invitrogen, Carlsbad, CA, USA). All assay experiments used 19.5 μL of 2 μM kinase and SYPRO Orange mixture. Compounds solubilized in dimethyl sulfoxide (DMSO) were used at a 12.5 μM final concentration, with a 2.5% concentration of DMSO per well. PCR plates were sealed using optically clear films and transferred to a C1000 thermal cycler with CFX-96 RT-PCR head (BioRad, Hercules, CA, USA). The fluorescence intensity was measured over a temperature gradient from 25 to 95 °C at a constant rate of 0.05 °C/s. Curve fitting and protein melting temperatures were calculated based on a Boltzmann function fitting to experimental data (GraphPad Prism 8). Protein with the addition of 2.5% DMSO was used as a reference. All experiments were carried out in triplicate, and the mean of the ΔT_m is reported. Compounds that provided negative values are presented as having a ΔT_m of 0 °C.

CAMKK1 and CAMKK2 Enzyme Assays. CAMKK1 and CAMKK2 activity was determined by measuring the transfer of radiolabeled phosphate from [γ-^{32}P]-ATP to a synthetic peptide substrate (CaMKKtide) as previously described.[66] Briefly, purified recombinant CAMKK1 or CAMKK2 (100 pM) was incubated in the assay buffer [50 mM HEPES (pH 7.4), 1 mM dithiothreitol, 0.02% (v/v) Brij-35] containing 200 μM CaMKKtide (Genscript), 100 μM $CaCl_2$, 1 μM CaM (Sigma-Aldrich, Castle Hill, NSW, Australia), 200 μM [γ-^{32}P]-ATP (Perkin Elmer, Boston, MA, USA), 5 mM $MgCl_2$ (Sigma-Aldrich, Castle Hill, NSW, Australia), and various concentrations of inhibitors (0−1 μM) in a standard 30 μL assay for 10 min at 30 °C. Reactions were terminated by spotting 15 μl onto P81 phosphocellulose paper (GE Lifesciences, Paramatta, NSW, Australia) and washing extensively in 1% phosphoric acid (Sigma-Aldrich, Castle Hill, NSW, Australia). Radioactivity was quantified by liquid scintillation counting.

CAMKK2 NanoBRET Assay. To quantify the cellular activity of these inhibitors, we developed a CAMKK2 NanoBRET target engagement assay.[63] Briefly, this assay utilizes an NL fused to the kinase domain of CAMKK2. This NL kinase fusion is then transiently transfected into HEK293 cells, and after 24 h, the tracer is added to the cells. When the tracer and the NL-CAMKK2 fusion come into proximity, they create a BRET signal that can be competed in a dose-dependent manner by the addition of cell-penetrant CAMKK2 inhibitors.

https://doi.org/10.1021/acs.jmedchem.0c02274
J. Med. Chem. 2021, 64, 10849−10877

Western Blot Analysis. C4-2 cells were plated in 6-well plates in the IMEM medium containing 0.5% fetal bovine serum. After 72 h, the cells were then treated with the compounds for 24 h before the media were aspirated and wells were washed twice in ice-cold phosphate-buffered saline. Cells were lysed using RIPA buffer containing phosphatase and the protease inhibitor cocktail while rotating for 30 min at 4 °C. In each lane, 30 μg/well of protein lysate was loaded into a 10% sodium dodecyl sulfate-polyacrylamide gel electrophoresis gel and run for 1 h and 30 min. Gels were then transferred overnight in a TRIS-glycine/methanol transfer buffer onto a poly(vinylidene difluoride) membrane at 4 °C. Membranes were blocked, incubated with primary overnight at 4 °C, washed, incubated with secondary at room temperature (rt) for 1 h, washed, and then developed on an Azure Biosystems C-600 imager.

[Cell signaling: phospho-AMPKα (Thr172) (40H9) rabbit mAb: Cat#: 2535; AMPKα (D5A2) Rabbit mAb Cat#: 5831; BD Bioscience: CAMKK mouse mAb Cat# 610544; Sigma: GAPDH rabbit pAb: Cat# G9545; secondary antibody: goat anti-rabbit IgG (H + L)-HRP conjugate was from Bio-Rad (Cat#:1706515)].

Crystallization, Data Collection, and Structure Determination. Crystallization of the CAMKK2-kinase domain bound to **13g** or UNC10244803 followed a previously established protocol.[38] Briefly, the inhibitor (dissolved in 100% DMSO) was added to the protein in 3-fold molar excess and incubated on ice for approximately 30 min. The mixture was centrifuged at 21,000*g* for 10 minutes at 4 °C before setting up 150 nL volume sitting drops at three ratios (2:1, 1:1, or 1:2 protein−inhibitor complex to reservoir solution). Crystallization experiments were performed at 20 °C. Crystal optimization used Newman's buffer system.[67] Crystals were cryoprotected in the mother liquor supplemented with 25−30% glycerol before flash cooling in liquid nitrogen for data collection. Diffraction data were collected at 100 K at the Advanced Photon Source 24ID-C or at the Diamond Light Source (DLS) I03 beamline.

Diffraction data were integrated with XDS[68] and scaled using AIMLESS from the CCP4 software suite.[69] The structure was solved by molecular replacement using Phaser[70] and the kinase domain of CAMKK2 as the search model (PDB ID 2ZV2).[71] Refinement was performed using REFMAC5,[72] and Coot[73] was used for model building. Structure validation was performed using MolProbity.[74] Structure factors and coordinates for the structure were deposited at the PDB (PDB ID 5UY6).

Chemistry. *General Chemistry Information.* All reagents and solvents, unless specifically stated, were used as obtained from their commercial sources without further purification. Solvents were degassed with nitrogen for cross-coupling reactions. Air- and moisture-sensitive reactions were performed under an inert atmosphere using nitrogen in a previously oven-dried or flame-dried reaction flask, and addition of reagents was done using a syringe. All microwave (μW) reactions were carried out in a Biotage Initiator EXP US 400W microwave synthesizer. Thin-layer chromatography (TLC) analyses were performed using 200 μm pre-coated sorbtech fluorescent TLC plates, and spots were visualized using UV light. High-resolution mass spectrometry samples were analyzed with a ThermoFisher Q Exactive HF-X (ThermoFisher, Bremen, Germany) mass spectrometer coupled with a Waters Acquity H-class liquid chromatograph system. All high-resolution mass spectrometry (HRMS) spectra were recorded *via* electrospray ionization (ESI). Column chromatography was undertaken with a Biotage Isolera One or Prime instrument. Nuclear magnetic resonance (NMR) spectrometry was run on a Varian Inova 400 MHz or Bruker AVANCE III 700 MHz spectrometer equipped with a TCI H-C/N-D 5 mm cryoprobe, and data were processed using the MestReNova processor. Chemical shifts are reported in ppm with residual solvent peaks referenced as the internal standard. All compounds were >95% pure by analytical LC.

*4-Bromo-2-cyclopentylbenzoic Acid (**2**).* 4-Bromo-2-fluorobenzoic acid (2.00 g, 9.00 mmol) was dissolved in tetrahydrofuran (THF) (20.0 mL) and cooled to 0 °C. Cyclopentylmagnesium bromide solution (16.0 mL of a 2 M solution, 32.0 mmol) was added dropwise. The reaction was stirred at 0 °C for 4 h. 2 M HCl (25.0 mL) was then slowly added to the solution, followed by EtOAc (40.0 mL). The organic phase was separated, concentrated, and purified using column chromatography (10% EtOAc/hexane) to afford 4-bromo-2-cyclopentylbenzoic acid **2** (1.70 g, 71%) as a pure white solid. The NMR data for this compound match those previously reported.[38]

^{1}H NMR (400 MHz, DMSO-d_6): δ 13.07 (s, 1H), 7.60−7.56 (m, 2H), 7.45 (dd, J = 8.3, 2.1 Hz, 1H), 3.68 (tt, J = 9.5, 7.5 Hz, 1H), 2.03−1.94 (m, 2H), 1.82−1.72 (m, 2H), 1.67−1.46 (m, 4H). ^{13}C NMR (100 MHz, DMSO-d_6): δ 168.9, 148.6, 131.2, 131.1, 129.5, 128.6, 125.1, 41.2, 34.2, 25.2; LCMS: $[M + H]^+$ m/z, 269.0.

*2-Cyclopentyl-4-(4,4,5,5-tetramethyl-1,3,2-dioxaborolan-2-yl)-benzoic Acid (**3**).* To a stirred solution of 4-bromo-2-cyclopentylbenzoic acid **2** (2.50 g, 9.30 mmol) and bis(pinacolato)diboron (2.80 g, 11.0 mmol) in dioxane (50.0 mL) were added $PdCl_2$(dppf)·CH_2Cl_2 (0.76 g, 0.96 mmol) and KOAc (3.60 g, 37.0 mmol). The solution was heated to 95 °C for 2 h. Once cooled to rt, the solution was diluted with EtOAc and filtered through a celite pad. The solution was concentrated, and the crude product was purified by column chromatography (10% EtOAc/hexane) to afford 2-cyclopentyl-4-(4,4,5,5-tetramethyl-1,3,2-dioxaborolan-2-yl)benzoic acid **3** (2.30 g, 78%) as an off-white solid.

^{1}H NMR (400 MHz, DMSO-d_6): δ 13.00 (s, 1H), 7.69 (d, J = 1.1 Hz, 1H), 7.60 (d, J = 7.6 Hz, 1H), 7.53 (dd, J = 7.6, 1.1 Hz, 1H), 3.62 (tt, J = 9.8, 7.4 Hz, 1H), 2.05−1.95 (m, 2H), 1.83−1.73 (m, 2H), 1.69−1.45 (m, 4H), 1.29 (s, 12H); ^{13}C NMR (100 MHz, DMSO-d_6): δ 169.7, 144.4, 134.9, 132.1, 131.5, 128.2, 83.9, 41.2, 34.4, 25.2, 24.7; LCMS: $[M + H]^+$ m/z, 317.2.

*Methyl 2-Cyclopentyl-4-(4,4,5,5-tetramethyl-1,3,2-dioxaborolan-2-yl)benzoate (**4**).* To a stirred solution of methyl 4-bromo-2-cyclopentylbenzoate **SI1** (1.50 g, 5.29 mmol) and bis(pinacolato)-diboron (1.88 g, 7.42 mmol) in dioxane (35.0 mL) were added $Pd(dppf)Cl_2$ (194 mg, 0.26 mmol) and KOAc (1.56 g, 15.9 mmol). The solution was heated to 100 °C for 2 h. Once cooled to rt, the solution was filtered through a pad of Celite and washed with 100 mL of EtOAc. The volatiles were removed *in vacuo*, and the crude residue was purified *via* column chromatography (0−5% EtOAc/hexane) to afford methyl 2-cyclopentyl-4-(4,4,5,5-tetramethyl-1,3,2-dioxaborolan-2-yl)benzoate **4** (1.37 g, 78%) as oil which slowly solidified into a white solid under vacuum.

^{1}H NMR (400 MHz, DMSO-d_6): δ 7.70 (d, J = 1.1 Hz, 1H), 7.60 (d, J = 7.7 Hz, 1H), 7.56 (d, J = 1.1 Hz, 1H), 3.83 (s, 3H), 3.50 (tt, J = 9.9, 7.5 Hz, 1H), 2.04−1.93 (m, 2H), 1.85−1.70 (m, 2H), 1.70−1.44 (m, 4H), 1.30 (s, 12H); ^{13}C NMR (100 MHz, DMSO-d_6): δ 168.3, 144.6, 133.6, 132.2, 131.6, 128.3, 84.0, 52.2, 41.3, 34.3, 25.2, 24.7; LCMS: $[M + H]^+$ m/z, 330.2.

*Methyl 2-Cyclopentyl-4-(1-((2-(trimethylsilyl)ethoxy)methyl)-1H-pyrrolo[2,3-b]pyridin-3-yl)benzoate (**6**).* To a stirred solution of 3-bromo-1-((2-(trimethylsilyl)ethoxy)methyl)-1*H*-pyrrolo[2,3-*b*]-pyridine (450 mg, 1.37 mmol) and methyl 2-cyclopentyl-4-(4,4,5,5-tetramethyl-1,3,2-dioxaborolan-2-yl)benzoate **4** (681 mg, 2.06 mmol) in PhMe (8.0 mL) and H_2O (1.00 mL) were added Pd(OAc)2 (15.4 mg, 68.7 μmol), K3PO4 (934 mg, 4.40 mmol), and P(Cy)3 (38.6 mg, 137 μmol). The reaction mixture was heated to 100 °C for 18 h and allowed to cool to rt, filtered through a pad of Celite, and washed with EtOAc (10 mL). The filtrate was concentrated *in vacuo*, and the crude was purified by column chromatography eluting with 0−30% EtOAc/hexane to afford methyl 2-cyclopentyl-4-(1-((2-(trimethylsilyl)-ethoxy)methyl)-1*H*-pyrrolo[2,3-*b*]pyridin-3-yl)benzoate (545 mg, 88%) as a light-yellow solid (LCMS: $[M + H]^+$ m/z, 327.3). A solution of the above material ("SEM-protected **6**"), 2-cyclopentyl-4-(1-((2-(trimethylsilyl)ethoxy)methyl)-1*H*-pyrrolo[2,3-*b*]pyridin-3-yl)benzoate (500 mg, 1.11 mmol), in CH_2Cl_2 (10 mL) was treated with trifluoroacetyl (3.50 mL, 45.5 mmol). The solution was stirred at 25 °C for 2 h and then neutralized with sat. $NaHCO_3$ (50 mL). The solution was extracted with EtOAc (3 × 100 mL), and the combined organic phases were washed with sat. NaCl solution, dried (Na_2SO_4), filtered, and concentrated *in vacuo*. The residue was dissolved in ethanol (40.0 mL), and NaOAc (1.82 mg, 22.2 mmol) was added. The mixture was stirred at 50 °C for 20 h and allowed to cool to rt. The solution was diluted with H_2O (50 mL) and EtOAc (75.0 mL).

https://doi.org/10.1021/acs.jmedchem.0c02274
J. Med. Chem. 2021, 64, 10849−10877

The layers were separated, and the aqueous phase was extracted with EtOAc (2 × 75 mL). The combined organics were washed with a saturated NaCl solution (50 mL), dried (Na_2SO_4), filtered, and concentrated *in vacuo*. The crude material was purified by column chromatography (0−30% EtOAc/hexane) to afford methyl 2-cyclopentyl-4-(1*H*-pyrrolo[2,3-*b*]pyridin-3-yl)benzoate **6** (245 mg, 69%) as a deep-yellow solid.

^{1}H NMR (400 MHz, DMSO-d_6): δ 12.10−12.05 (m, 1H), 8.32−8.24 (m, 2H), 8.05 (d, J = 2.7 Hz, 1H), 7.78−7.72 (m, 2H), 7.63 (dd, J = 8.1, 1.7 Hz, 1H), 7.20 (dd, J = 8.0, 4.6 Hz, 1H), 3.84 (s, 3H), 3.79−3.67 (m, 1H), 2.11−1.98 (m, 2H), 1.88−1.77 (m, 2H), 1.74−1.58 (m, 4H). ^{13}C NMR (101 MHz, DMSO-d_6): δ 167.9, 149.2, 147.2, 143.1, 138.7, 130.3, 127.4, 127.2, 125.1, 124.1, 123.2, 117.2, 116.4, 113.4, 51.9, 41.3, 34.3, 25.2; LCMS: $[M + H]^+$ m/z, 320.4.

*2-Cyclopentyl-4-(1H-pyrrolo[2,3-b]pyridin-3-yl)benzoic Acid (**7**).* Methyl 2-cyclopentyl-4-(1*H*-pyrrolo[2,3-*b*]pyridin-3-yl)benzoate (100 mg, 0.312 mmol) was dissolved in methanol (8.00 mL), followed by the addition of 50% NaOH solution (170 μL, 3.12 mmol). The mixture was heated to 75 °C for 1 h, allowed to cool, and extracted with diethyl ether (20.0 mL). The aqueous layer was then acidified to pH 5 with 1 M HCl and extracted with CH_2Cl_2 (15 mL). The organic layer was then dried (Na_2SO_4), filtered, and concentrated *in vacuo* to afford 2-cyclopentyl-4-(1*H*-pyrrolo[2,3-*b*]pyridin-3-yl)-benzoic acid **7** (85.0 mg, 89%) as a pale-yellow solid.

^{1}H NMR (400 MHz, DMSO-d_6): δ 12.64 (s, 1H), 12.12−12.08 (m, 1H), 8.32−8.27 (m, 2H), 8.03 (d, J = 2.6 Hz, 1H), 7.78−7.71 (m, 2H), 7.60 (dd, J = 8.1, 1.8 Hz, 1H), 7.22 (dd, J = 8.0, 4.7 Hz, 1H), 3.92−3.81 (m, 1H), 2.07 (d, J = 14.0 Hz, 2H), 1.82 (t, J = 5.8 Hz, 2H), 1.73−1.61 (m, 4H). ^{13}C NMR (101 MHz, DMSO-d_6): δ 169.3, 148.3, 147.1, 142.3, 138.1, 130.4, 128.6, 128.2, 125.2, 124.2, 123.2, 117.7, 116.4, 113.8, 41.2, 34.4, 25.3; HRMS: calcd for $C_{19}H_{18}N_2O_2$ $[M + H]^+$ m/z, 307.1447; found, 307.1426; mp range 238−242 °C.

*Methyl 4-(5-Chloro-1-methyl-1H-pyrrolo[2,3-b]pyridin-3-yl)-2-cyclopentylbenzoate (**9**).* 5-Chloro-3-iodo-1-methyl-1*H*-pyrrolo[2,3-*b*]pyridine (100 mg, 0.34 mmol), methyl 2-cyclopentyl-4-(4,4,5,5-tetramethyl-1,3,2-dioxaborolan-2-yl)benzoate (113 mg, 0.34 mmol), Pd(dppf)Cl_2·CH_2Cl_2 (28.0 mg, 34.0 μmol), and Cs_2CO_3 (334 mg, 1.00 mmol) were loaded into a microwave vial. A 3:1 mixture of dioxane/water (2 mL) was added before the vial was flushed with nitrogen and capped. The solution was stirred at rt for 16 h. Once cooled, the solution was diluted with EtOAc (2.00 mL) and water (2.00 mL). The layers were separated, and the aqueous phase was extracted with EtOAc (2 × 3.00 mL). The combined organics were dried (Na_2SO_4), filtered, and concentrated *in vacuo*. The crude was purified *via* column chromatography (5−20% EtOAc/hexane) to afford methyl 4-(5-chloro-1-methyl-1*H*-pyrrolo[2,3-*b*]pyridin-3-yl)-2-cyclopentylbenzoate **9** (217 mg, 69%) as a white solid.

^{1}H NMR (400 MHz, $CDCl_3$): δ 8.34 (d, J = 2.2 Hz, 1H), 8.15 (d, J = 2.0 Hz, 1H), 7.86 (d, J = 8.1 Hz, 1H), 7.60 (d, J = 1.6 Hz, 1H), 7.49 (s, 1H), 7.42 (dd, J = 8.1, 1.7 Hz, 1H), 3.97 (s, 3H), 3.93 (s, 3H), 3.92−3.84 (m, 1H), 2.31−2.06 (m, 2H), 1.92−1.80 (m, 2H), 1.80−1.71 (m, 2H), 1.71−1.59 (m, 4H); ^{13}C NMR (100 MHz, $CDCl_3$): δ 168.5, 148.6, 146.3, 141.7, 137.6, 130.8, 128.5, 128.3, 127.6, 125.0, 124.4, 123.6, 119.3, 114.2, 52.0, 41.7, 34.9, 31.8, 25.7; HRMS: calcd for $C_{21}H_{22}N_2O_2Cl$ $[M + H]^+$ m/z, 369.1369; found: m/z, 369.1348; mp range 144−148 °C.

*2-Cyclopentyl-4-(1-methyl-5-phenyl-1H-pyrrolo[2,3-b]pyridin-3-yl)benzoic Acid (**10**).* Methyl 4-(5-chloro-1-methyl-1*H*-pyrrolo[2,3-*b*]pyridin-3-yl)-2-cyclopentylbenzoate **9** (100 mg, 0.27 mmol), phenylboronic acid (40.0 mg, 0.32 mmol), $Pd_2(dba)_3$ (12.0 mg, 13.0 μmol), XPhos (13.0 mg, 27.0 μmol), and Cs_2CO_3 (265 mg, 0.81 mmol) were loaded into a microwave vial. A 3:1 mixture of dioxane/water (2 ml) was added, and the vial was flushed with nitrogen and capped. The solution was heated to 120 °C for 16 h. Once cooled, the solution was diluted with EtOAc (2 mL) and water (2.00 mL). The layers were separated, and the aqueous phase was extracted with EtOAc (2 × 3.00 mL). The combined organics were dried (Na_2SO_4), filtered, and concentrated *in vacuo*. The crude was purified *via* column chromatography (5−10% EtOAc/hexane) to afford the methyl ester intermediate. The methyl ester was saponified in a solution of aq LiOH (1.00 mL, 1 M) and dioxane (1.00 mL) at 100 °C for 16 h. The solution was cooled to rt, diluted with water (2 mL), and then acidified with aq HCl (1 M) until pH 4. The solution was extracted with EtOAc (2 × 3.00 mL). The combined organics were dried (Na_2SO_4), filtered, and concentrated *in vacuo*. The solid was washed with cold water (5.00 mL), followed by hexane (10.0 mL), and dried to afford 2-cyclopentyl-4-(1-methyl-5-phenyl-1*H*-pyrrolo[2,3-*b*]-pyridin-3-yl)benzoic acid **10** (77.0 mg, 72%) as an off-white solid.

^{1}H NMR (400 MHz, DMSO-d_6): δ 12.75 (br s, 1H), 8.63 (d, J = 2.1 Hz, 1H), 8.43 (d, J = 2.1 Hz, 1H), 8.15 (s, 1H), 7.83−7.67 (m, 5H), 7.50 (dd, J = 8.4, 7.0 Hz, 2H), 7.43−7.34 (m, 1H), 3.94−3.85 (m, 1H), 3.92 (s, 3H), 2.12−1.99 (m, 2H), 1.88−1.76 (m, 2H), 1.75−1.58 (m, 4H); ^{13}C NMR (100 MHz, DMSO-d_6): δ 169.7, 148.0, 147.7, 142.4, 139.2, 138.2, 131.0, 130.0, 129.6, 129.5, 128.9, 127.6, 126.1, 124.5, 123.6, 117.9, 113.3, 41.4, 34.8, 31.6, 25.8; HRMS: calcd for $C_{26}H_{25}N_2O_2$ $[M + H]^+$ m/z, 397.1916; found m/z, 397.1911; mp range 199−201 °C.

*2-Cyclopentyl-4-(1-methyl-1H-pyrrolo[2,3-b]pyridin-3-yl)benzoic Acid (**11**).* 3-Bromo-1-methyl-1*H*-pyrrolo[2,3-*b*]pyridine (100 mg, 0.47 mmol), methyl 2-cyclopentyl-4-(4,4,5,5-tetramethyl-1,3,2-dioxaborolan-2-yl)benzoate (180 mg, 0.54 mmol), $Pd_2(dba)_3$ (22.0 mg, 24 μmol), XPhos (23.0 mg, 48.0 μmol), and Cs_2CO_3 (540 mg, 1.66 mmol) were loaded into a microwave vial. A 3:1 mixture of dioxane/water (2.00 mL) was added, and the vial was flushed with nitrogen and capped. The solution was heated to 120 °C for 16 h. Once cooled, the solution was diluted with EtOAc (2.0 mL) and water (2.00 mL). The layers were separated, and the aqueous phase was extracted with EtOAc (2 × 3.00 mL). The combined organics were dried (Na_2SO_4), filtered, and concentrated *in vacuo*. The crude was purified *via* column chromatography (0−20% EtOAc/hexane) to afford the methyl ester intermediate. The methyl ester was saponified in a solution of aq LiOH (2.00 mL, 1.00 M) and dioxane (2.00 mL) at 100 °C for 16 h. The solution was cooled to rt, diluted with water (2.00 mL), and then acidified with aq HCl (1.00 M) until pH 4. The solution was extracted with EtOAc (2 × 3.00 mL). The combined organics were dried (Na_2SO_4), filtered, and concentrated *in vacuo*. The solid was washed with cold water (5.00 mL), followed by hexane (10.0 mL), and dried to afford **11** (113 mg, 75%) as an off-white solid.

^{1}H NMR (400 MHz, DMSO-d_6): δ 8.33 (d, J = 2.2 Hz, 1H), 8.29 (d, J = 2.2 Hz, 1H), 8.20 (s, 1H), 7.75 (d, J = 8.1 Hz, 1H), 7.65 (d, J = 1.8 Hz, 1H), 7.59 (dd, J = 8.1, 1.8 Hz, 1H), 3.91−3.80 (m, 1H) 3.87 (s, 3H), 2.12−1.96 (m, 2H), 1.82 (m, 2H), 1.71−159 (m, 4H); ^{13}C NMR (100 MHz, DMSO-d_6): δ 169.3, 147.0, 146.3, 141.0, 136.9, 130.7, 130.5, 129.1, 126.8, 124.0, 123.4, 123.1, 118.2, 112.3, 41.1, 34.3, 31.3, 25.3; HRMS: calcd for $C_{20}H_{21}N_2O_2$ $[M + H]^+$ m/z, 321.1603; found m/z, 321.1596; mp range 181−184 °C.

*Ethyl 2-Chloronicotinate (**12b**).* To a solution of 2-chloronicotinic acid (5.00 g, 31.7 mmol) in toluene (35.0 mL) was added dropwise with stirring triethyl orthoacetate (17.5 mL, 95.2 mmol). The mixture was heated to reflux for 16 h and allowed to cool to rt, and the resultant solution was washed with sat. $NaHCO_3$ (50.0 mL). The organic phase was dried with $MgSO_4$, and the solvent was removed *in vacuo* to afford the title compound, ethyl 2-chloronicotinate **12b** (5.40 g, 92%), as a clear oil.

^{1}H NMR (400 MHz, DMSO-d_6): δ 8.58 (dd, J = 4.8, 2.0 Hz, 1H), 8.24 (dd, J = 7.7, 2.0 Hz, 1H), 7.57 (dd, J = 7.7, 4.8 Hz, 1H), 4.35 (q, J = 7.1 Hz, 2H), 1.32 (t, J = 7.1 Hz, 3H); ^{13}C NMR (101 MHz, DMSO-d_6): δ 164.1, 152.2, 147.8, 140.2, 127.1, 123.2, 61.8, 13.9; LCMS: $[M + H]^+$ m/z, 186.0.

*Ethyl 5-Bromo-2-chloronicotinate (**13b**).* To a solution of 5-bromo-2-chloronicotinic acid (10.0 g, 42.0 mmol) in ethanol (60.0 mL) was added slowly H_2SO_4 (9.10 g, 5.0 mL, 93.0 mmol). The reaction mixture was heated to reflux for 16 h. The mixture was concentrated *in vacuo*, re-dissolved in aq $NaHCO_3$ (150 mL), and extracted with EtOAc (2 × 300 mL). The combined organic layers were dried over Na_2SO_4 and concentrated to give the desired product, **13b** (10.5 g, 92%), as a light-yellowish oil.

^{1}H NMR (400 MHz, DMSO-d_6): δ 8.76 (d, J = 2.5 Hz, 1H), 8.47 (d, J = 2.5 Hz, 1H), 4.35 (q, J = 7.1 Hz, 2H), 1.33 (t, J = 7.1 Hz, 3H);

https://doi.org/10.1021/acs.jmedchem.0c02274
J. Med. Chem. 2021, 64, 10849−10877

^{13}C NMR (100 MHz, DMSO-d_6): δ 162.88, 152.79, 146.65, 142.12, 128.34, 118.85, 62.24, 13.83; LCMS: $[M + H]^+$ m/z, 186.0.

*Ethyl 2,5-Dichloronicotinate (**14b**).* Prepared following the procedure for **12b** using 2,5-dichloronicotinic acid (10.0 g, 42.0 mmol). After purification, ethyl 2,5-dichloronicotinate **14b** (11.0 g, 99%) was afforded as a clear oil.

^{1}H NMR (400 MHz, DMSO-d_6): δ 8.69 (d, J = 2.6 Hz, 1H), 8.38 (d, J = 2.6 Hz, 1H), 4.35 (q, J = 7.1 Hz, 2H), 1.33 (t, J = 7.1 Hz, 3H). ^{13}C NMR (100 MHz, DMSO-d_6): δ 162.9, 150.6, 146.1, 139.5, 130.3, 128.0, 62.3, 13.8; LCMS: $[M + H]^+$ m/z, 220.1.

*Ethyl 3-Hydroxyfuro[2,3-b]pyridine-2-carboxylate (**12c**).* To a suspension of sodium hydride, 60% dispersed in mineral oil, (5.60 g, 0.14 mol) in 1,2-dimethoxyethane (60.0 mL) was added ethyl 2-hydroxyacetate (13.0 mL, 0.13 mol) under ice cooling and stirring. The ice bath was removed, and the solution was allowed warm to rt. After 30 min, a solution of ethyl 2-chloronicotinate (10.0 g, 54.0 mmol) in 100 mL of 1,2-dimethoxyethane was slowly added and the mixture was heated to 75 °C for 2 h. The solvent was removed *in vacuo*, and the residual solid was re-dissolved in aq $NaHCO_3$ solution (150 mL) and EtOAc (250 mL). The aq layer was acidified with AcOH (pH 4) and extracted with CH_2Cl_2 (3 × 200 mL). The combined organic phases were dried over Na_2SO_4 and concentrated *in vacuo*. Purification by flash column chromatography (10% EtOAc/hexane) afforded ethyl 3-hydroxyfuro[2,3-*b*]pyridine-2-carboxylate **12c** (8.5 g, 76%) as a pale-white solid.

^{1}H NMR (400 MHz, $CDCl_3$): δ 8.53 (dd, J = 4.8, 1.8 Hz, 1H), 8.11 (dd, J = 7.8, 1.8 Hz, 1H), 7.30 (dd, J = 7.8, 4.8 Hz, 1H), 4.48 (q, J = 7.1 Hz, 2H), 1.45 (t, J = 7.1 Hz, 3H).

LCMS: $[M + H]^+$ m/z, 208.1.

*Ethyl 5-Bromo-3-hydroxyfuro[2,3-b]pyridine-2-carboxylate (**13c**).* Prepared following the procedure for **12c** using ethyl 5-bromo-2-chloronicotinate **13b** (18.0 g, 68.0 mmol). After purification, ethyl 5-bromo-3-hydroxyfuro[2,3-*b*]pyridine-2-carboxylate **13c** (19.0 g, 76%) was afforded as a light-brown solid.

^{1}H NMR (400 MHz, DMSO-d_6): δ 11.34−11.30 (m, 1H), 8.58 (d, J = 2.3 Hz, 1H), 8.53 (d, J = 2.3 Hz, 1H), 4.32 (q, J = 7.1 Hz, 2H), 1.31 (t, J = 7.1 Hz, 3H); ^{13}C NMR (100 MHz, DMSO-d_6): δ 158.7, 156.7, 148.8, 144.7, 133.5, 127.2, 115.9, 114.3, 60.4, 14.3; LCMS: $[M + H]^+$ m/z, 286.0.

*Ethyl 5-Chloro-3-hydroxythieno[2,3-b]pyridine-2-carboxylate (**14c**).* Prepared following the procedure for **12c** using ethyl 2,5-dichloronicotinate **14b** (15.0 g, 68.0 mmol) and ethyl 2-mercaptoacetate (15.0 mL, 0.14 mmol). After purification, ethyl 5-chloro-3-hydroxythieno[2,3-*b*]pyridine-2-carboxylate **14c** (12.4 g, 71%) was afforded as a light-orange solid.

^{1}H NMR (400 MHz, DMSO-d_6): δ 11.04 (s, 1H), 8.73 (d, J = 2.4 Hz, 1H), 8.41 (d, J = 2.4 Hz, 1H), 4.33 (q, J = 7.1 Hz, 2H), 1.31 (t, J = 7.1 Hz, 3H); ^{13}C NMR (100 MHz, DMSO-d_6): δ 162.6, 155.7, 152.2, 149.4, 130.3, 127.7, 126.7, 105.5, 61.1, 14.2; LCMS: $[M + H]^+$ m/z, 258.0.

*Furo[2,3-b]pyridin-3(2H)-one (**12d**).* A mixture of ethyl 3-hydroxyfuro[2,3-*b*]pyridine-2-carboxylate **12c** (6.00 g, 30.0 mmol) in ethanol (100 mL) and sodium hydroxide (5.00 g, 100 mmol) dissolved in 15.0 mL of water was refluxed for 1 h. After evaporation of the solvent, the yellow-orange crystalline mass was dissolved in water (100 mL), acidified to pH 2−3 with conc. HCl, and heated to reflux for 45 min. Once cooled, the solution was neutralized with sodium bicarbonate and extracted with chloroform. The organic phase was dried (Na_2SO_4) and filtered, and the solvent was removed *in vacuo* to afford furo[2,3-*b*]pyridin-3(2*H*)-one **12d** (2.70 g, 67%) as a light-brown solid. The title compound was isolated as a mixture of keto−enol tautomers (9:1).

^{1}H NMR (400 MHz, DMSO-d_6): δ 9.71 (s, 0H), 8.60 (dd, J = 4.9, 2.0 Hz, 1H), 8.15 (dd, J = 7.5, 1.9 Hz, 1H), 7.27−7.22 (m, 1H), 4.89 (s, 2H); ^{13}C NMR (101 MHz, DMSO-d_6): δ 197.7, 177.1, 156.9, 134.3, 118.8, 113.6, 74.6; LCMS: $[M + H]^+$ m/z, 136.1.

*5-Bromofuro[2,3-b]pyridin-3(2H)-one (**13d**).* Prepared following the procedure for **12d** using ethyl 5-bromo-3-hydroxyfuro[2,3-*b*]pyridine-2-carboxylate **13c** (10.0 g, 35.0 mmol). After purification, 5-bromofuro[2,3-*b*]pyridin-3(2*H*)-one **13d** (6.30 g, 84%) was afforded as a brown solid.

^{1}H NMR (400 MHz, DMSO-d_6): δ 8.71 (d, J = 2.5 Hz, 1H), 8.42 (d, J = 2.5 Hz, 1H), 4.96 (s, 2H); ^{13}C NMR (100 MHz, DMSO): δ 196.4, 175.6, 156.9, 136.3, 115.5, 113.2, 75.8; LCMS: $[M + H]^+$ m/z, 213.4.

*5-Chlorothieno[2,3-b]pyridin-3(2H)-one (**14d**).* Prepared following the procedure for **12d** using ethyl 5-chloro-3-hydroxythieno[2,3-*b*]pyridine-2-carboxylate **14c** (3.0g, 12 mmol). After purification, 5-chlorothieno[2,3-*b*]pyridin-3(2*H*)-one **14d** (1.0 g, 50%) was isolated as an orange solid composed of keto- and enol-isomers.

^{1}H NMR (400 MHz, DMSO-d_6): δ 10.46 (s, 1H), 8.77 (d, J = 2.5 Hz, 1H), 8.56 (dd, J = 2.3, 0.5 Hz, 1H), 8.16 (d, J = 2.4 Hz, 1H), 8.11 (d, J = 2.5 Hz, 1H), 6.70 (d, J = 0.5 Hz, 1H), 4.18 (s, 2H); ^{13}C NMR (101 MHz, DMSO-d_6): δ 196.8, 172.1, 156.5, 154.7, 145.4, 145.3, 133.2, 127.9, 127.8, 126.9, 126.0, 100.9, 40.8; LCMS: $[M + H]^+$ m/z, 186.4.

*Furo[2,3-b]pyridin-3-yl Trifluoromethanesulfonate (**12e**).* A solution of **12d** (450 mg, 3.33 mmol) in CH_2Cl_2 (8.00 mL) was cooled to 0 °C. DIPEA (0.70 mL, 4.00 mmol) was added, followed by dropwise addition of trifluoromethanesulfonic anhydride (788 μL, 4.66 mmol). The reaction mixture was slowly warmed to rt and stirred for 2 h and then quenched with water. The aqueous phase was extracted with CH_2Cl_2, and the combined organic extracts were dried, filtered, and concentrated *in vacuo*. The residue was purified by column chromatography (10% EtOAc/hexane) to afford furo[2,3-*b*]pyridin-3-yl trifluoromethanesulfonate **12e** (640 mg, 72%) as a brown oil.

^{1}H NMR (400 MHz, $CDCl_3$): δ 8.55−8.41 (m, 1H), 8.03 (dd, J = 7.8, 1.7 Hz, 1H), 7.91 (s, 1H), 7.43−7.35 (m, 1H); ^{13}C NMR (101 MHz, $CDCl_3$): δ 158.81, 146.35, 135.28, 132.54, 129.95, 128.17, 120.11, 118.71 (q, J = 321.6 Hz); LCMS: $[M + H]^+$ m/z, 268.2.

*5-Bromofuro[2,3-b]pyridin-3-yl Trifluoromethanesulfonate (**13e**).* Prepared following the procedure for **12e** using 5-bromofuro-[2,3-*b*]pyridin-3(2*H*)-one **13d** (10.0 g, 47.0 mmol). After purification, 5-bromofuro[2,3-*b*]pyridin-3-yl trifluoromethanesulfonate **13e** (12.8 g, 79%) was isolated as a light-brown oil which solidified upon standing.

^{1}H NMR (400 MHz, $CDCl_3$): δ 8.50 (dd, J = 2.2, 0.4 Hz, 1H), 8.14 (d, J = 2.2 Hz, 1H), 7.92 (s, 1H); LCMS: $[M + H]^+$ m/z, 347.1.

*5-Chlorothieno[2,3-b]pyridin-3-yl Trifluoromethanesulfonate (**14e**).* Prepared following the procedure for **12e** using 5-chlorothieno-[2,3-*b*]pyridin-3(2*H*)-one **14d** (800 mg, 4.31 mmol). After purification, 5-Chlorothieno[2,3-*b*]pyridin-3-yl trifluoromethanesulfonate **14e** (1.00 g, 74%) was isolated as a brown oil.

^{1}H NMR (400 MHz, $CDCl_3$): δ 8.60 (d, J = 2.3 Hz, 1H), 8.02 (d, J = 2.3 Hz, 1H), 7.55 (d, J = 0.5 Hz, 1H); ^{13}C NMR (101 MHz, $CDCl_3$): δ 155.34, 147.62, 134.57, 129.60, 127.41, 125.23, 118.67 (q, J = 321.2 Hz), 118.13; LCMS: $[M + H]^+$ m/z, 318.4.

*2-Cyclopentyl-4-(furo[2,3-b]pyridin-3-yl)benzoic Acid (**12f**).* A microwave vial was loaded with furo[2,3-*b*]pyridin-3-yl trifluoromethanesulfonate **12e** (250 mg, 936 μmol), 2-cyclopentyl-4-(4,4,5,5-tetramethyl-1,3,2-dioxaborolan-2-yl)benzoic acid **3** (444 mg, 1.40 mmol), $Pd(PPh_3)_4$ (11.0 mg, 9.50 μmol), sodium carbonate (397 mg, 3.74 mmol), MeOH (2.00 mL), and CH_2Cl_2 (0.50 mL). The vial was sealed and heated to 90 °C for 2 h. The solution was neutralized with aq HCl (10 mL) and then extracted with ethyl acetate (2 × 20.0 mL). The organic phases were combined and dried (Na_2SO_4), filtered, and concentrated *in vacuo*. The crude was purified *via* column chromatography (30% EtOAc/hexane) to afford **12f** (217 mg, 76%) as an off-white solid.

^{1}H NMR (400 MHz, DMSO-d_6): δ 12.94 (s, 1H), 8.67 (s, 1H), 8.41 (d, J = 6.3 Hz, 2H), 7.81−7.75 (m, 2H), 7.67 (dd, J = 8.0, 1.8 Hz, 1H), 7.52−7.46 (m, 1H), 3.84−3.73 (m, 1H), 2.07−2.03 (m, 2H), 1.86−1.81 (m, 2H), 1.73−1.62 (m, 4H); ^{13}C NMR (101 MHz, DMSO-d_6): δ 169.2, 161.9, 147.0, 144.5, 143.0, 133.7, 131.0, 130.2, 124.8, 123.9, 120.2, 119.9, 117.4, 41.3, 34.3, 25.2; HRMS calcd for $C_{19}H_{17}NO_3$: $[M + H]^+$ m/z, 308.1287; found, 308.1266; mp range 164−168 °C.

https://doi.org/10.1021/acs.jmedchem.0c02274
J. Med. Chem. 2021, 64, 10849−10877

*Methyl 4-(5-Bromofuro[2,3-b]pyridin-3-yl)-2-cyclopentylbenzoate (**13f**).* Prepared following the procedure for **12f** using 5-bromofuro[2,3-*b*]pyridin-3-yl trifluoromethanesulfonate **13e** (100 mg, 0.29 mmol) and **4** (95.4 mg, 0.29 mmol). After purification, methyl 4-(5-bromofuro[2,3-*b*]pyridin-3-yl)-2-cyclopentylbenzoate **13f** (68 mg, 59%) was isolated as an off-white solid.

^{1}H NMR (400 MHz, DMSO-d_6): δ 8.74 (s, 1H), 8.56 (d, J = 1.8 Hz, 1H), 8.48 (d, J = 1.6 Hz, 1H), 7.75 (d, J = 8.2 Hz, 2H), 7.69 (dd, J = 7.9, 1.7 Hz, 1H), 3.85 (s, 3H), 3.71−3.58 (m, 1H), 2.08−1.96 (m, 2H), 1.87−1.76 (m, 2H), 1.73−1.61 (m, 4H); ^{13}C NMR (101 MHz, DMSO-d_6): δ 167.9, 160.5, 147.0, 144.9, 144.8, 133.4, 132.3, 130.2, 130.0, 125.0, 124.1, 119.6, 119.5, 115.3, 52.2, 41.4, 34.2, 25.2.

*Methyl 4-(5-Chlorothieno[2,3-b]pyridin-3-yl)-2-cyclopentylbenzoate (**14f**).* Prepared following the procedure for **12f** using 5-chlorothieno[2,3-*b*]pyridin-3-yl trifluoromethanesulfonate **14e** (950 mg, 2.99 mmol) and **4** (988 mg, 2.99 mmol). After purification, methyl 4-(5-chlorothieno[2,3-*b*]pyridin-3-yl)-2-cyclopentylbenzoate **14f** (870 mg, 78%) was isolated as a near-white solid.

^{1}H NMR (400 MHz, DMSO-d_6): δ 8.69 (d, J = 2.3 Hz, 1H), 8.27−8.24 (m, 2H), 7.79 (d, J = 8.0 Hz, 1H), 7.66 (d, J = 1.8 Hz, 1H), 7.57 (dd, J = 8.0, 1.7 Hz, 1H), 3.87 (s, 3H), 3.71−3.61 (m, 1H), 2.08−2.01 (m, 2H), 1.85−1.75 (m, 2H), 1.69−1.62 (m, 4H); ^{13}C NMR (100 MHz, DMSO-d_6): δ 168.0, 159.5, 147.1, 145.4, 137.1, 133.6, 131.3, 130.2, 130.0, 129.7, 128.1, 128.0, 126.6, 125.3, 52.2, 41.4, 34.3, 25.2.

*2-Cyclopentyl-4-(5-phenylfuro[2,3-b]pyridin-3-yl)benzoic Acid (**13g**).* 4-(5-Bromofuro[2,3-*b*]pyridin-3-yl)-2-cyclopentylbenzoic acid, **13f** (48.0 mg, 0.12 mmol), phenylboronic acid (30.0 mg, 0.25 mmol), Na_2CO_3 (40.0 mg, 0.37 mmol), and $Pd(PPh_3)_4$ (14.0 mg, 12 μmol) were dissolved in a 4:1 mixture of dioxane (2.5 mL) and heated to 90 °C under nitrogen for 16 h. The mixture was neutralized to pH 6−7 with aq HCl and extracted with ethyl acetate (5.00 mL). The combined organics were dried (Na_2SO_4), filtered, and concentrated *in vacuo*. The crude residue was purified using flash column chromatography (30% EtOAc/hexane) to obtain the methyl ester intermediate which was immediately dissolved in MeOH (3.0 mL), added aq NaOH (small excess), and heated to 70 °C for 1 h. After cooling, H_2O (4.0 mL) was added and the mixture was extracted with diethyl ether (2 × 4.0 mL). The aqueous phase was acidified to pH 6 with aq HCl, extracted with CH_2Cl_2 (6.00 mL), and concentrated to afford 2-cyclopentyl-4-(5-phenylfuro[2,3-*b*]pyridin-3-yl)benzoic acid **13g** (39 mg, 82%) as a white solid.

^{1}H NMR (400 MHz, DMSO-d_6): δ 12.95 (s, 1H), 8.72 (s, 1H), 8.67 (d, J = 2.2 Hz, 1H), 8.53 (d, J = 2.2 Hz, 1H), 7.82 (d, J = 1.5 Hz, 1H), 7.81−7.79 (m, 4H), 7.56−7.50 (m, 2H), 7.47−7.41 (m, 1H), 3.86−3.77 (m, 1H), 2.11−2.01 (m, 2H), 1.87−1.79 (m, 2H), 1.73−1.62 (m, 4H); ^{13}C NMR (101 MHz, DMSO-d_6): δ 169.3, 161.6, 147.0, 143.8, 143.2, 137.5, 133.6, 132.9, 131.0, 130.3, 129.1, 128.2, 127.8, 127.5, 125.0, 124.1, 120.2, 117.6, 41.2, 34.4, 25.3; HRMS: calcd for $C_{25}H_{21}NO_3$ [M + H]$^+$ m/z, 384.1600; found, 384.1593; mp range 259−262 °C.

*2-Cyclopentyl-4-(5-phenylthieno[2,3-b]pyridin-3-yl)benzoic Acid (**14g**).* Methyl 4-(5-chlorothieno[2,3-*b*]pyridin-3-yl)-2-cyclopentylbenzoate **14f** (150 mg, 403 μmol), phenylboronic acid (73.8 mg, 605 μmol), $Pd_2(dba)_3$ (18.5 mg, 20.2 μmol), dicyclohexyl(2′,4′,6′-triisopropyl-[1,1′-biphenyl]-2-yl)phosphane (28.8 mg, 60.5 μmol), and Cs_2CO_3 (394 mg, 1.21 mmol) were dissolved in dioxane (3.00 mL) and H_2O (0.8 mL). The solution was heated to 90 °C for 16 h. The reaction mixture was allowed to cool to rt, neutralized to pH 7 with aq HCl, and extracted with ethyl acetate (15 mL). The combined organic phases were dried (Na_2SO_4), filtered, and concentrated *in vacuo*. The crude was purified by column chromatography (25% EtOAc/hexane) to afford the methyl ester intermediate. This material was dissolved in MeOH (6 mL), added aq NaOH (small excess), and heated to 70 °C for 1 h. After cooling, H_2O (8 mL) was added and the mixture was extracted with diethyl ether (2 × 10.0 mL). The aqueous phase was acidified to pH 6, extracted with CH_2Cl_2 (10 mL), and concentrated to afford 2-cyclopentyl-4-(5-phenylthieno[2,3-*b*]pyridin-3-yl)benzoic acid **14g** (116 mg, 72%) as a yellow solid.

^{1}H NMR (400 MHz, DMSO-d_6): δ 12.94 (s, 1H), 8.96 (d, J = 2.1 Hz, 1H), 8.38 (d, J = 2.2 Hz, 1H), 8.17 (s, 1H), 7.83−7.77 (m, 3H), 7.72 (d, J = 1.7 Hz, 1H), 7.62 (dd, J = 8.0, 1.7 Hz, 1H), 7.55−7.50 (m, 2H), 7.47−7.41 (m, 1H), 3.87−3.78 (m, 1H), 2.09−2.04 (m, 2H), 1.83−1.78 (m, 2H), 1.71−1.63 (m, 4H); ^{13}C NMR (100 MHz, DMSO-d_6): δ 169.4, 160.6, 147.0, 145.8, 137.3, 137.3, 134.4, 132.5, 131.2, 130.4, 130.1, 129.2, 128.1, 128.1, 127.3, 126.5, 126.2, 125.3, 41.2, 34.5, 25.3; HRMS: calcd for $C_{25}H_{21}NO_2S$ [M + H]$^+$ m/z, 400.1371; found, 400.1365; mp range 269−273 °C.

*2-Cyclopentyl-4-(thieno[2,3-b]pyridin-3-yl)benzoic Acid (**12g**).* Prepared following the procedure for **12f** using 3-bromothieno[2,3-*b*]pyridine **15e** (50.0 mg, 0.23 mmol). After purification, 2-cyclopentyl-4-(thieno[2,3-*b*]pyridin-3-yl)benzoic acid **12g** (66.0 mg, 88%) was afforded as a light-brown solid.

^{1}H NMR (400 MHz, DMSO-d_6): δ 12.99 (s, 1H), 8.65 (dd, J = 4.6, 1.6 Hz, 1H), 8.27 (dd, J = 8.2, 1.6 Hz, 1H), 8.10 (s, 1H), 7.80 (d, J = 8.0 Hz, 1H), 7.64 (d, J = 1.8 Hz, 1H), 7.56−7.50 (m, 2H), 3.85−3.76 (m, 1H), 2.08−2.03 (m, 2H), 1.82−1.78 (m, 2H), 1.72−1.58 (m, 4H); ^{13}C NMR (176 MHz, DMSO-d_6): δ 172.6, 164.7, 150.1, 149.9, 140.4, 137.4, 134.5, 133.7, 133.4, 133.1, 129.5, 128.4, 128.4, 123.4, 44.4, 37.5, 28.4; HRMS: calcd for $C_{19}H_{17}NO_2S$ [M + H]$^+$ m/z, 324.1058; found, 324.1054; mp range 194−197 °C.

*Methyl 4-(5-Bromopyrazolo[1,5-a]pyridin-3-yl)-2-cyclopentylbenzoate (**17**).* 5-Bromo-3-iodopyrazolo[1,5-*a*]pyridine (200 mg, 0.62 mmol) and methyl 2-cyclopentyl-4-(4,4,5,5-tetramethyl-1,3,2-dioxaborolan-2-yl)benzoate **4** (194 mg, 0.60 mmol) were dissolved in a 3:1 solution of dioxane/water (4.00 mL). $Pd_2(dba)_3$ (28 mg, 31 μmol), XPhos (30.0 mg, 62.0 μmol), and Cs_2CO_3 (605 mg, 1.90 mmol) were added. The mixture was stirred at rt for 16 h. The aqueous phase was removed, and the solution was concentrated *in vacuo*. The crude was purified *via* column chromatography (0−20% EtOAc/hexane) to afford ethyl 4-(5-bromopyrazolo[1,5-*a*]pyridin-3-yl)-2-cyclopentylbenzoate **17** (189 mg, 76%) as a mustard yellow solid.

^{1}H NMR (400 MHz, $CDCl_3$): δ 8.36 (dd, J = 7.3, 0.8 Hz, 1H), 8.16 (s, 1H), 7.94 (dd, J = 2.1, 0.8 Hz, 1H), 7.86 (dd, J = 8.1, 0.4 Hz, 1H), 7.57 (d, J = 1.8 Hz, 1H), 7.40 (dd, J = 8.1, 1.8 Hz, 1H), 6.91 (ddd, J = 7.3, 2.1, 0.4 Hz, 1H), 3.93 (s, 3H), 3.91−3.83 (m, 1H), 2.24−2.11 (m, 2H), 1.93−1.81 (m, 2H), 1.81−1.72 (m, 2H), 1.71−1.61 (m, 2H); ^{13}C NMR (100 MHz, $CDCl_3$): δ 168.5, 148.7, 141.6, 137.6, 135.8, 130.9, 129.7, 128.4, 125.3, 123.7, 119.7, 118.7, 116.0, 112.4, 52.0, 41.7, 34.8, 25.7; HRMS: calcd for $C_{20}H_{20}N_2O_2Br$ [M + H]$^+$ m/z, 399.0708; found m/z, 399.0705; mp range 182−184 °C.

*Methyl 4-(5-Chloropyrazolo[1,5-a]pyrimidin-3-yl)-2-cyclopentylbenzoate (**18**).* 5-Chloro-3-iodopyrazolo[1,5-*a*]pyrimidine (500 mg, 1.79 mmol) and methyl 2-cyclopentyl-4-(4,4,5,5-tetramethyl-1,3,2-dioxaborolan-2-yl)benzoate **4** (591 mg) were dissolved in a 10:1 mixture of dioxane/water (10.0 mL). $Pd(dppf)Cl_2{\cdot}CH_2Cl_2$ (73.0 mg, 0.9 mmol) and Cs_2CO_3 (1.75 g, 5.37 mmol) were added, and the solution was heated to 80 °C for 16 h. The solution was allowed to cool to rt, the aqueous phase was removed, and the organic phase was concentrated *in vacuo*. The crude was purified *via* column chromatography (10−20% EtOAc/hexane) to afford methyl 4-(5-chloropyrazolo[1,5-*a*]pyrimidin-3-yl)-2-cyclopentylbenzoate **18** (270 mg, 44%) as a bright-yellow solid.

^{1}H NMR (400 MHz, $CDCl_3$): δ 8.59 (d, J = 7.2 Hz, 1H), 8.48 (s, 1H), 8.12 (d, J = 1.5 Hz, 1H), 7.92−7.78 (m, 2H), 6.86 (d, J = 7.2 Hz, 1H), 3.99−3.86 (m, 4H), 2.28−2.04 (m, 2H), 1.97−1.84 (m, 2H), 1.84−1.61 (m, 4H); ^{13}C NMR (100 MHz, $CDCl_3$): δ 168.6, 150.8, 148.6, 143.9, 136.5, 134.4, 130.6, 128.3, 124.5, 122.8, 110.1, 109.4, 51.9, 41.7, 34.8, 25.8; HRMS: calcd for $C_{19}H_{19}N_3O_2Cl$ [M + H]$^+$ m/z, 356.1165; found m/z, 356.1161; mp range 163−166 °C.

*2-Cyclopentyl-4-(5-phenylpyrazolo[1,5-a]pyridin-3-yl)benzoic Acid (**19**).* Methyl 4-(5-bromopyrazolo[1,5-*a*]pyridin-3-yl)-2-cyclopentylbenzoate **17** (100 mg, 0.25 mmol), phenylboronic acid (37.0 mg, 0.30 mmol), $Pd(PPh_3)_4$ (29.0 mg, 25.0 μmol), and Cs_2CO_3 (245 mg, 0.75 mmol) were loaded into a microwave vial. A 3:1 mixture of dioxane/water (1.50 mL) was added, and the vial was flushed with nitrogen and sealed. The mixture was irradiated at 120 °C for 30 min. Once cooled, the solution was diluted with EtOAc (2.00 mL) and

https://doi.org/10.1021/acs.jmedchem.0c02274
J. Med. Chem. 2021, 64, 10849−10877

water (2.00 mL). The layers were separated, and the aqueous phase was extracted with EtOAc (2 × 3.00 mL). The combined organics were dried (Na_2SO_4), filtered, and concentrated *in vacuo*. The crude was purified *via* column chromatography (5−10% EtOAc/hexane) to afford the methyl ester intermediate. The methyl ester was saponified in a solution of aq LiOH (1.00 mL, 1.00 M) and dioxane (1.00 mL) at 100 °C for 16 h. The solution was cooled to rt, diluted with water (2.00 mL), and then acidified with aq HCl (1 M) until pH 4. The solution was extracted with EtOAc (2 × 3.00 mL). The combined organics were dried (Na_2SO_4), filtered, and concentrated *in vacuo*. The solid was washed with cold water (5.00 mL), followed by hexane (10.0 mL), and dried to afford the acid (68.0 mg, 71%) as a yellow solid.

^{1}H NMR (700 MHz, DMSO-d_6): δ 8.83 (d, J = 6.9 Hz, 1H), 8.50 (s, 1H), 8.10 (s, 1H), 8.02 (s, 1H), 7.85 (d, J = 7.1 Hz, 2H), 7.79 (d, J = 7.8 Hz, 1H), 7.72 (s, 1H), 7.67 (d, J = 7.6 Hz, 1H), 7.53 (t, J = 6.9 Hz, 2H), 7.45 (t, J = 6.8 Hz, 1H), 7.33 (d, J = 6.8 Hz, 1H), 3.91−3.85 (m, 1H), 2.10−2.01 (m, 2H), 1.88−1.78 (m, 2H), 1.73−1.60 (m, 4H); ^{13}C NMR (176 MHz, DMSO-d_6): δ 169.2, 147.2, 141.4, 137.6, 136.9, 136.5, 135.7, 131.5, 131.4, 130.5, 129.7, 129.3, 129.1, 128.9, 128.7, 128.5, 126.7, 124.5, 123.4, 113.5, 111.9, 111.7, 41.1, 34.3, 25.3; HRMS: calcd for $C_{25}H_{23}N_2O_2$ [M + H]$^+$ m/z, 383.1759; found m/z, 383.1754; mp range 153−155 °C.

*2-Cyclopentyl-4-(5-phenylpyrazolo[1,5-a]pyrimidin-3-yl)benzoic Acid (**20**).* Methyl 4-(5-chloropyrazolo[1,5-*a*]pyrimidin-3-yl)-2-cyclopentylbenzoate **18** (100 mg, 0.28 mmol), phenylboronic acid (41.0 mg, 0.33 mmol), $Pd(PPh_3)_4$ (32.0 mg, 28.0 μmol), and Cs_2CO_3 (275 mg, 0.84 mmol) were loaded into a microwave vial. A 3:1 mixture of dioxane/water (2.00 mL) was added, and the vial was flushed with nitrogen and capped. The solution was irradiated at 120 °C for 30 min. Once cooled, the solution was diluted with EtOAc (2.00 mL) and water (2.00 mL). The layers were separated, and the aqueous phase was extracted with EtOAc (2 × 3.00 mL). The combined organics were dried (Na_2SO_4), filtered, and concentrated *in vacuo*. The crude was purified *via* column chromatography (5−10% EtOAc/hexane) to afford the methyl ester intermediate. The methyl ester was saponified in a solution of aq LiOH (1.00 mL, 1.00 M) and dioxane (1.00 mL) at 100 °C for 16 h. The solution was cooled to rt, diluted with water (2.00 mL), and then acidified with aq HCl (1.00 M) until pH 4. The solution was extracted with EtOAc (2 × 3.00 mL). The combined organics were dried (Na2SO4), filtered, and concentrated *in vacuo*. The solid was washed with cold water (5.00 mL), followed by hexane (10.0 mL), and dried to afford 2-cyclopentyl-4-(5-phenylpyrazolo[1,5-*a*]pyrimidin-3-yl)benzoic acid **20** (87.0 mg, 81%) as a bright-yellow solid.

^{1}H NMR (700 MHz, DMSO-d_6): δ 12.94 (s, 1H), 9.24 (dd, J = 7.6, 2.8 Hz, 1H), 8.87 (s, 1H), 8.65 (s, 1H), 8.39−8.28 (m, 2H), 7.95 (d, J = 8.1 Hz, 1H), 7.84−7.72 (m, 2H), 7.61−7.55 (m, 3H), 3.98−3.91 (m, 1H), 2.15−2.09 (m, 2H), 1.93−1.86 (m, 2H), 1.77−1.68 (m, 4H); ^{13}C NMR (176 MHz, DMSO-d_6): 169.2, 155.9, 147.3, 144.3, 143.6, 137.0, 136.6, 135.3, 131.0, 130.1, 129.0 (2 × ArCH), 128.4, 127.2 (2 × ArCH), 123.8, 122.1, 108.2, 105.9, 41.0, 34.7, 25.6; HRMS: calcd for $C_{24}H_{22}N_3O_2$ [M + H]$^+$ m/z, 384.1712; found, m/z 384.1707; mp range 210−214 °C.

*2-Cyclopentyl-4-(pyrazolo[1,5-a]pyridin-3-yl)benzoic Acid (**21**).* 3-Bromopyrazolo[1,5-*a*]pyridine (100 mg, 0.50 mmol), 2-cyclopentyl-4-(4,4,5,5-tetramethyl-1,3,2-dioxaborolan-2-yl)benzoic acid **3** (193 mg, 0.61 mmol), $Pd_2(dba)_3$ (23.0 mg, 25.0 μmol), XPhos (24.0 mg, 51.0 μmol), and Cs_2CO_3 (579 mg, 1.80 mmol) were loaded into a microwave vial. A 3:1 mixture of dioxane/water (3.00 mL) was added, and the vial was flushed with nitrogen and sealed. The mixture was heated to 120 °C for 16 h. Once cooled, the solution was diluted with EtOAc (2.00 mL) and water (2.00 mL). The mixture was acidified to pH 4 with 1.00 M aq HCl solution. The layers were separated, and the aqueous phase was extracted with EtOAc (2 × 3.00 mL). The combined organics were dried (Na_2SO_4), filtered, and concentrated *in vacuo*. The crude was purified *via* column chromatography (50−100% EtOAc/hexane) to afford 2-cyclopentyl-4-(pyrazolo[1,5-*a*]pyridin-3-yl)benzoic acid **21** (64.0 mg, 41%) as a yellow solid.

^{1}H NMR (400 MHz, DMSO-d_6): δ 12.78 (br s, 1H), 8.76 (d, J = 7.0 Hz, 1H), 8.47 (s, 1H), 7.94 (d, J = 9.0 Hz, 1H), 7.77 (d, J = 8.1 Hz, 1H), 7.67 (d, J = 1.6 Hz, 1H), 7.57 (dd, J = 8.1, 1.7 Hz, 1H), 7.39 (ddd, J = 8.9, 6.7, 1.0 Hz, 1H), 6.99 (td, J = 6.9, 1.1 Hz, 1H), 3.90−3.79 (m, 1H), 2.09−1.97 (m, 2H), 1.88−1.76 (m, 2H), 1.73−1.58 (m, 4H); ^{13}C NMR (101 MHz, DMSO-d_6): δ 169.2, 147.1, 140.8, 136.3, 135.8, 130.5, 129.6, 128.7, 125.4, 124.2, 123.2, 117.1, 112.7, 110.9, 41.2, 34.3, 25.2; HRMS (ESI): calcd for $C_{19}H_{19}N_2O_2$ [M + H]$^+$ m/z, 307.1446; found m/z, 307.1439; mp range 167−169 °C.

*2-Cyclopentyl-4-(pyrazolo[1,5-a]pyrimidin-3-yl)benzoic Acid (**22**).* 3-Bromopyrazolo[1,5-*a*]pyrimidine (150 mg, 0.75 mmol), 2-cyclopentyl-4-(4,4,5,5-tetramethyl-1,3,2-dioxaborolan-2-yl)benzoic acid **3** (287 mg, 0.90 mmol), $Pd(PPh_3)_4$ (87.0 mg, 75.0 μmol), and Cs_2CO_3 (864 mg, 2.65 mmol) were loaded into a microwave vial. A 3:1 mixture of dioxane/water (2.00 mL) was added, and the vial was flushed with nitrogen and capped. The solution was irradiated at 120 °C for 30 min. Once cooled, the solution was diluted with EtOAc (2.00 mL) and water (2.00 mL). The mixture was acidified to pH 4 with 1 M aq HCl solution. The layers were separated, and the aqueous phase was extracted with EtOAc (2 × 3.00 mL). The combined organics were dried (Na_2SO_4), filtered, and concentrated *in vacuo*. The crude was purified *via* column chromatography (50−100% EtOAc/hexane) to afford 2-cyclopentyl-4-(pyrazolo[1,5-*a*]pyrimidin-3-yl)benzoic acid **22** (137 mg, 59%) as a bright-yellow solid.

^{1}H NMR (700 MHz, DMSO-d_6): δ 12.74 (br s, 1H), 9.24−9.12 (d, J = 6.0 Hz, 1H), 8.87 (d, J = 2.9 Hz, 1H), 8.72 (s, 1H), 8.25 (s, 1H), 8.03 (d, J = 8.2 Hz, 1H), 7.75 (dd, J = 8.1, 2.8 Hz, 1H), 7.14 (dt, J = 7.4, 3.5 Hz, 1H), 3.89−3.83 (m, 1H), 2.08−2.01 (m, 2H), 1.88−1.82 (m, 2H), 1.71−1.63 (m, 4H); ^{13}C NMR (176 MHz, DMSO-d_6): δ 169.3, 150.9, 146.9, 144.5, 143.2, 136.6, 135.0, 130.1, 128.6, 123.6, 122.5, 109.0, 108.2, 41.2, 34.3, 25.2; HRMS: calcd for $C_{18}H_{18}N_3O_2$ [M + H]$^+$ m/z, 308.1399; found m/z, 308.1393; mp range 196−199 °C.

*Methyl 4-(6-Chloro-[1,2,4]triazolo[4,3-b]pyridazin-3-yl)-2-cyclopentylbenzoate (**24**).* 3-Bromo-6-chloro-[1,2,4]triazolo[4,3-*b*]-pyridazine (924 mg, 3.96 mmol), methyl 2-cyclopentyl-4-(4,4,5,5-tetramethyl-1,3,2-dioxaborolan-2-yl)benzoate **4** (1.31 g, 3.96 mmol), K_2CO_3 (1.64 g, 11.9 mmol), and $Pd(PPh_3)_4$ (320 mg, 0.28 mmol) in a mixture of dioxane (12.0 mL) and water (3.00 mL) were degassed and put under a N_2 atmosphere. The reaction mixture was heated to 90 °C and stirred for 16 h. The reaction mixture was diluted with aq HCl (50.0 mL) to pH 6 and extracted with EtOAc (2 × 75.0 mL), and the combined organic phases were concentrated *in vacuo*. The crude residue was purified *via* column chromatography (35% EtOAc/hexane) to afford methyl 4-(6-chloro-[1,2,4]triazolo[4,3-*b*]pyridazin-3-yl)-2-cyclopentylbenzoate **24** (1.20 g, 85%) as a grayish solid. ^{1}H NMR (400 MHz, DMSO-d_6): δ 8.58 (d, J = 9.7 Hz, 1H), 8.47 (d, J = 1.7 Hz, 1H), 8.21 (dd, J = 8.2, 1.7 Hz, 1H), 7.87 (d, J = 8.2 Hz, 1H), 7.59 (d, J = 2.8 Hz, 1H), 3.88 (s, 3H), 3.77−3.66 (m, 1H), 2.14−2.03 (m, 2H), 1.91−1.79 (m, 2H), 1.75−1.58 (m, 4H). LCMS: [M + H]$^+$ m/z, 356.2.

*2-Cyclopentyl-4-(6-phenyl-[1,2,4]triazolo[4,3-b]pyridazin-3-yl)-benzoic Acid (**25**).* Following the procedure for **14g** using 4-(6-chloro-[1,2,4]triazolo[4,3-*b*]pyridazin-3-yl)-2-cyclopentylbenzoate **24** (220 mg, 0.62 mmol). After purification, cyclopentyl-4-(6-phenyl-[1,2,4]triazolo[4,3-*b*]pyridazin-3-yl)benzoic acid **25** (200 mg, 84%) was afforded as a near-yellow solid.

^{1}H NMR (400 MHz, DMSO-d_6): δ 13.14 (s, 1H), 8.74 (d, J = 1.7 Hz, 1H), 8.58 (d, J = 9.8 Hz, 1H), 8.32 (dd, J = 8.2, 1.7 Hz, 1H), 8.21−8.18 (m, 2H), 8.07 (d, J = 9.8 Hz, 1H), 7.89 (d, J = 8.2 Hz, 1H), 7.65−7.59 (m, 3H), 3.91−3.82 (m, 1H), 2.15−2.11 (m, 2H), 1.88−1.83 (m, 2H), 1.72−1.66 (m, 4H); ^{13}C NMR (100 MHz, DMSO-d_6): δ 169.2, 153.5, 146.6, 146.4, 144.5, 134.1, 133.0, 131.1, 129.7, 129.1, 128.7, 127.4, 125.6, 125.2, 124.2, 119.9, 41.1, 34.7, 25.6; HRMS: calcd for $C_{23}H_{20}N_4O_2$ [M + H]$^+$ m/z, 385.1665; found, 385.1659; mp range 228−231 °C.

*4-([1,2,4]Triazolo[4,3-b]pyridazin-3-yl)-2-cyclopentylbenzoic Acid (**26**).* 3-Bromo-[1,2,4]triazolo[4,3-*b*]pyridazine (150 mg, 754 μmol), methyl 2-cyclopentyl-4-(4,4,5,5-tetramethyl-1,3,2-dioxaborolan-2-yl)benzoate **4** (373 mg, 1.13 mmol), XPhos (53.9 mg, 113

https://doi.org/10.1021/acs.jmedchem.0c02274
J. Med. Chem. 2021, 64, 10849−10877

μmol), Cs_2CO_3 (516 mg, 1.58 mmol), and $Pd_2(dba)_3$ (34.5 mg, 0.04 mmol) in a 3:1 mixture of dioxane/water (4.00 mL) were heated to 90 °C under a N_2 atmosphere for 16 h. The reaction mixture was diluted with aq HCl (25.0 mL, pH 6) and extracted with EtOAc (2 × 50.0 mL); the organic phases were combined, concentrated, and purified using flash column chromatography (40% EtOAc/hexane) to afford 4-([1,2,4]triazolo[4,3-*b*]pyridazin-3-yl)-2-cyclopentylbenzoic acid **26** (178.0 mg, 77%) as an off-white solid.

^{1}H NMR (400 MHz, DMSO-d_6): δ 13.14 (s, 1H), 8.79 (dd, *J* = 4.3, 1.5 Hz, 1H), 8.50−8.46 (m, 2H), 8.29 (dd, *J* = 8.2, 1.7 Hz, 1H), 7.86 (d, *J* = 8.2 Hz, 1H), 7.44 (dd, *J* = 9.4, 4.3 Hz, 1H), 3.86−3.75 (m, 1H), 2.14−2.04 (m, 2H), 1.89−1.79 (m, 2H), 1.74−1.58 (m, 4H); ^{13}C NMR (100 MHz, DMSO-d_6): δ 169.2, 146.8, 146.4, 146.3, 145.1, 133.1, 129.6, 128.6, 125.4, 125.3, 124.1, 120.9, 41.3, 34.4, 25.3; HRMS: calcd for $C_{17}H_{16}N_4O_2$ [M + H]$^+$ *m*/*z*, 309.1352; found, 309.1346; mp range 208−211 °C.

*4-Chloro-1-methyl-2-phenyl-1H-pyrrolo[2,3-b]pyridine (**28**).* 4-Chloro-2-iodo-1-methyl-1*H*-pyrrolo[2,3-*b*]pyridine (75.0 mg, 0.25 mmol), phenylboronic acid (31.0 mg, 0.25 mmol), Cs_2CO_3 (251 mg, 0.77 mmol), and $Pd(PPh_3)_4$ (30.0 mg, 0.02 mmol) were loaded into a microwave vial. A 3:1 mixture of dioxane/water (2.00 mL) was added, and the vial was flushed with nitrogen and capped. The solution was irradiated at 120 °C for 30 min. Once cooled, the solution was diluted with EtOAc (2.00 mL) and water (2.00 mL). The layers were separated, and the aqueous phase was extracted with EtOAc (2 × 3.00 mL). The combined organics were dried (Na_2SO_4), filtered, and concentrated *in vacuo*. The crude was purified *via* column chromatography (10% EtOAc/hexane) to afford 4-chloro-1-methyl-2-phenyl-1*H*-pyrrolo[2,3-*b*]pyridine **28** (58.0 mg, 93%) as a white-gray solid.

^{1}H NMR (400 MHz, $CDCl_3$): δ 8.23 (d, *J* = 5.2 Hz, 1H), 7.63−7.40 (m, 5H), 7.12 (d, *J* = 5.2 Hz, 1H), 6.63 (s, 1H), 3.89 (s, 3H); ^{13}C NMR (101 MHz, $CDCl_3$): δ 149.6, 142.6, 142.5, 135.3, 131.7, 129.1 (2 × ArCH), 128.7 (2 × ArCH), 128.6, 119.9, 116.2, 97.9, 30.3; mp range 113−116 °C.

*2-Cyclopentyl-4-(1-methyl-2-phenyl-1H-pyrrolo[2,3-b]pyridin-4-yl)benzoic Acid (**29**).* 4-Chloro-1-methyl-2-phenyl-1*H*-pyrrolo[2,3-*b*]pyridine **28** (60.0 mg, 0.25 mmol), methyl 2-cyclopentyl-4-(4,4,5,5-tetramethyl-1,3,2-dioxaborolan-2-yl)benzoate **4** (98.0 mg, 0.30 mmol), $Pd(PPh_3)_4$ (29.0 mg, 25.0 μmol), and Cs_2CO_3 (242 mg, 0.74 mmol) were loaded into a microwave vial. A 3:1 mixture of dioxane/water (2.00 mL) was added, and the vial was flushed with nitrogen and capped. The solution was irradiated at 120 °C for 30 min. Once cooled, the solution was diluted with EtOAc (2.00 mL) and water (2.00 mL). The layers were separated, and the aqueous phase was extracted with EtOAc (2 × 3.00 mL). The combined organics were dried (Na_2SO_4), filtered, and concentrated *in vacuo*. The crude was purified *via* column chromatography (5−10% EtOAc/hexane) to afford the methyl-substituted ester intermediate. The methyl ester was saponified in a solution of aq LiOH (1.00 mL, 1.00 M) and dioxane (1.00 mL) at 100 °C for 16 h. The solution was cooled to rt, diluted with water (2.00 mL), and then acidified with aq HCl (1.00 M) until pH 4. The solution was extracted with EtOAc (2 × 3.00 mL). The combined organics were dried (Na_2SO_4), filtered, and concentrated *in vacuo*. The solid was washed with cold water (5.00 mL), followed by hexane (10.0 mL), and dried to afford 2-cyclopentyl-4-(1-methyl-2-phenyl-1*H*-pyrrolo[2,3-*b*]pyridin-4-yl)-benzoic acid **29** (79.0 mg, 80%) as a brown-yellow solid.

^{1}H NMR (700 MHz, DMSO-d_6): δ 8.40 (d, *J* = 4.9 Hz, 1H), 7.82 (d, *J* = 8.0 Hz, 1H), 7.80 (d, *J* = 1.7 Hz, 1H), 7.71 (t, *J* = 7.7 Hz, 3H), 7.56 (t, *J* = 7.5 Hz, 2H), 7.50 (t, *J* = 7.4 Hz, 1H), 7.33 (d, *J* = 4.9 Hz, 1H), 6.73 (s, 1H), 3.89 (s, 3H), 3.86−3.76 (m, 1H), 2.12−2.04 (m, 2H), 1.84−1.77 (m, 2H), 1.70−1.59 (m, 4H); ^{13}C NMR (176 MHz, DMSO-d_6): δ 169.3, 149.5, 146.7, 143.0, 142.2, 140.8, 139.4, 131.8, 131.6, 130.0, 128.9 (2 × ArCH), 128.8 (2 × ArCH), 128.6, 126.5, 125.5, 117.5, 115.1, 98.1, 41.2, 34.4, 29.9, 25.3; HRMS: calcd for $C_{26}H_{25}N_2O_2$ [M + H]$^+$ *m*/*z*, 397.1916; found *m*/*z*, 397.1908; mp range 187−189 °C.

*2-Cyclopentyl-4-(1-methyl-1H-pyrrolo[2,3-b]pyridin-4-yl)benzoic Acid (**30**).* 4-Chloro-1-methyl-1*H*-pyrrolo[2,3-*b*]pyridine (75.0 mg, 0.45 mmol), methyl 2-cyclopentyl-4-(4,4,5,5-tetramethyl-1,3,2-dioxaborolan-2-yl)benzoate **4** (180 mg, 0.54 mmol), $Pd(PPh_3)_4$ (52.0 mg, 45.0 μmol), and Cs_2CO_3 (440 mg, 1.40 mmol) were loaded into a microwave vial. A 3:1 mixture of dioxane/water (3.00 mL) was added, and the vial was flushed with nitrogen and capped. The solution was irradiated at 120 °C for 30 min. Once cooled, the solution was diluted with EtOAc (2.00 mL) and water (2.00 mL). The layers were separated, and the aqueous phase was extracted with EtOAc (2 × 3.00 mL). The combined organics were dried (Na_2SO_4), filtered, and concentrated *in vacuo*. The crude was purified *via* column chromatography (5−10% EtOAc/hexane) to afford the methyl ester intermediate. The methyl ester was saponified in a solution of aq LiOH (1.00 mL, 1.00 M) and dioxane (1.00 mL) at 100 °C for 16 h. The solution was cooled to rt, diluted with water (2.00 mL), and then acidified with aq HCl (1.00 M) until pH 4. The solution was extracted with EtOAc (2 × 3.00 mL). The combined organics were dried (Na_2SO_4), filtered, and concentrated *in vacuo*. The solid was washed with cold water (5.00 mL), followed by hexane (10.0 mL), and dried to afford 2-cyclopentyl-4-(1-methyl-1*H*-pyrrolo[2,3-*b*]pyridin-4-yl)-benzoic acid **30** (97.0 mg, 67%) as a pale-yellow solid.

^{1}H NMR (700 MHz, DMSO-d_6): δ 13.01 (s, 1H), 8.36 (s, 1H), 7.81 (d, *J* = 7.6 Hz, 1H), 7.76 (s, 1H), 7.67−7.61 (m, 2H), 7.27 (s, 1H), 6.57 (s, 1H), 3.87 (s, 3H), 3.80 (dd, *J* = 19.7, 12.5 Hz, 1H), 2.13−2.00 (m, 2H), 1.87−1.74 (m, 2H), 1.71−1.56 (m, 4H); ^{13}C NMR (100 MHz, DMSO-d_6): δ 169.3, 147.9, 146.6, 142.6, 140.8, 139.9, 131.7, 131.0, 129.9, 126.5, 125.4, 117.5, 114.3, 97.8, 41.1, 34.4, 31.2, 25.3; HRMS: calcd for $C_{20}H_{21}N_2O_2$ [M + H]$^+$ *m*/*z*, 321.1603; found *m*/*z*, 321.1595; mp range 201−203 °C.

*Methyl 2-Cyclopentyl-4-(2,3-diaminopyridin-4-yl)benzoate (**32**).* 4-Chloropyridine-2,3-diamine (103 mg, 0.71 mmol) and methyl 2-cyclopentyl-4-(4,4,5,5-tetramethyl-1,3,2-dioxaborolan-2-yl)benzoate **4** (250 mg, 0.75 mmol) were dissolved in a 10:1 mixture of dioxane/H_2O (10.0 mL). $Pd_2(dba)_3$ (69.0 mg, 75 μmol), XPhos (72.0 mg, 150 μmol), and Cs_2CO_3 (740 mg, 2.30 mmol) were added. The solution was heated to 100 °C for 16 h. Once cooled to rt, the aqueous phase was removed and the organic phase was concentrated *in vacuo*. The crude was purified *via* column chromatography (25−75% EtOAc/hexane) to afford methyl 2-cyclopentyl-4-(2,3-diaminopyridin-4-yl)benzoate **32** (169 mg, 71%) as a dark-brown solid.

^{1}H NMR (400 MHz, $CDCl_3$): δ 7.82 (d, *J* = 8.0 Hz, 1H), 7.66 (d, *J* = 5.3 Hz, 1H), 7.47 (d, *J* = 1.8 Hz, 1H), 7.31−7.23 (dd, 1H), 6.61 (d, *J* = 5.3 Hz, 1H), 4.63 (br s, 2H), 3.93 (s, 3H), 3.86−3.71 (m, 1H), 3.61 (br s, 2H), 2.19−2.07 (m, 2H), 1.90−1.73 (m, 2H), 1.75−1.65 (m, 2H), 1.65−1.50 (m, 2H); ^{13}C NMR (100 MHz, $CDCl_3$): δ 168.5, 149.1, 148.4, 140.6, 136.8, 133.8, 130.4, 130.4, 127.2, 126.6, 125.5, 116.3, 52.2, 41.7, 35.0, 25.7; HRMS: calcd for $C_{18}H_{22}N_3O_2$ [M + H]$^+$ *m*/*z*, 312.1712; found *m*/*z*, 312.1704; mp range 125−129 °C.

*2-Cyclopentyl-4-(3H-imidazo[4,5-b]pyridin-7-yl)benzoic Acid (**33**).* Methyl 2-cyclopentyl-4-(2,3-diaminopyridin-4-yl)benzoate **32** (100 mg, 0.32 mmol) was dissolved in MeOH (1 mL). Sulfamic acid (3.00 mg, 32.0 μmol) and trimethyl orthoformate (85.0 mg, 0.80 mmol) were added, and the mixture was stirred at rt for 1 h. The solvent was removed *in vacuo*, and the residue was dissolved in EtOAc (10.0 mL) and water (10.0 mL). The phases were separated, and the aqueous phase was extracted with EtOAc (2 × 10.0 mL). The combined organics were dried (Na_2SO_4), filtered, and concentrated *in vacuo*. The crude residue was purified by column chromatography (50−100% EtOAc/hexane). The isolated methyl ester was dissolved in dioxane (1.00 mL) and aq LiOH (1.00 mL of a 1.00 M solution). The solution was heated to 100 °C for 16 h, cooled, and diluted with EtOAc (3.00 mL) and water (3.00 mL). The mixture was acidified to pH 4 with 1.00 M aq HCl solution. The layers were separated, and the aqueous phase was extracted with EtOAc (3 × 3.00 mL). The combined organics were dried (Na_2SO_4), filtered, and concentrated *in vacuo* to afford 2-cyclopentyl-4-(3H-imidazo[4,5-*b*]pyridin-7-yl)-benzoic acid **33** (45 mg, 46%) as a white solid.

^{1}H NMR (700 MHz, DMSO-d_6): δ 13.23 (s, 1H), 8.51 (s, 1H), 8.45 (s, 1H), 8.41 (d, *J* = 4.7 Hz, 1H), 8.11 (d, *J* = 8.1 Hz, 1H), 7.79 (d, *J* = 8.1 Hz, 1H), 7.59 (d, *J* = 4.7 Hz, 1H), 3.80 (t, *J* = 8.7 Hz, 1H), 2.10−2.03 (br m, 2H), 1.87−1.73 (br m, 2H), 1.67 (m, 4H); ^{13}C

https://doi.org/10.1021/acs.jmedchem.0c02274
J. Med. Chem. 2021, 64, 10849−10877

NMR (176 MHz, DMSO-d_6): δ 171.9, 169.4, 148.8, 146.1, 144.2, 143.8, 138.2, 136.5, 132.1, 131.8, 129.3, 127.6, 125.8, 115.3, 41.3, 34.4, 25.2; HRMS: calcd for $C_{18}H_{18}N_3O_2$ $[M + H]^+$ m/z, 308.1399; found, m/z 308.1392; mp range 183−186 °C.

*2-Cyclopentyl-4-(2-phenyl-3H-imidazo[4,5-b]pyridin-7-yl)-benzoic Acid (**34**).* Benzoic acid (47.0 mg, 0.38 mmol) and CDI (63.0 mg, 0.38 mmol) were loaded into a microwave vial and dissolved in dimethylformamide (DMF) (1.0 mL). The solution was cooled to 0 °C and stirred for 30 min. Methyl 2-cyclopentyl-4-(2,3-diaminopyridin-4-yl)benzoate **4** (100 mg, 0.32 mmol) was added, and the vial was sealed. The mixture was heated to 200 °C for 10 min and allowed to cool to rt, and water (3.00 mL) was added, causing a precipitate to form. The precipitate was filtered and washed with cold water (10.0 mL) and hexane (10.0 mL). The precipitate was dissolved in dioxane (1.00 mL) and aq LiOH (1.00 mL of a 1.00 M solution). The solution was heated to 100 °C for 16 h and then diluted with EtOAc (3.00 mL) and water (3.00 mL). The mixture was acidified to pH 4 with 1 M aq HCl solution. The layers were separated, and the aqueous phase was extracted with EtOAc (3 × 3.00 mL). The combined organics were dried (Na_2SO_4), filtered, and concentrated *in vacuo*. The crude was purified *via* column chromatography (50−100% EtOAc/hexane) to afford 2-cyclopentyl-4-(2-phenyl-3H-imidazo[4,5-*b*]pyridin-7-yl)benzoic acid **34** (93.0 mg, 76%) as a white solid.

^{1}H NMR (700 MHz, DMSO-d_6): δ 8.55−8.44 (m, 2H), 8.33 (d, J = 6.3 Hz, 2H), 8.05 (d, J = 6.7 Hz, 1H), 7.84 (d, J = 7.8 Hz, 1H), 7.67 (s, 1H), 7.61 (d, J = 6.6 Hz, 3H), 3.93−3.79 (m, 1H), 2.18−2.05 (m, 2H), 1.93−1.83 (m, 2H), 1.82−1.66 (m, 4H); ^{13}C NMR (176 MHz, DMSO-d_6): δ 169.4, 150.2, 146.6, 137.7, 132.4, 131.1, 129.5, 129.1, 128.0, 127.1, 125.6, 116.2, 41.1, 39.5, 34.5, 25.4; HRMS: calcd for $C_{24}H_{22}N_3O_2$ $[M + H]^+$ m/z, 384.1712; found m/z, 384.1704; mp range 196−199 °C.

*4-Chloro-6-iodothieno[3,2-d]pyrimidine (**35b**).* An oven-dried 250 mL three-neck round-bottom flask provided with a pressure-equalizing addition funnel was cooled under N_2. 4-Chlorothieno[3,2-*d*]pyrimidine **35a** (3.40 g, 20.0 mmol) was added under positive N_2 pressure, followed by the addition of anhydrous THF (65.0 mL). The solution was cooled down to −78 °C; LDA (12.0 mL, 24.0 mmol) was added dropwise over 5 min, and the mixture was stirred at −78 °C for 20 min. A solution of I_2 (6.08 g, 24.0 mmol) in anhydrous THF (15.0 mL) was added dropwise over 10 min using the equalizing addition funnel. The resulting mixture was stirred at −78 °C for 30 min, allowed to warm up to rt over 1 h, and then stirred for 16 h. The reaction was quenched with saturated NH_4Cl/ice and diluted with $CHCl_3$ (200 mL). The layers were separated, and the aqueous layer was extracted with $CHCl_3$ (2 × 50.0 mL). The combined organics were rinsed with aq $Na_2S_2O_3$ (2 × 25.0 mL) and sat. NaCl solution (2 × 25.0 mL), dried (Na_2SO_4), filtered, and concentrated *in vacuo*. The crude was purified *via* column chromatography (0−100% hexane/EtOAc), affording 4-chloro-6-iodothieno[3,2-*d*]pyrimidine **35b** (4.60 g, 68%) as a clear brown solid.

^{1}H NMR (400 MHz, $CDCl_3$): δ 8.90 (s, 1H), 7.84 (s, 1H); ^{13}C NMR (176 MHz, DMSO-d_6): δ 162.6, 154.9, 154.8, 151.7, 134.8, 134.2, 97.4.

*4-Chloro-6-phenylthieno[3,2-d]pyrimidine (**36**).* 4-Chloro-6-iodothieno[3,2-*d*]pyrimidine **35b** (1.01 mmol, 300 mg), phenylboronic acid (1.01 mmol, 125 mg), $NaHCO_3$ (1.01 mmol, 85.0 mg), CsF (1.01 mmol, 155 mg), and $Pd(Ph_3)_4$ (35.0 mg, 0.03 mmol) were dissolved in a 3:1 mixture of dioxane/water (7.00 mL). The reaction mixture was stirred at reflux for 3 h. The volatiles were removed under reduced pressure, and the crude was purified *via* column chromatography (hexane/EtOAc 0−30%) to afford 4-chloro-6-phenylthieno[3,2-*d*]pyrimidine **36** (175 mg, 70%) as a white solid.

^{1}H NMR (400 MHz, DMSO-d_6): δ 9.04 (s, 1H), 8.26 (s, 1H), 8.05−7.97 (m, 2H), 7.62−7.52 (m, 3H).

*2-Cyclopentyl-4-(6-phenylthieno[3,2-d]pyrimidin-4-yl)benzoic Acid (**37**).* A 5 mL microwave vial was loaded with pyrimidine **36** (55.0 mg, 0.22 mmol) and 2-cyclopentyl-4-(4,4,5,5-tetramethyl-1,3,2-dioxaborolan-2-yl)benzoic acid **3** (70.0 mg, 0.22 mmol), Cs_2CO_3 (0.45 mmol, 150 mg), and $Pd(Ph_3)_4$ (5 mol %, 13.0 mg). The solids were dissolved in a solution of 1,4-dioxane/water (3:1, 1.50 mL). The vial was sealed, and the reaction mixture was irradiated at 125 °C for 15 min. The volatiles were removed *in vacuo*, and remaining solids were suspended in ice/water before the pH was adjusted to 2−3 with 2 M HCl. After an initial purification over silica gel, the compound was further purified by recrystallization from diethyl ether, affording 2-cyclopentyl-4-(6-phenylthieno[3,2-*d*]pyrimidin-4-yl)benzoic acid **37** (12.0 mg, 15%) as a white solid.

^{1}H NMR (400 MHz, DMSO-d_6): δ 13.25 (s, 1H), 9.30 (s, 1H), 8.23 (s, 2H), 8.07 (dd, J = 8.1, 1.8 Hz, 1H), 8.00 (dd, J = 7.1, 2.5 Hz, 2H), 7.89 (d, J = 8.1 Hz, 1H), 7.62−7.52 (m, 3H), 3.80 (p, J = 8.3 Hz, 1H), 2.18−2.06 (m, 2H), 1.92−1.78 (m, 2H), 1.75−1.60 (m, 4H); ^{13}C NMR (176 MHz, DMSO-d_6): δ 169.2, 162.98, 157.7, 155.2, 153.6, 146.6, 138.9, 134.4, 131.9, 130.6, 129.8, 129.5, 127.4, 126.8, 126.6, 125.4, 120.3, 41.3, 34.5, 25.3; HRMS calcd for $C_{24}H_{20}N_2O_2S$ $[M + H]^+$, 401.1324; found, 401.1329; mp range >250 °C.

*2-Cyclopentyl-4-(thieno[3,2-d]pyrimidin-4-yl)benzoic Acid (**38**).* A 5 mL microwave vial was loaded with 4-chlorothieno[3,2-*d*]pyrimidine **35a** (0.41 mmol, 70.0 mg), 2-cyclopentyl-4-(4,4,5,5-tetramethyl-1,3,2-dioxaborolan-2-yl)benzoic acid **3** (0.41 mmol, 130 mg), Cs_2CO_3 (0.82 mmol, 270 mg), and $Pd(Ph_3)_4$ (5 mol %, 25.0 mg). The solids were dissolved in a solution of 1,4-dioxane/water (3:1, 1.50 mL). The vial was sealed, and the reaction mixture was irradiated at 125 °C for 15 min. The volatiles were removed *in vacuo*, and the remaining solids were suspended with ice/water before the pH was adjusted to 2−3 with 2 M HCl(aq). The crude was purified *via* column chromatography (CH_2Cl_2/MeOH/HOAc, 95:4:1−90:9:1), affording 2-cyclopentyl-4-(thieno[3,2-*d*]pyrimidin-4-yl)-benzoic acid **38** (70.0 mg, 48%) as a white solid.

^{1}H NMR (400 MHz, DMSO-d_6): δ 13.24 (s, 1H), 9.31 (s, 1H), 8.60 (d, J = 5.5 Hz, 1H), 8.22 (d, J = 1.7 Hz, 1H), 8.04 (dd, J = 8.1, 1.7 Hz, 1H), 7.88 (d, J = 8.1 Hz, 1H), 7.76 (d, J = 5.5 Hz, 1H), 3.80 (p, J = 8.4, 7.9 Hz, 1H), 2.16−2.06 (m, 2H), 1.89−1.79 (m, 2H), 1.74−1.60 (m, 4H); ^{13}C NMR (176 MHz, DMSO-d_6): δ 169.2, 162.1, 158.3, 154.7, 146.6, 139.0, 138.9, 134.4, 129.8, 127.6, 126.6, 125.5, 124.5, 41.2, 34.5, 25.4; HRMS calcd for $C_{18}H_{16}N_2O_2S$ $[M + H]^+$, 325.1011; found, 325.1011; mp range 205−209 °C.

*Methyl 4-(6-Bromothieno[2,3-d]pyrimidin-4-yl)-2-cyclopentyl-benzoate (**40**).* A 5 mL microwave vial was loaded with 6-bromo-4-chlorothieno[2,3-*d*]pyrimidine **39b** (0.40 mmol, 100 mg), methyl 2-cyclopentyl-4-(4,4,5,5-tetramethyl-1,3,2-dioxaborolan-2-yl)benzoate **4** (0.36 mmol, 120 mg), Cs_2CO_3 (0.60 mmol, 195 mg), and $Pd(Ph_3)_4$ (5 mol %, 23.0 mg). The solids were dissolved in a solution of 1,4-dioxane/water (3:1, 1.5 mL). The vial was sealed, and the reaction mixture was irradiated at 145 °C for 15 min. The volatiles were removed *in vacuo*, and the crude was purified *via* column chromatography (0−5% hexane/EtOAc) to afford methyl 4-(6-bromothieno[2,3-*d*]pyrimidin-4-yl)-2-cyclopentylbenzoate **40** (50.0 mg, 30%) as a white solid.

^{1}H NMR (400 MHz, DMSO-d_6): δ 8.95 (s, 1H), 8.22 (s, 1H), 7.98 (d, J = 1.9 Hz, 1H), 7.83−7.76 (m, 2H), 3.86 (s, 3H), 3.63−3.57 (m, 1H), 2.08−2.00 (m, 2H), 1.90−1.81 (m, 2H), 1.75−1.63 (m, 4H).

*2-Cyclopentyl-4-(6-phenylthieno[2,3-d]pyrimidin-4-yl)benzoic Acid (**41**).* Methyl 4-(6-bromothieno[2,3-*d*]pyrimidin-4-yl)-2-cyclopentylbenzoate **40** (0.11 mmol, 45.0 mg), phenylboronic acid (0.12 mmol, 15.0 mg), Cs_2CO_3 (0.38 mmol, 52.0 mg), and $Pd(Ph_3)_4$ (5 mol %, 6.00 mg) were dissolved in a solution of 1,4-dioxane/water (3:1, 2.00 mL). The reaction mixture was stirred at reflux for 3 h. The volatiles were removed *in vacuo*, and the crude was purified *via* column chromatography (0−10% EtOAc/hexane). The material was further purified using preparative TLC silica plates, affording methyl 2-cyclopentyl-4-(6-phenylthieno[2,3-*d*]pyrimidin-4-yl)benzoate (25 mg, 55%) as a white solid. The methyl ester was saponified as follows: methyl 2-cyclopentyl-4-(6-phenylthieno[2,3-*d*]pyrimidin-4-yl)benzoate (0.06 mmol, 25.0 mg) was dissolved in 1,4-dioxane (2.50 mL). LiOH (0.30 mmol, 7.00 mg) was dissolved in H_2O (0.50 mL) and added to the solution. This mixture was stirred at 80 °C for 4 h. Solvents were removed *in vacuo*; the material was suspended in ice/water, and the pH was adjusted to 2−3 with 2 M HCl. The resulting solid was filtrated, thoroughly rinsed with water, and air- and vacuum-

https://doi.org/10.1021/acs.jmedchem.0c02274
J. Med. Chem. 2021, 64, 10849−10877

dried, affording 2-cyclopentyl-4-(6-phenylthieno[2,3-*d*]pyrimidin-4-yl)benzoic acid **41** (17.0 mg, 70%) as a white solid.

^{1}H NMR (400 MHz, DMSO-d_6): δ 13.11 (s, 1H), 9.16 (s, 1H), 8.16 (s, 1H), 8.13−8.06 (m, 2H), 7.83 (dd, J = 4.3, 2.4 Hz, 2H), 7.78−7.74 (m, 1H), 7.68−7.63 (m, 3H), 3.68−3.62 (m, 1H), 2.10−1.98 (m, 2H), 1.87−1.79 (m, 2H), 1.70−1.62 (m, 4H); ^{13}C NMR (176 MHz, DMSO-d_6): δ 169.1, 168.8, 159.9, 153.4, 146.8, 142.8, 136.9, 134.9, 130.7, 130.2, 129.4, 129.0, 128.9, 126.7, 124.9, 124.4, 117.7, 41.4, 34.2, 25.1; HRMS (HESI) calcd for $C_{24}H_{20}N_2O_2S$ [M + H]$^+$, 401.1324; found, 401.1330; mp range >250 °C.

*2-Cyclopentyl-4-(thieno[2,3-d]pyrimidin-4-yl)benzoic Acid (**42**).* Prepared following the procedure for **38** using 4-chlorothieno[2,3-*d*]pyrimidine **35a** (70.0 mg, 0.41 mmol) and 2-cyclopentyl-4-(4,4,5,5-tetramethyl-1,3,2-dioxaborolan-2-yl)benzoic acid **3** (130 mg, 0.41 mmol). After purification, 2-cyclopentyl-4-(thieno[2,3-*d*]pyrimidin-4-yl)benzoic acid **42** (72.0 mg, 55%) was afforded as a white solid.

^{1}H NMR (400 MHz, DMSO-d_6): δ 9.19 (s, 1H), 8.09 (d, J = 6.1 Hz, 1H), 7.98 (d, J = 1.6 Hz, 1H), 7.87−7.79 (m, 2H), 7.68 (d, J = 6.1 Hz, 1H), 3.83−3.70 (m, 1H), 2.12−2.02 (m, 2H), 1.86−1.74 (m, 2H), 1.65−1.56 (m, 4H); ^{13}C NMR (176 MHz, DMSO-d_6): δ 169.3, 169.3, 159.2, 153.1, 146.2, 139.4, 133.9, 129.5, 129.3, 127.4, 127.4, 126.4, 120.7, 41.3, 34.4, 25.3; HRMS (HESI) calcd for $C_{18}H_{16}N_2O_2S$ [M + H]$^+$, 325.1011; found, 325.1013; mp range 146−149.5 °C.

*Methyl 4-(6-Chloroquinolin-4-yl)-2-cyclopentylbenzoate (**44**).* 4,6-Dichloroquinoline (1.00 g, 5.05 mmol) and 2-cyclopentyl-4-(4,4,5,5-tetramethyl-1,3,2-dioxaborolan-2-yl)benzoate **4** (1.58 g, 4.80 mmol) were dissolved in a 10:1 solution of dioxane/water (27.5 mL). $Pd_2(dba)_3$ (231 mg, 0.25 mmol), XPhos (240 mg, 0.51 mmol), and Cs_2CO_3 (4.94 g, 15.2 mmol) were added, and the mixture was stirred for 16 h at 25 °C. The solution was diluted with EtOAc (20.0 mL) and water (25.0 mL). The layers were separated, and the aqueous phase was extracted with EtOAc (3 × 20.0 mL). The combined organics were dried (Na_2SO_4), filtered, and concentrated *in vacuo*. The crude was purified *via* column chromatography (10−30% EtOAc/hexane) to afford methyl 4-(6-chloroquinolin-4-yl)-2-cyclopentylbenzoate **44** (1.54 g, 83%) as a white solid.

^{1}H NMR (400 MHz, $CDCl_3$): δ 8.96 (d, J = 4.4 Hz, 1H), 8.15 (d, J = 9.0 Hz, 1H), 7.90 (d, J = 8.0 Hz, 1H), 7.84 (d, J = 2.3 Hz, 1H), 7.69 (dd, J = 9.0, 2.3 Hz, 1H), 7.51 (d, J = 1.6 Hz, 1H), 7.42−7.33 (m, 2H), 3.97 (s, 3H), 3.89−3.78 (m, 1H), 2.23−2.12 (m, 2H), 1.86−1.69 (m, 4H), 1.63 (ddd, J = 16.2, 12.9, 8.8 Hz, 2H); ^{13}C NMR (100 MHz, $CDCl_3$): δ 168.5, 145.0, 148.1, 147.2, 146.9, 140.4, 133.0, 131.5, 131.1, 130.5, 130.0, 128.1, 127.2, 126.4, 124.5, 121.8, 77.0, 52.3, 41.8, 35.9, 25.7; HRMS: calcd for $C_{22}H_{21}ClNO_2$ [M + H]$^+$ m/z, 366.1260; found m/z, 366.1246; mp range 137−139 °C.

*2-Cyclopentyl-4-(6-phenylquinolin-4-yl)benzoic Acid (**45**).* Methyl 4-(6-chloroquinolin-4-yl)-2-cyclopentylbenzoate **44** (100 mg, 0.27 mmol) and phenylboronic acid (66.0 mg, 0.32 mmol) were dissolved in a 10:1 solution of dioxane/water (12 mL). $Pd_2(dba)_3$ (25 mg, 0.03 mmol), XPhos (29.0 mg, 0.06 mmol), and Cs_2CO_3 (264 mg, 0.81 mmol) were added, and the solution was heated to 80 °C for 16 h. Once cooled, the solution was diluted with EtOAc (10 mL) and water (10 mL). The layers were separated, and the aqueous phase was extracted with EtOAc (3 × 10 mL). The combined organics were dried (Na_2SO_4), filtered, and concentrated *in vacuo*. The crude was purified *via* column chromatography (10−30% EtOAc/hexane) to afford methyl 2-cyclopentyl-4-(6-phenylquinolin-4-yl)benzoate as an intermediate. The intermediate methyl ester was dissolved in dioxane (1 mL) and aq LiOH (1 mL of a 1 M solution). The solution was heated to 100 °C for 16 h and then acidified to pH 4 with 1 M aq HCl, causing a precipitate to form. The solid was collected by filtration, washed with cold water (4 mL) and Et_2O (10 mL), and dried under vacuum to afford 2-cyclopentyl-4-(6-phenylquinolin-4-yl)benzoic acid **45** (81 mg, 76%) as an off-white solid.

^{1}H NMR (400 MHz, DMSO-d_6): δ 9.15 (d, J = 4.8 Hz, 1H), 8.39 (d, J = 8.6 Hz, 1H), 8.32 (d, J = 8.7 Hz, 1H), 8.13 (d, J = 1.7 Hz, 1H), 7.87 (d, J = 7.9 Hz, 1H), 7.84−7.79 (m, 1H), 7.74−7.69 (m, 3H), 7.59 (dd, J = 8.0, 1.6 Hz, 1H), 7.51 (t, J = 7.4 Hz, 2H), 7.47−7.41 (m, 1H), 3.88−3.72 (m, 1H), 2.14−2.01 (m, 2H), 1.84−1.71 (m, 2H), 1.71−1.50 (m, 4H); ^{13}C NMR (176 MHz, DMSO): δ 169.3, 146.4, 145.2, 139.8, 138.9, 138.8, 132.8, 130.7, 129.6, 129.3, 129.2, 128.3, 128.1, 127.1, 126.8, 126.2, 123.0, 122.3, 119.4, 99.5, 41.2, 34.5, 25.3; HRMS: calcd for $C_{27}H_{24}NO_2$ [M + H]$^+$ m/z, 394.1807; found m/z, 394.1786; mp range 164−167 °C.

*2-Cyclopentyl-4-(quinolin-4-yl)benzoic Acid (**46**).* Prepared following the procedure for **21** using 4-chloroquinoline (100 mg, 611 μmol). After purification, 2-cyclopentyl-4-(quinolin-4-yl)benzoic acid **46** (l60 mg, 83%) was afforded as a white solid.

^{1}H NMR (400 MHz, DMSO-d_6): δ 13.09 (s, 1H), 8.97 (d, J = 4.4 Hz, 1H), 8.14−8.11 (m, 1H), 7.8−7.78 (m, 3H), 7.62 (ddd, J = 8.3, 6.9, 1.3 Hz, 1H), 7.56 (d, J = 1.7 Hz, 1H), 7.50 (d, J = 4.4 Hz, 1H), 7.44 (dd, J = 7.9, 1.7 Hz, 1H), 3.85−3.73 (m, 1H), 2.11−2.00 (m, 2H), 1.81−1.71 (m, 2H), 1.70−1.54 (m, 4H); ^{13}C NMR (100 MHz, DMSO-d_6): δ 169.4, 150.2, 148.1, 146.8, 146.6, 140.0, 132.1, 129.6, 129.6, 129.5, 127.8, 127.2, 126.7, 125.7, 125.2, 121.5, 41.2, 34.5, 25.3; HRMS: calcd for $C_{21}H_{19}NO_2$ [M − H]$^-$ m/z, 316.1338; found, 316.1339; mp range 259−263 °C.

*Methyl 2-Cyclopentyl-4-(6-hydroxyquinazolin-4-yl)benzoate (**48**).* Prepared following the procedure for **32** using 4-chloroquinazolin-6-ol **47b** (50.0 mg, 0.28 mmol). After purification, methyl 2-cyclopentyl-4-(6-hydroxyquinazolin-4-yl)benzoate **48** (63.0 mg, 65%) was afforded as a thick oil.

^{1}H NMR (400 MHz, DMSO-d_6): δ 9.42 (s, 1H), 8.16 (d, J = 9.0 Hz, 1H), 8.10 (dd, J = 9.0, 2.3 Hz, 1H), 7.99−7.98 (m, 1H), 7.88−7.84 (m, 3H), 7.71 (dd, J = 7.9, 1.7 Hz, 1H), 3.70−3.62 (m, 1H), 2.13−2.01 (m, 2H), 1.81−1.75 (m, 2H), 1.72−1.57 (m, 4H); ^{13}C NMR (101 MHz, DMSO-d_6): δ 167.9, 166.2, 154.7, 149.0, 146.4, 138.9, 134.8, 132.6, 132.3, 130.8, 129.4, 128.4, 127.1, 125.2, 122.9, 52.4, 41.3, 34.4, 25.2.

*2-Cyclopentyl-4-(6-phenylquinazolin-4-yl)benzoic Acid (**49**).* Methyl 2-cyclopentyl-4-(6-phenylquinazolin-4-yl)benzoate **SI4** (170 mg, 0.41 mmol) was dissolved in MeOH (3.5 mL) and aq NaOH (1 mL). The resulting solution was heated to 70 °C for 1 h and allowed to cool to rt, added water (4 mL), and extracted with ether (2 × 10 mL). The aqueous phase was acidified with 1 N HCl (pH 6) and then extracted with EtOAc. The organic phase was dried (Na_2CO_3) and concentrated to afford 2-cyclopentyl-4-(6-phenylquinazolin-4-yl)-benzoic acid **49** (150 mg, 91%) as a light-yellow solid.

^{1}H NMR (400 MHz, DMSO-d_6): δ 13.19 (s, 1H), 9.39 (s, 1H), 8.39 (dd, J = 8.8, 2.1 Hz, 1H), 8.24−8.19 (m, 2H), 7.92 (d, J = 1.7 Hz, 1H), 7.87 (d, J = 7.9 Hz, 1H), 7.78−7.73 (m, 3H), 7.51 (t, J = 7.4 Hz, 2H), 7.45 (d, J = 7.3 Hz, 1H), 3.86−3.75 (m, 1H), 2.12−2.04 (m, 2H), 1.80−1.74 (m, 2H), 1.69−1.60 (m, 4H); ^{13}C NMR (101 MHz, DMSO-d_6): δ 169.4, 167.0, 154.4, 149.9, 146.1, 139.8, 139.0, 138.8, 133.5, 133.4, 129.3, 129.2, 129.2, 128.5, 128.3, 127.2, 127.1, 123.7, 122.5, 41.2, 34.5, 25.3; HRMS: calcd for $C_{26}H_{22}N_2O_2$ [M − H]$^-$ m/z, 393.1607; found, 393.1603; mp range 265−269 °C.

*2-Cyclopentyl-4-(quinazolin-4-yl)benzoic Acid (**50**).* 4-Chloroquinazoline (100 mg, 0.60 mmol), 2-cyclopentyl-4-(4,4,5,5-tetramethyl-1,3,2-dioxaborolan-2-yl)benzoate **4** (240 mg, 0.72 mmol), $Pd(PPh_3)_4$ (70.0 mg, 60.0 μmol), and Cs_2CO_3 (0.60 g, 1.80 mmol) were loaded into a microwave vial. A solution of dioxane/water (6.0 mL of a 10:1 mix) was added, and the vial was flushed with nitrogen. The mixture was irradiated at 100 °C for 30 min. Once cooled, the aqueous layer was removed and the remaining volatiles were removed *in vacuo*. The crude was purified *via* column chromatography, and the intermediate ester was isolated. The ester was dissolved in dioxane (1 mL) and aq LiOH (1 mL of a 1 M solution). The solution was heated to 100 °C for 16 h and then acidified to pH 4 with 1 M aq HCl, causing a precipitate to form. The solid was collected by filtration, washed with cold H_2O, and then dried under vacuum to afford the quinazoline (128 mg, 67%) as a pale-white solid.

^{1}H NMR (400 MHz, DMSO-d_6): δ 9.38 (s, 1H), 8.15−8.03 (m, 3H), 7.85 (d, J = 7.9 Hz, 1H), 7.78 (ddd, J = 9.7, 6.8, 1.4 Hz, 3H), 7.66 (dd, J = 7.9, 1.7 Hz, 1H), 3.83−3.73 (m, 1H), 2.11−2.02 (m, 2H), 1.81−1.71 (m, 2H), 1.70−1.57 (m, 4H); ^{13}C NMR (101 MHz, DMSO-d_6): δ 169.3, 167.0, 154.3, 150.3, 146.0, 139.0, 134.4, 133.5, 129.1, 128.6, 128.4, 128.2, 127.08, 126.6, 122.3, 41.3, 34.4, 25.2; HRMS: calcd for $C_{20}H_{19}N_2O_2$ [M + H]$^+$ m/z, 319.1446; found, m/z 319.1427; mp range 120−122 °C.

https://doi.org/10.1021/acs.jmedchem.0c02274
J. Med. Chem. 2021, 64, 10849−10877

*2-Cyclopentyl-4-(2-methylquinolin-4-yl)benzoic Acid (**52**).* Prepared following the procedure for **21** using 4-chloro-2-methylquinoline **51** (200 mg, 1.13 mmol). After purification, 2-cyclopentyl-4-(2-methylquinolin-4-yl)benzoic acid **52** (290 mg, 77%) was afforded as an off-white solid.

^{1}H NMR (400 MHz, DMSO-d_6): δ 13.08 (s, 1H), 8.01 (dd, J = 8.5, 1.5 Hz, 1H), 7.81 (d, J = 7.9 Hz, 1H), 7.78−7.72 (m, 2H), 7.56−7.52 (m, 2H), 7.43−7.39 (m, 2H), 3.86−3.74 (m, 1H), 2.70 (s, 3H), 2.12−2.00 (m, 2H), 1.78−1.74 (m, 2H), 1.67−1.56 (m, 4H); ^{13}C NMR (176 MHz, DMSO-d_6): δ 172.6, 161.6, 151.0, 150.0, 149.3, 143.2, 135.4, 132.6, 132.5, 132.0, 130.8, 129.7, 129.3, 128.1, 127.2, 125.3, 44.4, 37.6, 28.4, 27.9; HRMS: calcd for $C_{22}H_{21}NO_2$ $[M - H]^-$ m/z, 332.1651; found, 332.1642; mp range 271−275 °C.

*2-Cyclopentyl-4-(1,6-naphthyridin-4-yl)benzoic Acid (**54**).* Prepared following the procedure for **21** using 4-chloro-1,6-naphthyridine **53** (80.0 mg, 0.49 mmol). After purification, 2-cyclopentyl-4-(1,6-naphthyridin-4-yl)benzoic acid **54** (110 mg, 54%) was afforded as a yellow solid.

^{1}H NMR (400 MHz, DMSO-d_6): δ 13.14 (s, 1H), 9.24−9.15 (m, 2H), 8.79 (d, J = 5.8 Hz, 1H), 8.01 (dd, J = 5.9, 0.9 Hz, 1H), 7.84 (d, J = 7.9 Hz, 1H), 7.71−7.65 (m, 2H), 7.54 (dd, J = 7.9, 1.8 Hz, 1H), 3.84−3.73 (m, 1H), 2.09−2.04 (m, 2H), 1.80−1.71 (m, 2H), 1.71−1.56 (m, 4H); ^{13}C NMR (176 MHz, DMSO-d_6): δ 169.88, 155.32, 150.85, 150.45, 147.84, 146.88, 146.7, 138.4, 133.1, 129.9, 128.4, 127.3, 123.5, 122.3, 121.5, 41.6, 34.8, 25.6; HRMS calcd for $C_{20}H_{18}N_2O_2$ $[M - H]^-$ m/z, 319.1447; found, 319.1427; mp range 195−200 °C.

*2-Cyclopentyl-4-(pyrimidin-4-yl)benzoic Acid (**56**).* 4-Chloropyrimidine (162 mg, 1.40 mmol) and Cs_2CO_3 (1.32 g, 4.00 mmol) were dissolved in 1,2-DME (4.00 mL) and H_2O (0.70 mL). $Pd(PPh_3)_4$ (78 mg, 68 μmol) and **3** (503 mg, 1.60 mmol) were added, and the solution was stirred at 120 °C for 30 min. The resulting suspension was filtered through Celite under vacuum. The filter cake was washed with ethyl acetate, and the filtrate was dried (Na_2SO_4), filtered, and concentrated *in vacuo*. The crude product was purified by column chromatography [0−50% EtOAc(0.01% acetic acid)/hexane] to afford 2-cyclopentyl-4-(pyrimidin-4-yl)benzoic acid **56** (29 mg, 8%) as a white solid.

^{1}H NMR (700 MHz, DMSO-d_6): δ 13.14 (br s, 1H), 9.28 (s, 1H), 8.92−8.87 (m, 1H), 8.25 (s, 1H), 8.20−8.16 (m, 1H), 8.06 (d, J = 7.7 Hz, 1H), 7.77 (d, J = 7.7 Hz, 1H), 3.72 (p, J = 8.0 Hz, 1H), 2.09−2.01 (m, 2H), 1.87−1.79 (m, 2H), 1.73−1.59 (m, 4H); ^{13}C NMR (176 MHz, DMSO-d_6): δ 169.3, 158.8, 158.8, 158.3, 146.4, 138.3, 134.5, 129.7, 125.1, 124.2, 117.7, 41.4, 34.4, 25.3; HRMS: calcd for $C_{16}H_{15}N_2O_2$ $[M - H]^-$ m/z, 267.1138; found, 267.1139; mp range 245 °C.

*2-Cyclopentyl-4-(2-phenylpyrimidin-4-yl)benzoic Acid (**58**).* 4-Chloro-2-phenylpyrimidine (155 mg, 0.81 mmol) and Cs_2CO_3 (775 mg, 2.40 mmol) were dissolved in 1,2-DME (2.40 mL) and H_2O (0.40 mL). $Pd(PPh_3)_4$ (48.0 mg, 42.0 μmol) and **3** (307 mg, 0.97 mmol) were added, and the solution was stirred at 120 °C for 30 min. The resulting suspension was filtered through Celite under vacuum. The filter cake was washed with ethyl acetate, and the filtrate was dried (Na_2SO_4), filtered, and concentrated *in vacuo*. The crude product was purified by column chromatography [0−10% EtOAc-(0.01% acetic acid)/hexane] to afford 2-cyclopentyl-4-(2-phenylpyrimidin-4-yl)benzoic acid **58** (21 mg, 8%) as a white solid.

^{1}H NMR (700 MHz, DMSO-d_6): δ 13.16 (br s, 1H), 9.04−8.95 (m, 1H), 8.52 (d, J = 6.0 Hz, 2H), 8.33 (s, 1H), 8.21 (d, J = 7.6 Hz, 1H), 8.15−8.07 (m, 1H), 7.82 (d, J = 7.6 Hz, 1H), 7.63−7.53 (m, 3H), 3.76 (p, J = 8.8 Hz, 1H), 2.12−2.03 (m, 2H), 1.90−1.82 (m, 2H), 1.75−1.65 (m, 4H); ^{13}C NMR (176 MHz, DMSO-d_6): δ 169.4, 163.4, 162.3, 158.9, 146.4, 138.5, 137.2, 134.5, 131.0, 129.7, 128.8, 127.8, 125.3, 124.3, 115.7, 41.4, 34.4, 25.3; HRMS: calcd for $C_{22}H_{21}N_2O_2$ $[M + H]^+$ m/z, 345.1598; found, 345.1600; mp range >250 °C.

*Methyl 4-(2-Aminopyrimidin-4-yl)-2-cyclopentylbenzoate (**60**).* 4-Chloropyrimidin-2-amine (501 mg, 3.90 mmol) and Cs_2CO_3 (3.81 mg, 12.0 mmol) were dissolved in 1,2-DME (8.00 mL) and H_2O (2.00 mL). $Pd(PPh_3)_4$ (238 mg, 0.21 mmol) and **4** (1.50 g, 4.50 mmol) were added, and the solution was irradiated at 120 °C for 30 min. The resulting suspension was filtered through Celite under vacuum. The filter cake was washed with ethyl acetate, and the filtrate was dried (Na_2SO_4), filtered, and concentrated *in vacuo*. The crude product was purified by column chromatography (20% EtOAc/hexane) to afford methyl 4-(2-aminopyrimidin-4-yl)-2-cyclopentylbenzoate **60** (523 mg, 45%) as a white solid.

^{1}H NMR (400 MHz, DMSO-d_6): δ 8.34 (d, J = 5.2 Hz, 1H), 8.13 (d, J = 1.7 Hz, 1H), 7.93 (dd, J = 8.1, 1.7 Hz, 1H), 7.73 (d, J = 8.1 Hz, 1H), 7.19 (d, J = 5.2 Hz, 1H), 6.74 (s, 2H), 3.85 (s, 3H), 3.69−3.54 (m, 1H), 2.11−1.96 (m, 2H), 1.90−1.75 (m, 2H), 1.73−1.55 (m, 3H); ^{13}C NMR (100 MHz, DMSO-d_6): δ 168.00, 163.81, 162.68, 159.31, 146.28, 139.90, 132.37, 129.51, 124.83, 124.03, 106.29, 52.23, 41.48, 34.34, 25.20; mp range 178 °C.

*4-(2-Aminopyrimidin-4-yl)-2-cyclopentylbenzoic Acid Hydrochloride (**61**·HCl).* Methyl 4-(2-aminopyrimidin-4-yl)-2-cyclopentylbenzoate **60** (40.0 mg, 0.13 mmol) was dissolved in 1,4-dioxane (1.00 mL). 1 M LiOH (1.00 mL) was added, and the solution was stirred at 100 °C for 17 h. HCl (6.00 M, 6.00 mL) was added, resulting in precipitate formation. The precipitate was filtered and washed with HCl (6.00 M). The precipitate was dried under reduced pressure to afford 4-(2-aminopyrimidin-4-yl)-2-cyclopentylbenzoic acid hydrochloride **61**·HCl (35.0 mg, 85%) as a white solid.

^{1}H NMR (400 MHz, DMSO-d_6): δ 8.54−8.14 (br s, 1H) 8.53 (d, J = 6.3 Hz, 1H), 8.22 (d, J = 1.8 Hz, 1H), 8.05 (dd, J = 8.2, 1.8 Hz, 1H), 7.77 (d, J = 8.2 Hz, 1H), 7.61 (d, J = 6.3 Hz, 1H), 3.73−3.60 (m, 1H), 2.10−1.98 (m, 2H), 1.90−1.76 (m, 2H), 1.73−1.57 (m, 4H); ^{13}C NMR (100 MHz, DMSO-d_6): δ 169.2, 168.3, 157.1, 150.3, 146.1, 136.7, 136.0, 129.5, 126.1, 125.3, 106.5, 41.5, 34.4, 25.2; HRMS: calcd for $C_{16}H_{18}N_3O_2$ $[M + H]^+$ m/z, 284.1394; found, 284.1394; mp range >250 °C.

*2-Cyclopentyl-4-(2-(phenylamino)pyrimidin-4-yl)benzoic Acid Hydrochloride (**62**·HCl).* Methyl 2-cyclopentyl-4-(2-(phenylamino)-pyrimidin-4-yl)benzoate **SI5** (20 mg, 54 μmol) was dissolved in 1,4-dioxane (1.0 mL). 1 M LiOH (1.0 mL) was added, and the solution was stirred for at 100 °C for 16 h. HCl (6.0 M, 6.0 mL) was added, resulting in precipitate formation. The precipitate was filtered and washed with HCl (6.0 M). The precipitate was dried under reduced pressure to afford 2-cyclopentyl-4-(2-(phenylamino)pyrimidin-4-yl)-benzoic acid hydrochloride (**62**·HCl) (12 mg, 63%) as a yellow solid.

^{1}H NMR (700 MHz, DMSO-d_6): δ 13.10 (br s, 1H), 9.74 (s, 1H), 8.61−8.55 (m, 1H), 8.29 (s, 1H), 8.00 (d, J = 7.4 Hz, 1H), 7.86 (d, J = 7.3 Hz, 2H), 7.77 (d, J = 7.4 Hz, 1H), 7.50−7.46 (m, 1H), 7.33−7.27 (m, 2H), 7.01−6.96 (m, 1H), 3.77 (p, J = 9.6 Hz, 1H), 2.13−2.03 (m, 2H), 1.89−1.80 (m, 2H), 1.73−1.61 (m, 4H); ^{13}C NMR (176 MHz, DMSO-d_6): δ 169.3, 162.6, 160.1, 159.3, 146.4, 140.5, 139.0, 134.0, 129.6, 128.4, 125.1, 124.0, 121.5, 119.0, 108.3, 41.2, 34.5, 25.4; HRMS: calcd for $C_{22}H_{22}N_3O_2$ $[M + H]^+$ m/z, 360.4365; found, 360.1712; mp range >250 °C.

■ ASSOCIATED CONTENT

Supporting Information

The Supporting Information is available free of charge at https://pubs.acs.org/doi/10.1021/acs.jmedchem.0c02274.

Mass spectrometry methods, compound characterization spectra, CAMKK2 in cell target engagement NanoBRET data, *p*-AMPK Western blot images, details on docking studies, and treespot images of kinase selectivity data (PDF)

Compound selectivity data (CSV)

Compound molecular formula strings (XLSX)

■ AUTHOR INFORMATION

Corresponding Authors

John W. Scott − *St Vincent's Institute and Department of Medicine, The University of Melbourne, Fitzroy 3065, Australia; Mary MacKillop Institute for Health Research,*

https://doi.org/10.1021/acs.jmedchem.0c02274
J. Med. Chem. 2021, 64, 10849−10877

Australian Catholic University, Melbourne 3000, Australia; The Florey Institute of Neuroscience and Mental Health, Parkville 3052, Australia; Phone: +61-3-9231-3510; Email: jscott@svi.edu.au

David H. Drewry − *Structural Genomics Consortium and Division of Chemical Biology and Medicinal Chemistry, UNC Eshelman School of Pharmacy, University of North Carolina at Chapel Hill, Chapel Hill, North Carolina 27599, United States; UNC Lineberger Comprehensive Cancer Center, UNC Eshelman School of Pharmacy, University of North Carolina at Chapel Hill, Chapel Hill, North Carolina 27599, United States;* orcid.org/0000-0001-5973-5798; Phone: +1-919-602-1327; Email: david.drewry@unc.edu

Authors

Benjamin J. Eduful − *Structural Genomics Consortium and Division of Chemical Biology and Medicinal Chemistry, UNC Eshelman School of Pharmacy, University of North Carolina at Chapel Hill, Chapel Hill, North Carolina 27599, United States*

Sean N. O'Byrne − *Structural Genomics Consortium and Division of Chemical Biology and Medicinal Chemistry, UNC Eshelman School of Pharmacy, University of North Carolina at Chapel Hill, Chapel Hill, North Carolina 27599, United States*

Louisa Temme − *Structural Genomics Consortium and Division of Chemical Biology and Medicinal Chemistry, UNC Eshelman School of Pharmacy, University of North Carolina at Chapel Hill, Chapel Hill, North Carolina 27599, United States*

Christopher R. M. Asquith − *Structural Genomics Consortium and Division of Chemical Biology and Medicinal Chemistry, UNC Eshelman School of Pharmacy, University of North Carolina at Chapel Hill, Chapel Hill, North Carolina 27599, United States; Department of Pharmacology, School of Medicine, University of North Carolina at Chapel Hill, Chapel Hill, North Carolina 27599, United States;* orcid.org/0000-0001-5871-3458

Yi Liang − *Structural Genomics Consortium and Division of Chemical Biology and Medicinal Chemistry, UNC Eshelman School of Pharmacy, University of North Carolina at Chapel Hill, Chapel Hill, North Carolina 27599, United States*

Alfredo Picado − *Structural Genomics Consortium and Division of Chemical Biology and Medicinal Chemistry, UNC Eshelman School of Pharmacy, University of North Carolina at Chapel Hill, Chapel Hill, North Carolina 27599, United States*

Joseph R. Pilotte − *Structural Genomics Consortium and Division of Chemical Biology and Medicinal Chemistry, UNC Eshelman School of Pharmacy, University of North Carolina at Chapel Hill, Chapel Hill, North Carolina 27599, United States*

Mohammad Anwar Hossain − *Structural Genomics Consortium and Division of Chemical Biology and Medicinal Chemistry, UNC Eshelman School of Pharmacy, University of North Carolina at Chapel Hill, Chapel Hill, North Carolina 27599, United States;* orcid.org/0000-0001-8684-8755

Carrow I. Wells − *Structural Genomics Consortium and Division of Chemical Biology and Medicinal Chemistry, UNC Eshelman School of Pharmacy, University of North Carolina at Chapel Hill, Chapel Hill, North Carolina 27599, United States;* orcid.org/0000-0003-4799-6792

William J. Zuercher − *Structural Genomics Consortium and Division of Chemical Biology and Medicinal Chemistry, UNC Eshelman School of Pharmacy, University of North Carolina at Chapel Hill, Chapel Hill, North Carolina 27599, United States*

Carolina M. C. Catta-Preta − *Centro de Química Medicinal (CQMED), Centro de Biologia Molecular e Engenharia Genética (CBMEG), Universidade Estadual de Campinas (UNICAMP), Campinas, São Paulo 13083-875, Brazil; Structural Genomics Consortium, Departamento de Genética e Evolução, Instituto de Biologia, UNICAMP, Campinas, São Paulo 13083-886, Brazil*

Priscila Zonzini Ramos − *Centro de Química Medicinal (CQMED), Centro de Biologia Molecular e Engenharia Genética (CBMEG), Universidade Estadual de Campinas (UNICAMP), Campinas, São Paulo 13083-875, Brazil; Structural Genomics Consortium, Departamento de Genética e Evolução, Instituto de Biologia, UNICAMP, Campinas, São Paulo 13083-886, Brazil*

André de S. Santiago − *Centro de Química Medicinal (CQMED), Centro de Biologia Molecular e Engenharia Genética (CBMEG), Universidade Estadual de Campinas (UNICAMP), Campinas, São Paulo 13083-875, Brazil; Structural Genomics Consortium, Departamento de Genética e Evolução, Instituto de Biologia, UNICAMP, Campinas, São Paulo 13083-886, Brazil*

Rafael M. Couñago − *Centro de Química Medicinal (CQMED), Centro de Biologia Molecular e Engenharia Genética (CBMEG), Universidade Estadual de Campinas (UNICAMP), Campinas, São Paulo 13083-875, Brazil; Structural Genomics Consortium, Departamento de Genética e Evolução, Instituto de Biologia, UNICAMP, Campinas, São Paulo 13083-886, Brazil*

Christopher G. Langendorf − *St Vincent's Institute and Department of Medicine, The University of Melbourne, Fitzroy 3065, Australia*

Kévin Nay − *St Vincent's Institute and Department of Medicine, The University of Melbourne, Fitzroy 3065, Australia; Mary MacKillop Institute for Health Research, Australian Catholic University, Melbourne 3000, Australia*

Jonathan S. Oakhill − *St Vincent's Institute and Department of Medicine, The University of Melbourne, Fitzroy 3065, Australia; Mary MacKillop Institute for Health Research, Australian Catholic University, Melbourne 3000, Australia*

Thomas L. Pulliam − *Department of Cancer Systems Imaging, University of Texas MD Anderson Cancer Center, Houston, Texas 77054, United States; Center for Nuclear Receptors and Cell Signaling and Department of Biology and Biochemistry, University of Houston, Houston, Texas 77204, United States*

Chenchu Lin − *Department of Cancer Systems Imaging, University of Texas MD Anderson Cancer Center, Houston, Texas 77054, United States; The University of Texas MD Anderson Cancer Center UTHealth Graduate School of Biomedical Sciences, Houston, Texas 77030, United States*

Dominik Awad − *Department of Cancer Systems Imaging, University of Texas MD Anderson Cancer Center, Houston, Texas 77054, United States; The University of Texas MD Anderson Cancer Center UTHealth Graduate School of Biomedical Sciences, Houston, Texas 77030, United States*

Timothy M. Willson − *Structural Genomics Consortium and Division of Chemical Biology and Medicinal Chemistry, UNC Eshelman School of Pharmacy, University of North Carolina*

https://doi.org/10.1021/acs.jmedchem.0c02274
J. Med. Chem. 2021, 64, 10849−10877

at Chapel Hill, Chapel Hill, North Carolina 27599, United States; orcid.org/0000-0003-4181-8223

Daniel E. Frigo − *Department of Cancer Systems Imaging, University of Texas MD Anderson Cancer Center, Houston, Texas 77054, United States; Center for Nuclear Receptors and Cell Signaling and Department of Biology and Biochemistry, University of Houston, Houston, Texas 77204, United States; Department of Genitourinary Medical Oncology, University of Texas MD Anderson Cancer Center, Houston, Texas 77030, United States; The Methodist Hospital Research Institute, Houston, Texas 77030, United States;* orcid.org/0000-0002-0713-471X

Complete contact information is available at: https://pubs.acs.org/10.1021/acs.jmedchem.0c02274

Author Contributions

⊥⊥B.J.E., S.N.O., and L.T. contributed equally to this work. The manuscript was written through contributions of all authors. All authors have given approval to the final version of the manuscript.

Funding

This research was funded in part by the National Cancer Institute of the National Institutes of Health (grant numbers R01CA218442 and R01CA184208) and was supported by the NIH Illuminating the Druggable Genome program (grant number 1U24DK116204-01), FAPESP (Fundação de Amparo à Pesquisa do Estado de São Paulo) (2013/50724-5 and 2014/50897-0), and CNPq (Conselho Nacional de Desenvolvimento Cientifico e Tecnológico) (465651/2014-3). The SGC is a registered charity (number 1097737) that receives funds from AbbVie, Bayer Pharma AG, Boehringer Ingelheim, the Canada Foundation for Innovation, Eshelman Institute for Innovation, Genome Canada, Innovative Medicines Initiative (EU/EFPIA) [ULTRA-DD grant no. 115766], Janssen, Merck KGaA Darmstadt Germany, MSD, Novartis Pharma AG, Ontario Ministry of Economic Development and Innovation, Pfizer, Takeda, and Wellcome [106169/ZZ14/Z]. J.W.S. and J.S.O. are funded by National Health and Medical Research Council (NHMRC) grants GNT1138102 and GNT1145265, respectively. P.Z.R. received CAPES (Coordenação de Aperfeiçoamento de Pessoal de Nível Superior) postdoctoral fellowship (88887.136432/2017-00). A.d.S.S. is an FAPESP postdoctoral fellow (2019/14275-8). C.G.L. is an NHMRC early career fellow (GNT1143080). C.L. is supported by an Antje Wuelfrath Gee and Harry Gee, Jr. Family Legacy Scholarship. D.A. is supported by an American Legion Auxiliary Fellowship. Acknowledgements for beamlines/crystallography: this work is based upon research conducted at the Northeastern Collaborative Access Team beamlines (GU51510, GU56413), which are funded by the National Institute of General Medical Sciences from the National Institutes of Health (P41 GM103403). The Pilatus 6M detector on the 24-ID-C beamline is funded by an NIH-ORIP HEI grant (S10 RR029205). This research used resources of the Advanced Photon Source, a U.S. Department of Energy (DOE) Office of Science User Facility, operated for the DOE Office of Science by Argonne National Laboratory under contract no. DE-AC02-06CH11357. We thank Diamond Light Source for access to beam line I03 (proposal number MX10619-74).

Notes

The authors declare no competing financial interest.

PDB ID codes: 5UY6; 5UYJ. Authors will release the atomic coordinates upon article publication.

■ ACKNOWLEDGMENTS

We are grateful for LC−MS/HRMS support provided by Dr. Brandie Ehrmann and Diane E. Wallace in the Mass Spectrometry Core Laboratory at the University of North Carolina at Chapel Hill. The core is supported by the National Science Foundation under grant no. CHE-1726291.

■ ABBREVIATIONS

CAMKK2, calcium-calmodulin protein kinase kinase 2; AMPK, AMP-activated protein kinase; AKT, protein kinase B (PKB); siRNA, small interfering RNA; HCC, hepatocellular carcinoma; NAFLD, non-alcoholic fatty liver disease; GRK3, G protein-coupled receptor kinase 3; CK2, casein kinase 2; CDKL2, cyclin-dependent kinase-like 3; AhR, aryl hydrocarbon receptor; ATP, adenosine triphosphate; SEM, trimethylsilylethoxymethyl; CDI, 1,1-carbodiimidazole; DME, dimethoxyethane; DSF, differential scanning fluorimetry; PoC, percentage of control; ADMET, absorption, distribution, metabolism, excretion, and toxicology; LE, ligand efficiency; LLE, lipophilic ligand efficiency; DMSO, dimethylsulfoxide; BRET, bioluminescence resonance energy transfer

■ REFERENCES

(1) Chin, D.; Means, A. R. Calmodulin: a prototypical calcium sensor. *Trends Cell Biol.* **2000**, *10*, 322−328.

(2) Hook, S. S.; Means, A. R. Ca(2+)/CaM-dependent kinases: from activation to function. *Annu. Rev. Pharmacol. Toxicol.* **2001**, *41*, 471−505.

(3) Sharma, R. K.; Parameswaran, S. Calmodulin-binding proteins: A journey of 40 years. *Cell Calcium* **2018**, *75*, 89−100.

(4) Clapham, D. E. Calcium signaling. *Cell* **2007**, *131*, 1047−1058.

(5) Racioppi, L.; Means, A. R. Calcium/calmodulin-dependent protein kinase kinase 2: roles in signaling and pathophysiology. *J. Biol. Chem.* **2012**, *287*, 31658−31665.

(6) Anderson, K. A.; Means, R. L.; Huang, Q.-H.; Kemp, B. E.; Goldstein, E. G.; Selbert, M. A.; Edelman, A. M.; Fremeau, R. T.; Means, A. R. Components of a calmodulin-dependent protein kinase cascade. Molecular cloning, functional characterization and cellular localization of Ca2+/calmodulin-dependent protein kinase kinase beta. *J. Biol. Chem.* **1998**, *273*, 31880−31889.

(7) Hawley, S. A.; Pan, D. A.; Mustard, K. J.; Ross, L.; Bain, J.; Edelman, A. M.; Frenguelli, B. G.; Hardie, D. G. Calmodulin-dependent protein kinase kinase-beta is an alternative upstream kinase for AMP-activated protein kinase. *Cell Metab.* **2005**, *2*, 9−19.

(8) Karacosta, L. G.; Foster, B. A.; Azabdaftari, G.; Feliciano, D. M.; Edelman, A. M. A regulatory feedback loop between Ca2+/calmodulin-dependent protein kinase kinase 2 (CaMKK2) and the androgen receptor in prostate cancer progression. *J. Biol. Chem.* **2012**, *287*, 24832−24843.

(9) Lin, F.; Marcelo, K. L.; Rajapakshe, K.; Coarfa, C.; Dean, A.; Wilganowski, N.; Robinson, H.; Sevick, E.; Bissig, K.-D.; Goldie, L. C.; Means, A. R.; York, B. The camKK2/camKIV relay is an essential regulator of hepatic cancer. *Hepatology* **2015**, *62*, 505−520.

(10) Liu, D.-M.; Wang, H.-J.; Han, B.; Meng, X.-Q.; Chen, M.-H.; Yang, D.-B.; Sun, Y.; Li, Y.-L.; Jiang, C.-L. CAMKK2, regulated by promoter methylation, is a prognostic marker in diffuse gliomas. *CNS Neurosci. Ther.* **2016**, *22*, 518−524.

(11) Massie, C. E.; Lynch, A.; Ramos-Montoya, A.; Boren, J.; Stark, R.; Fazli, L.; Warren, A.; Scott, H.; Madhu, B.; Sharma, N.; Bon, H.; Zecchini, V.; Smith, D.-M.; Denicola, G. M.; Mathews, N.; Osborne, M.; Hadfield, J.; Macarthur, S.; Adryan, B.; Lyons, S. K.; Brindle, K. M.; Griffiths, J.; Gleave, M. E.; Rennie, P. S.; Neal, D. E.; Mills, I. G.

The androgen receptor fuels prostate cancer by regulating central metabolism and biosynthesis. *EMBO J.* **2011**, *30*, 2719−2733.
(12) Rodriguez-Mora, O. G.; LaHair, M. M.; McCubrey, J. A.; Franklin, R. A. Calcium/calmodulin-dependent kinase I and calcium/calmodulin-dependent kinase kinase participate in the control of cell cycle progression in MCF-7 human breast cancer cells. *Cancer Res.* **2005**, *65*, 5408−5416.
(13) Shima, T.; Mizokami, A.; Miyagi, T.; Kawai, K.; Izumi, K.; Kumaki, M.; Ofude, M.; Zhang, J.; Keller, E. T.; Namiki, M. Down-regulation of calcium/calmodulin-dependent protein kinase kinase 2 by androgen deprivation induces castration-resistant prostate cancer. *Prostate* **2012**, *72*, 1789−1801.
(14) Subbannayya, Y.; Syed, N.; Barbhuiya, M. A.; Raja, R.; Marimuthu, A.; Sahasrabuddhe, N.; Pinto, S. M.; Manda, S. S.; Renuse, S.; Manju, H.; Zameer, M. A. L.; Sharma, J.; Brait, M.; Srikumar, K.; Roa, J. C.; Vijaya Kumar, M.; Kumar, K. V.; Prasad, T. K.; Ramaswamy, G.; Kumar, R. V.; Pandey, A.; Gowda, H.; Chatterjee, A. Calcium calmodulin dependent kinase kinase 2 - a novel therapeutic target for gastric adenocarcinoma. *Canc. Biol. Ther.* **2015**, *16*, 336−345.
(15) Yano, S.; Tokumitsu, H.; Soderling, T. R. Calcium promotes cell survival through CaM-K kinase activation of the protein-kinase-B pathway. *Nature* **1998**, *396*, 584−587.
(16) Spengler, K.; Zibrova, D.; Woods, A.; Langendorf, C. G.; Scott, J. W.; Carling, D.; Heller, R. Protein kinase A negatively regulates VEGF-induced AMPK activation by phosphorylating CaMKK2 at serine 495. *Biochem. J.* **2020**, *477*, 3453−3469.
(17) Gocher, A. M.; Azabdaftari, G.; Euscher, L. M.; Dai, S.; Karacosta, L. G.; Franke, T. F.; Edelman, A. M. Akt activation by Ca(2+)/calmodulin-dependent protein kinase kinase 2 (CaMKK2) in ovarian cancer cells. *J. Biol. Chem.* **2017**, *292*, 14188−14204.
(18) Schmitt, J. M.; Abell, E.; Wagner, A.; Davare, M. A. ERK activation and cell growth require CaM kinases in MCF-7 breast cancer cells. *Mol. Cell. Biochem.* **2010**, *335*, 155−171.
(19) Frigo, D. E.; Howe, M. K.; Wittmann, B. M.; Brunner, A. M.; Cushman, I.; Wang, Q.; Brown, M.; Means, A. R.; McDonnell, D. P. CaM kinase kinase beta-mediated activation of the growth regulatory kinase AMPK is required for androgen-dependent migration of prostate cancer cells. *Cancer Res.* **2011**, *71*, 528−537.
(20) Fu, H.; He, H.-c.; Han, Z.-d.; Wan, Y.-p.; Luo, H.-w.; Huang, Y.-q.; Cai, C.; Liang, Y.-x.; Dai, Q.-s.; Jiang, F.-n.; Zhong, W.-d. MicroRNA-224 and its target CAMKK2 synergistically influence tumor progression and patient prognosis in prostate cancer. *Tumour Biol.* **2015**, *36*, 1983−1991.
(21) White, M. A.; Tsouko, E.; Lin, C.; Rajapakshe, K.; Spencer, J. M.; Wilkenfeld, S. R.; Vakili, S. S.; Pulliam, T. L.; Awad, D.; Nikolos, F.; Katreddy, R. R.; Kaipparettu, B. A.; Sreekumar, A.; Zhang, X.; Cheung, E.; Coarfa, C.; Frigo, D. E. GLUT12 promotes prostate cancer cell growth and is regulated by androgens and CaMKK2 signaling. *Endocr. Relat. Canc.* **2018**, *25*, 453−469.
(22) Yasui, K.; Hashimoto, E.; Komorizono, Y.; Koike, K.; Arii, S.; Imai, Y.; Shima, T.; Kanbara, Y.; Saibara, T.; Mori, T.; Kawata, S.; Uto, H.; Takami, S.; Sumida, Y.; Takamura, T.; Kawanaka, M.; Okanoue, T.; Japan Nash Study Group, M. o. H. L.; Welfare of, J. Characteristics of patients with nonalcoholic steatohepatitis who develop hepatocellular carcinoma. *Clin. Gastroenterol. Hepatol.* **2011**, *9*, 428−433.
(23) Takuma, Y.; Nouso, K. Nonalcoholic steatohepatitis-associated hepatocellular carcinoma: our case series and literature review. *World J. Gastroenterol.* **2010**, *16*, 1436−1441.
(24) York, B.; Li, F.; Lin, F.; Marcelo, K. L.; Mao, J.; Dean, A.; Gonzales, N.; Gooden, D.; Maity, S.; Coarfa, C.; Putluri, N.; Means, A. R. Pharmacological inhibition of CaMKK2 with the selective antagonist STO-609 regresses NAFLD. *Sci. Rep.* **2017**, *7*, 11793.
(25) Price, D. J.; Drewry, D. H.; Schaller, L. T.; Thompson, B. D.; Reid, P. R.; Maloney, P. R.; Liang, X.; Banker, P.; Buckholz, R. G.; Selley, P. K.; McDonald, O. B.; Smith, J. L.; Shearer, T. W.; Cox, R. F.; Williams, S. P.; Reid, R. A.; Tacconi, S.; Faggioni, F.; Piubelli, C.; Sartori, I.; Tessari, M.; Wang, T. Y. An orally available, brain-penetrant CAMKK2 inhibitor reduces food intake in rodent model. *Bioorg. Med. Chem. Lett.* **2018**, *28*, 1958−1963.
(26) Anderson, K. A.; Ribar, T. J.; Lin, F.; Noeldner, P. K.; Green, M. F.; Muehlbauer, M. J.; Witters, L. A.; Kemp, B. E.; Means, A. R. Hypothalamic CaMKK2 contributes to the regulation of energy balance. *Cell Metab.* **2008**, *7*, 377−388.
(27) Langendorf, C. G.; O'Brien, M. T.; Ngoei, K. R. W.; McAloon, L. M.; Dhagat, U.; Hoque, A.; Ling, N. X. Y.; Dite, T. A.; Galic, S.; Loh, K.; Parker, M. W.; Oakhill, J. S.; Kemp, B. E.; Scott, J. W. CaMKK2 is inactivated by cAMP-PKA signaling and 14-3-3 adaptor proteins. *J. Biol. Chem.* **2020**, *295*, 16239−16250.
(28) Cary, R. L.; Waddell, S.; Racioppi, L.; Long, F.; Novack, D. V.; Voor, M. J.; Sankar, U. Inhibition of Ca(2)(+)/calmodulin-dependent protein kinase kinase 2 stimulates osteoblast formation and inhibits osteoclast differentiation. *J. Bone Miner. Res.* **2013**, *28*, 1599−1610.
(29) Pritchard, Z. J.; Cary, R. L.; Yang, C.; Novack, D. V.; Voor, M. J.; Sankar, U. Inhibition of CaMKK2 reverses age-associated decline in bone mass. *Bone* **2015**, *75*, 120−127.
(30) Lin, F.; Ribar, T. J.; Means, A. R. The Ca2+/calmodulin-dependent protein kinase kinase, CaMKK2, inhibits preadipocyte differentiation. *Endocrinology* **2011**, *152*, 3668−3679.
(31) Kang, X.; Cui, C.; Wang, C.; Wu, G.; Chen, H.; Lu, Z.; Chen, X.; Wang, L.; Huang, J.; Geng, H.; Zhao, M.; Chen, Z.; Müschen, M.; Wang, H.-Y.; Zhang, C. C. CAMKs support development of acute myeloid leukemia. *J. Hematol. Oncol.* **2018**, *11*, 30.
(32) Ma, Z.; Wen, D.; Wang, X.; Yang, L.; Liu, T.; Liu, J.; Zhu, J.; Fang, X. Growth inhibition of human gastric adenocarcinoma cells in vitro by STO-609 is independent of calcium/calmodulin-dependent protein kinase kinase-beta and adenosine monophosphate-activated protein kinase. *Am. J. Transl. Res.* **2016**, *8*, 1164−1171.
(33) O'Byrne, S. N.; Scott, J. W.; Pilotte, J. R.; Santiago, A. D. S.; Langendorf, C. G.; Oakhill, J. S.; Eduful, B. J.; Couñago, R. M.; Wells, C. I.; Zuercher, W. J.; Willson, T. M.; Drewry, D. H. In depth analysis of kinase cross screening data to identify CAMKK2 inhibitory scaffolds. *Molecules* **2020**, *25*, 325.
(34) Li, L.; Liu, C.; Amato, R. J.; Chang, J. T.; Du, G.; Li, W. CDKL2 promotes epithelial-mesenchymal transition and breast cancer progression. *Oncotarget* **2014**, *5*, 10840−10853.
(35) Billard, M. J.; Fitzhugh, D. J.; Parker, J. S.; Brozowski, J. M.; McGinnis, M. W.; Timoshchenko, R. G.; Serafin, D. S.; Lininger, R.; Klauber-Demore, N.; Sahagian, G.; Truong, Y. K.; Sassano, M. F.; Serody, J. S.; Tarrant, T. K. G protein coupled receptor kinase 3 regulates breast cancer migration, invasion, and metastasis. *PLoS One* **2016**, *11*, No. e0152856.
(36) Landesman-Bollag, E.; Romieu-Mourez, R.; Song, D. H.; Sonenshein, G. E.; Cardiff, R. D.; Seldin, D. C. Protein kinase CK2 in mammary gland tumorigenesis. *Oncogene* **2001**, *20*, 3247−3257.
(37) Monteiro, P.; Gilot, D.; Langouet, S.; Fardel, O. Activation of the aryl hydrocarbon receptor by the calcium/calmodulin-dependent protein kinase kinase inhibitor 7-oxo-7H-benzimidazo[2,1-a]benz-[de]isoquinoline-3-carboxylic acid (STO-609). *Drug Metab. Dispos.* **2008**, *36*, 2556−2563.
(38) Asquith, C. R. M.; Godoi, H. P.; Couñago, M. R.; Laitinen, T.; Scott, W. J.; Langendorf, G. C.; Oakhill, S. J.; Drewry, H. D.; Zuercher, J. W.; Koutentis, A. P.; Willson, M. T.; Kalogirou, S. A. 1,2,6-Thiadiazinones as novel narrow spectrum calcium/calmodulin-dependent protein kinase kinase 2 (CaMKK2) inhibitors. *Molecules* **2018**, *23*, 1221.
(39) Ghose, A. K.; Herbertz, T.; Pippin, D. A.; Salvino, J. M.; Mallamo, J. P. Knowledge based prediction of ligand binding modes and rational inhibitor design for kinase drug discovery. *J. Med. Chem.* **2008**, *51*, 5149−5171.
(40) Aronov, A. M.; Murcko, M. A. Toward a pharmacophore for kinase frequent hitters. *J. Med. Chem.* **2004**, *47*, 5616−5619.
(41) Xing, L.; Klug-Mcleod, J.; Rai, B.; Lunney, E. A. Kinase hinge binding scaffolds and their hydrogen bond patterns. *Bioorg. Med. Chem.* **2015**, *23*, 6520−6527.
(42) Irie, T.; Sawa, M. 7-Azaindole: A versatile scaffold for developing kinase inhibitors. *Chem. Pharm. Bull.* **2018**, *66*, 29−36.

https://doi.org/10.1021/acs.jmedchem.0c02274
J. Med. Chem. 2021, 64, 10849−10877

(43) Sherk, A. B.; Frigo, D. E.; Schnackenberg, C. G.; Bray, J. D.; Laping, N. J.; Trizna, W.; Hammond, M.; Patterson, J. R.; Thompson, S. K.; Kazmin, D.; Norris, J. D.; McDonnell, D. P. Development of a small-molecule serum- and glucocorticoid-regulated kinase-1 antagonist and its evaluation as a prostate cancer therapeutic. *Cancer Res.* **2008**, *68*, 7475−7483.
(44) Ishiyama, T.; Murata, M.; Miyaura, N. Palladium(0)-catalyzed cross-coupling reaction of alkoxydiboron with haloarenes: a direct procedure for arylboronic esters. *J. Org. Chem.* **1995**, *60*, 7508−7510.
(45) Merour, J.-Y.; Joseph, B. Synthesis and reactivity of 7-azaindoles (1H-pyrrolo(2,3-b)pyridine). *Curr. Org. Chem.* **2001**, *5*, 471−506.
(46) Morita, H.; Shiotani, S. Furopyridines. VI. Preparation and reactions of 2- and 3-substituted furo[2,3-b]pyridines. *J. Heterocycl. Chem.* **1986**, *23*, 1465−1469.
(47) Taylor, S. L.; Martin, J. C. Trifluoromethyl triflate: synthesis and reactions. *J. Org. Chem.* **1987**, *52*, 4147−4156.
(48) Fedorov, O.; Niesen, F. H.; Knapp, S. Kinase inhibitor selectivity profiling using differential scanning fluorimetry. *Methods Mol. Biol.* **2012**, *795*, 109−118.
(49) Santiago, A. D. S.; Couñago, R. M.; Ramos, P. Z.; Godoi, P. H. C.; Massirer, K. B.; Gileadi, O.; Elkins, J. M. Structural analysis of inhibitor binding to CAMKK1 Identifies Features Necessary for Design of Specific Inhibitors. *Sci. Rep.* **2018**, *8*, 14800.
(50) Davis, M. I.; Hunt, J. P.; Herrgard, S.; Ciceri, P.; Wodicka, L. M.; Pallares, G.; Hocker, M.; Treiber, D. K.; Zarrinkar, P. P. Comprehensive analysis of kinase inhibitor selectivity. *Nat. Biotechnol.* **2011**, *29*, 1046−1051.
(51) Profeta, G. S.; Dos Reis, C. V.; Santiago, A. D. S.; Godoi, P. H. C.; Fala, A. M.; Wells, C. I.; Sartori, R.; Salmazo, A. P. T.; Ramos, P. Z.; Massirer, K. B.; Elkins, J. M.; Drewry, D. H.; Gileadi, O.; Couñago, R. M. Binding and structural analyses of potent inhibitors of the human Ca(2+)/calmodulin dependent protein kinase kinase 2 (CAMKK2) identified from a collection of commercially-available kinase inhibitors. *Sci. Rep.* **2019**, *9*, 16452.
(52) Halgren, T. A.; Murphy, R. B.; Friesner, R. A.; Beard, H. S.; Frye, L. L.; Pollard, W. T.; Banks, J. L. Glide: a new approach for rapid, accurate docking and scoring. 2. Enrichment factors in database screening. *J. Med. Chem.* **2004**, *47*, 1750−1759.
(53) Beno, B. R.; Yeung, K.-S.; Bartberger, M. D.; Pennington, L. D.; Meanwell, N. A. A Survey of the role of noncovalent sulfur interactions in drug design. *J. Med. Chem.* **2015**, *58*, 4383−4438.
(54) Zhang, X.; Gong, Z.; Li, J.; Lu, T. Intermolecular sulfur...oxygen interactions: theoretical and statistical investigations. *J. Chem. Inf. Model.* **2015**, *55*, 2138−2153.
(55) Tokumitsu, H.; Inuzuka, H.; Ishikawa, Y.; Ikeda, M.; Saji, I.; Kobayashi, R. STO-609, a specific inhibitor of the Ca(2+)/calmodulin-dependent protein kinase kinase. *J. Biol. Chem.* **2002**, *277*, 15813−15818.
(56) Tokumitsu, H.; Inuzuka, H.; Ishikawa, Y.; Kobayashi, R. A single amino acid difference between alpha and beta Ca2+/calmodulin-dependent protein kinase kinase dictates sensitivity to the specific inhibitor, STO-609. *J. Biol. Chem.* **2003**, *278*, 10908−10913.
(57) Alsenz, J.; Kansy, M. High throughput solubility measurement in drug discovery and development. *Adv. Drug Deliv. Rev.* **2007**, *59*, 546−567.
(58) Hill, A. P.; Young, R. J. Getting physical in drug discovery: a contemporary perspective on solubility and hydrophobicity. *Drug Discov. Today* **2010**, *15*, 648−655.
(59) Lipinski, C. A.; Lombardo, F.; Dominy, B. W.; Feeney, P. J. Experimental and computational approaches to estimate solubility and permeability in drug discovery and development settings. *Adv. Drug Delivery Rev.* **1997**, *23*, 3−25.
(60) Mignani, S.; Rodrigues, J.; Tomas, H.; Jalal, R.; Singh, P. P.; Majoral, J.-P.; Vishwakarma, R. A. Present drug-likeness filters in medicinal chemistry during the hit and lead optimization process: how far can they be simplified? *Drug Discov. Today* **2018**, *23*, 605−615.
(61) Hopkins, A. L.; Keserü, G. M.; Leeson, P. D.; Rees, D. C.; Reynolds, C. H. The role of ligand efficiency metrics in drug discovery. *Nat. Rev. Drug Discov.* **2014**, *13*, 105−121.
(62) Saal, C.; Petereit, A. C. Optimizing solubility: kinetic versus thermodynamic solubility temptations and risks. *Eur. J. Pharm. Sci.* **2012**, *47*, 589−595.
(63) Vasta, J. D.; Corona, C. R.; Wilkinson, J.; Zimprich, C. A.; Hartnett, J. R.; Ingold, M. R.; Zimmerman, K.; Machleidt, T.; Kirkland, T. A.; Huwiler, K. G.; Ohana, R. F.; Slater, M.; Otto, P.; Cong, M.; Wells, C. I.; Berger, B.-T.; Hanke, T.; Glas, C.; Ding, K.; Drewry, D. H.; Huber, K. V. M.; Willson, T. M.; Knapp, S.; Müller, S.; Meisenheimer, P. L.; Fan, F.; Wood, K. V.; Robers, M. B. Quantitative, wide-spectrum kinase profiling in live cells for assessing the effect of cellular ATP on target engagement. *Cell Chem. Biol.* **2018**, *25*, 206−214.
(64) Green, M. F.; Anderson, K. A.; Means, A. R. Characterization of the CaMKKbeta-AMPK signaling complex. *Cell. Signal.* **2011**, *23*, 2005−2012.
(65) Niesen, F. H.; Berglund, H.; Vedadi, M. The use of differential scanning fluorimetry to detect ligand interactions that promote protein stability. *Nat. Protoc.* **2007**, *2*, 2212−2221.
(66) Xy Ling, N.; Langendorf, C. G.; Hoque, A.; Galic, S.; Loh, K.; Kemp, B. E.; Gundlach, A. L.; Oakhill, J. S.; Scott, J. W. Functional analysis of an R311C variant of Ca(2+) -calmodulin-dependent protein kinase kinase-2 (CaMKK2) found as a de novo mutation in a patient with bipolar disorder. *Bipolar Disord.* **2020**, *22*, 841−848.
(67) Newman, J. Novel buffer systems for macromolecular crystallization. *Acta Crystallogr., Sect. D: Biol. Crystallogr.* **2004**, *60*, 610−612.
(68) Kabsch, W. Xds. *Acta Crystallogr., Sect. D: Biol. Crystallogr.* **2010**, *66*, 125−132.
(69) Winn, M. D.; Ballard, C. C.; Cowtan, K. D.; Dodson, E. J.; Emsley, P.; Evans, P. R.; Keegan, R. M.; Krissinel, E. B.; Leslie, A. G. W.; McCoy, A.; McNicholas, S. J.; Murshudov, G. N.; Pannu, N. S.; Potterton, E. A.; Powell, H. R.; Read, R. J.; Vagin, A.; Wilson, K. S. Overview of the CCP4 suite and current developments. *Acta Crystallogr., Sect. D: Biol. Crystallogr.* **2011**, *67*, 235−242.
(70) McCoy, A. J.; Grosse-Kunstleve, R. W.; Adams, P. D.; Winn, M. D.; Storoni, L. C.; Read, R. J. Phaser crystallographic software. *J. Appl. Crystallogr.* **2007**, *40*, 658−674.
(71) Kukimoto-Niino, M.; Yoshikawa, S.; Takagi, T.; Ohsawa, N.; Tomabechi, Y.; Terada, T.; Shirouzu, M.; Suzuki, A.; Lee, S.; Yamauchi, T.; Okada-Iwabu, M.; Iwabu, M.; Kadowaki, T.; Minokoshi, Y.; Yokoyama, S. Crystal structure of the Ca(2)(+)/calmodulin-dependent protein kinase kinase in complex with the inhibitor STO-609. *J. Biol. Chem.* **2011**, *286*, 22570−22579.
(72) Murshudov, G. N.; Skubák, P.; Lebedev, A. A.; Pannu, N. S.; Steiner, R. A.; Nicholls, R. A.; Winn, M. D.; Long, F.; Vagin, A. A. REFMAC5 for the refinement of macromolecular crystal structures. *Acta Crystallogr., Sect. D: Biol. Crystallogr.* **2011**, *67*, 355−367.
(73) Emsley, P.; Lohkamp, B.; Scott, W. G.; Cowtan, K. Features and development of Coot. *Acta Crystallogr., Sect. D: Biol. Crystallogr.* **2010**, *66*, 486−501.
(74) Chen, V. B.; Arendall, W. B., 3rd; Headd, J. J.; Keedy, D. A.; Immormino, R. M.; Kapral, G. J.; Murray, L. W.; Richardson, J. S.; Richardson, D. C. MolProbity: all-atom structure validation for macromolecular crystallography. *Acta Crystallogr., Sect. D: Biol. Crystallogr.* **2010**, *66*, 12−21.

https://doi.org/10.1021/acs.jmedchem.0c02274
J. Med. Chem. 2021, 64, 10849−10877